الجمهورية الجزائرية الديمقراطية الشعبية
People's Democratic Republic OF Algeria
وزارة التعليم العالي و البحث العلمي
MINISTRY OF HIGHER EDUCATION AND SCIENTIFIC RESEARCH
جامعة الشهيد الشيخ العربي التبسي-تبسة
Echahid Cheikh Larbi Tebessi University-Tebessa
كلية العلوم و التكنولوجيا

Department of Electrical Engineering

A Master's Thesis

presented to obtain the diploma of Academic Master in Electrical Engineering
Discipline: Science and Technology
Specialty: Industrial Electrotechnic

THEME

ADVANCED CONTROL STRATEGY OF DFIG BASED WIND ENERGY CONVERSION SYSTEM

Presented and defended by:

- **Zaouiche Sihem**
- **Bentiba Nour elhouda**

Under jury members:

– **DJEBBAR Mohamed Salah**	**President**	**MCA**
– **BOUGARNE Abla**	**Supervisor**	**MCA**
– **METATLA Samir**	**Examinator**	**MCB**

2023/2024


بسم الله الرحمن الرحيم

Gratitude

First and foremost, we thank ALLAH for granting us the ability to accomplish this modest work.

Next, we would like to express our gratitude to our supervisor, Dr. BOUGARNE Abla, for her support, advice, and guidance, which have been beneficial for successfully completing this work.

We extend our appreciation to Dr. DJEBBAR Mohamed Salah, for agreeing to chair the jury.

We also wish to thank Dr. METATLA Samir, for accepting to examine this work.

Furthermore, we would like to thank all the teachers whom we had the honor of knowing and appreciating during our schooling.

We also extend our gratitude to our parents, for all the moral, financial, and psychological support, and particularly for the love they have bestowed upon us.

Lastly, our thanks go to all those who have contributed, directly or indirectly, to the realization of this modest work.

Bentiba nour elhouda
Zaouiche sihem

Dedication

To my beloved father, the noble Zaouiche Nacir, who provided me with invaluable guidance throughout my academic journey, constantly fueling my motivation and surrounding me with caring protection,

To my cherished mother, the beloved Kraidia Sadika, who walked alongside me and tirelessly prayed for my success,

To my beloved sisters, Fatma Ezzahra, Aouatef, Douaa,

To my dear friends, who shared unforgettable moments, sparkling laughter, and sincere friendship with me,

I dedicate this thesis with deep gratitude and infinite appreciation.

To my trusted partner, the eminent Bentiba Nour elhouda, whose contribution, sometimes discreet, sometimes evident, greatly contributed to the realization of this scientific work,

To my esteemed teachers, whose wisdom and erudition imparted the knowledge and passion that drive my pen,

To all those I know, who have crossed my path and offered me their kindness,

I extend my sincerest thanks to you all. Your unwavering support and unfaltering love have been the pillars of this achievement. Your constant presence in my life has been an endless source of inspiration and courage.

This thesis embodies not only my relentless efforts but also the fruit of your encouragement and unwavering support. I dedicate these pages to you with profound emotion and eternal gratitude.

May these words testify to my eternal gratitude towards all of you.

ZAOUICHE Sihem

Dedication

With all my feelings of respect. With the experience

of my gratitude, I dedicate my graduation and my joy

to my paradise, the apple of my eye, the source of my life and happiness,

my moon, and the thread of hope

that lights my path. My better half, Mom.

To the one who made me a person, my source of life, love, and affection.

To my support who was always by my side to encourage and support me, to my prince, Dad.

To my brothers and sister, and those who shared with me all the emotional moments

during the realization of this work.

To all the members of my extended family.

To my supervisor, « Dr. BOUGARNE Abla », for her patience, diligence,

and responsiveness during the preparation of this thesis.

Not forgetting my partner, « Sihem», for her moral support, patience,

and understanding throughout this project.

To my esteemed teachers, whose wisdom and erudition imparted the knowledge and passion that drive my pen,

To all my friends who have always encouraged me, and to whom I wish more success.

To everyone who loves me.

BENTIBA Nour elhouda

Summary

CHAPITER II

STUDY AND MODELLING OF THE WIND TURBINE

CHAPTER III

MODELING AND SIMULATION OF THE DOUBLY-FED INDUCTION MACHINE

CHAPTER VI

DPC FUZZY LOGIC CONTROL OF A WIND ENERGY CONVERSION SYSTEM BASED ON DFIG CONNECTED TO GRID

List of figures

List of tables

Acronyms

CDER	Center for Renewable Energy Development
CEGELEC	General Company of Electricity and Electronics
Sonelgaz	National Company of Electricity and Gas
INERGA	National Institute of Renewable Energies and Energy Efficiency
RE	Renewable Energies
WECS	Wind Energy Conversion System
HAWT	Horizontal Axis Wind Turbine
VAWT	Vertical Axis Wind Turbine
DFIG	Doubly Fed Induction Generator
PWM	Pulse Width Modulation
CP	Power Coefficient
MPPT	Maximum Power Point Tracking
PI	Proportional Integral
VCFO	Vector Control with Flux Orientation
DCFO	Direct Control with Flux Orientation
IRCFO	Indirect Control with Flux Orientation
OLTF	Open-Loop Transfer Function
CLTF	Closed-Loop Transfer Function.
DC	Direct current
AC	Alternating current

Nomenclature

P_n	Nominal power of the turbine [W]
V_n	Nominal wind speed [m/s]
V_m	Maximum wind speed [m/s]
β	Blade pitch angle [°]
R	Radius of the wind turbine or the length of the blades [m]
G	Speed multiplier gain
P_w	Wind power [W]
ρ	Air density [approximately 1.225 kg/m^3]
S	Area described by the rotating wind turbine blades [m^2]
λ	Speed ratio
λ_{opt}	The optimal specific speed of the turbine
Ω_t	Turbine rotation speed [rad/s]
C_p	Power coefficient
P_{aer}	Aerodynamic power extracted by the turbine [W]
C_t	Aerodynamic torque [N.m]
J_t	Turbine moment of inertia [Kg.m^2]
J_m	Moment of inertia of the DFIG [Kg.m^2]
f_v	Coefficient due to viscous friction of the DFIG [N.m/rad/s]
C_m	Mechanical torque on the DFIG shaft [N.m]
Ω_m	Rotation speed of the DFIG [rad/s]
J	Total inertia [Kg.m^2]
C_{em}	Electromagnetic torque of the DFIG [N.m]
V_{est}	Estimated wind speed [m/s]
V_s	Stator voltage [V]
V_r	Rotor voltage [V]
φ_s	Stator flux [W_b]
φ_r	Rotor flux [W_b]
I_s	Current statorique [A]
I_r	Current rotorique [A]
R_s	Stator resistance [Ohm]
R_r	Rotor resistance [Ohm]
l_s	Stator cyclic inductance [mH]

l_r	Rotor cyclic inductance [mH]
M_{sr}	Stator-rotor mutual inductance [mH]
M_s	Mutual inductance between stator phases [mH]
M_r	Mutual inductance between rotor phases [mH]
p	Number of pole pairs
θ	Park transformation angle
V_{ds},V_{qs}	Two-phase components of stator voltages [V]
V_{dr},V_{qr}	Two-phase components of rotor voltages [V]
I_{ds},I_{qs}	Two-phase components of stator currents [A]
I_{dr},I_{qr}	Two-phase components of rotor currents [A]
φ_{ds},φ_{qs}	Two-phase components of stator fluxes [Wb]
φ_{dr}, φ_{qr}	Two-phase components of rotor fluxes [Wb]
ω_s	Stator field pulsation [rad/s]
ω_r	Rotor field pulsation [rad/s]
s	Laplace operator
P_s	Active power statorique of the DFIG [W]
Q_s	Reactive power statorique of the DFIG [Var]
K_p	Proportional gain
K_i	Integral gain

GENERAL INTRODUCTION

General introduction

Currently, over 80% of the energy consumed worldwide comes from fossil fuels such as coal, oil, gas, and uranium. These resources, which have accumulated over geological time, are limited and non-renewable. The growing reliance on fossil fuels worsens the issue of resource depletion and increases price instability and uncertainty. At the same time, experts predict about a 30% increase in global electricity demand by 2050, highlighting the urgent need to seek alternative and sustainable solutions, such as renewable energies like solar and wind power.

In response to these challenges, wind energy offers environmental and economic benefits, though its reliance on weather conditions poses a challenge for the stability of the electrical grid. Research in wind energy has shown significant progress, with the introduction of advanced technologies such as optimized power sensors to best harness the wind's force. Wind systems generate electrical energy from wind speed, which is converted into mechanical energy by the generator.

Different types of generators are used in wind turbines, including the squirrel cage induction generator (SCIG), the doubly-fed induction generator (DFIG), and the wound rotor induction generator (WRIG). The DFIG stands out for its flexibility and ability to offer an excellent balance between performance and cost. Its design allows efficient regulation of the produced electrical energy, making it particularly suitable for variable wind conditions. Consequently, the DFIG is highly valued for its reliability and cost-effectiveness.

In the process of converting wind energy, the turbine first captures the wind's energy, then a generator transforms it into electrical energy. Wind turbines are generally classified into two categories: fixed-speed and variable-speed. Variable-speed turbines usually produce more energy than fixed-speed ones, reducing power fluctuations and improving the quality of the reactive energy provided. DFIGs are widely used in variable-speed turbines.

Many scientific studies have focused on the dynamic modeling and simulation of small wind systems to describe their dynamic physical model and predict the evolution of their outputs, such as current, voltage, and power.

The main objective of this thesis is to study the control techniques of the DFIG (Doubly-Fed Induction Generator) to improve the performance and optimize the production of a wind turbine. To achieve this, the thesis is organized into four chapters:

Chapter One: provides a general overview of the different types of renewable energy, their advantages and disadvantages, and Algeria's projects and prospects in this field.

Chapter Two: discusses the different types of wind turbines, highlighting the advantages and disadvantages of each type. It also covers the conversion system by identifying its main elements and components, as well as classification methods, and presents the model of each component in the chain. To improve system performance, we have also used the Maximum Power Point Tracking (MPPT) control strategy. Simulation results are presented, analyzed, and discussed at the end of this chapter.

Chapter Three: is dedicated to the modeling and simulation of the DFIG, which is a crucial step for the study of the system, with the presentation of its mathematical model for control purposes in the electrical energy production chain. We have included and analyzed the results at the end of the chapter.

Chapter Four: focuses on the direct control of active and reactive power on the stator side, allowing their adjustment according to the previously determined instructions by the network manager. Simulation results are presented to verify and validate the control strategies.

Finally, this thesis concludes with a general conclusion that proposes perspectives for the continuation of this work in the future.

CHAPITER I

RENEWABLE ENERGY GENERALITY

I.1 Introduction

Renewable energy is defined as deriving from sources that undergo natural replenishment, in contrast to non-renewable energy, which depletes its reserves. Over recent years, there has been a substantial surge in the development and utilization of renewable energies. The sustainability of energy systems in the forthcoming two decades will hinge upon the judicious management of traditional sources and an expanded incorporation of energy.

Consumers attain heightened security and demonstrate increased environmental conscientiousness through decentralized electricity production utilizing renewable energies. Nonetheless, certain regulations pertaining to the dimensions and operational methods of energy recovery systems are dictated by stochastic sources.

The present chapter will present a general study on the various renewable energy sources, particularly wind energy and its presence in Algeria.

I.2 Definition of renewable energy

Renewable energy, often abbreviated as RE, encompasses various methods of generating energy from sources or resources that are theoretically limitless, readily available without temporal constraints, or capable of replenishing more rapidly than their consumption rate. In general discourse, renewable energies are juxtaposed with fossil fuels, such as coal, oil, and natural gas, which have finite and non-renewable reserves within the human timeframe. In contrast, renewable energies derive from sources like sunlight or wind, considered theoretically inexhaustible on a human scale. While sometimes inaccurately labeled as "green energies" or "clean energies", renewable energies do possess ecological advantages. However, it is essential to note that they may not always be truly "green" or "clean," as they can also entail significant environmental consequences [1].

I.3 Recent technologies and innovations of renewable energies

Technologies and innovations associated with renewable energies are continually advancing as they are deployed, and new challenges emerge. In recent years, renewable energy technologies have focused on:

1. Energy Storage: Solutions for storing solar and wind energy have been developed to ensure a more continuous supply of electricity. These solutions include high-capacity batteries and storage systems utilizing hydrogen technologies.
2. Offshore Wind Energy: Offshore wind turbines have reached unprecedented heights and dimensions, providing higher efficiency and lower costs.

3. Solar Thermal Energy: This technology employs mirrors to concentrate solar light and generate heat, which can then be utilized to produce electricity or heat water. Despite being an ancient technology, it has often been overlooked in favor of photovoltaic panels but is now experiencing renewed development.

4. Advanced Biofuels: These biofuels are derived from non-food raw materials, such as agricultural and forestry waste, rather than food crops, thus avoiding competition with food production.

5. Geothermal Energy: Technologies for geothermal energy production have been enhanced, enabling the generation of electricity from increasingly lower heat sources.

I.4 Technical and economic constraints

I.4.1 Technical constraints

Despite the promising potential for significant development in the medium and long term, most renewable energy technologies have not yet attained sufficient maturity to compete with conventional energies on a large scale. Hydroelectricity stands as an exception, along with certain forms of renewable energy that are gradually becoming economically viable.

The technical constraints can be primarily categorized into three aspects:

- Firstly, there is a relatively low available power density, necessitating extensive collection areas and incurring high material costs.
- Secondly, the substantial variability of energy sources such as solar or wind energy, hydropower, and marine energy leads to wide fluctuations. Capturing energy when it is available requires intricate regulations.
- The third constraint involves the imperative need for storage. Since these energies manifest as flows, storage is essential for most applications, presenting a challenge due to the current lack of effective and economical energy storage solutions [2].

I.4.2 Economic constraints

The economic constraints encompass two main aspects:

- Firstly, there is a high investment cost associated with these technologies. Even when well developed, as in the case of hydroelectric power, these technologies remain relatively expensive in terms of initial investment, although their operating costs are generally low.
- Secondly, the necessity for backup adds an additional layer of economic constraints. In instances of source unavailability, alternative energy sources often need to be employed, incurring additional costs that may not be insignificant [2]

.

I.5 Different types of renewable energies

I.5.1 Wind energy

The global adoption of wind energy for electricity production is experiencing rapid growth. Wind energy, a consistently renewable resource, is harnessed to generate significant amounts of electricity through a device commonly known as a wind turbine or windmill. This apparatus converts a portion of the wind's kinetic energy into mechanical energy on the transmission shaft, subsequently converting it into electrical energy through an electromagnetic generator connected to the wind turbine. The mechanical coupling may be direct or indirect, depending on the specific application.

Currently, the most widely used wind turbines in the market are vertical-axis wind turbines, known for their compelling production profile. Another critical but less visible aspect pertains to small-scale production units, which are increasingly sought after for autonomous operations, supplying power to isolated or self-sufficient sites. Furthermore, with the introduction of new vertical-axis architectures, these units are finding applications in urban environments.

Irrespective of the machine type employed, operating as an autonomous generator entails unique constraints and specificities compared to large wind farms. In this context, the primary focus is on maintaining constant values for the amplitude and frequency of the generated voltage, regardless of the wind turbine's rotation speed and the power demanded within a specified range. Achieving this goal necessitates the implementation of a control system for the wind energy system [3].

Figure I.1 Wind turbines

I.5.1.1 Wind turbine in Algeria

Algeria has a considerable wind potential that can be exploited for the production of electrical energy, especially in the south where wind speeds are high and can exceed 4m/s (6m/s in the Tindouf region), and up to 7m/s in the Adrar region.

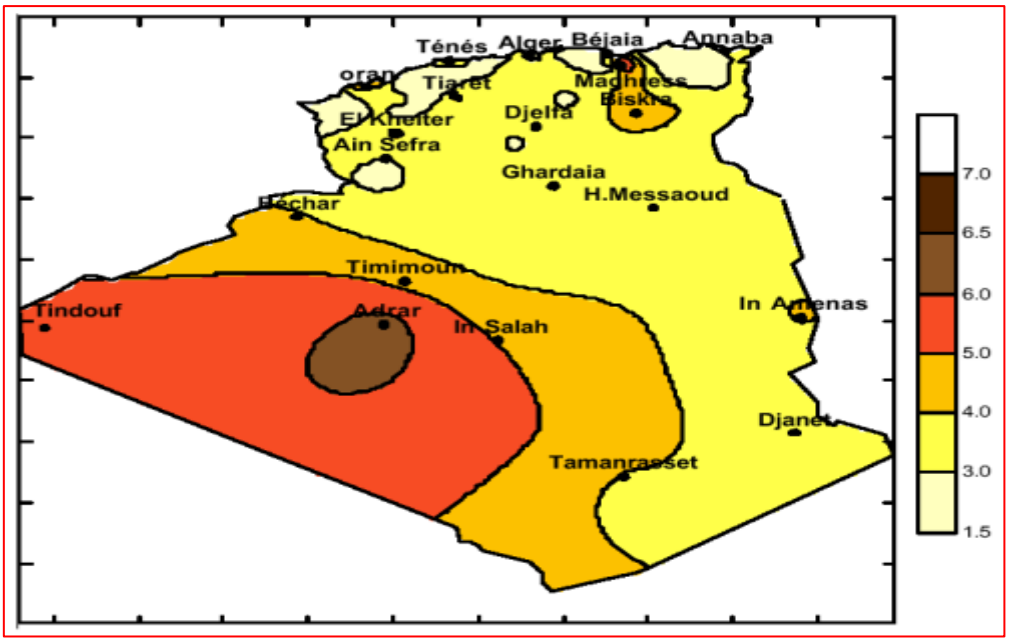

Figure I.2 Wind map in Algeria at 10 meters altitude [4]

The energy resources of Algeria have already been estimated by CDER since the 90s through the production of wind speed and available wind energy potential atlases in Algeria.

This has allowed the identification of nine windy areas that are likely to receive wind installations [5]:

• Two areas on the coast

• Three areas on the high plateaus

• And four areas in Saharan sites.

I.5.1.2 Adrar wind farm

In October 2011, the Adrar wind farm, which is intended to serve as a pilot project for the government's 420 MW wind plan by 2024, was commissioned by the Minister of Energy, Youcef Yousfi.

Consisting of 12 wind turbines with a unit power of 0.85MW each (for a total capacity of 10 megawatts), the Adrar wind farm, located on an area of 30 hectares in the Kabertene zone 72 km north of the capital of the wilaya, required nearly 32 months of work. Started in October

2011, the construction work of the Adrar wind farm was entrusted to the French company CEGELEC in partnership with a group composed of subsidiary companies of Sonelgaz, ETTERKIB and INERGA. In The occurrence, with a total cost of 2.8 billion dinars, was supposed to be completed in the second quarter of 2013. This new electricity production plant, the first of its kind on a national scale, is part of a vast plan of renewable energy generation projects of 22 GW by 2030, including 1.7 GW in wind power. In terms of renewable energy, the government's plan is significantly delayed. The plan, launched in 2011, was supposed to be carried out in three phases. The first phase (2011-2013) was dedicated to studies and the launch of pilot projects; the second phase (2014-2015) to the implementation of the first installations, and the third phase (2016-2020) to the launch of large-scale industry.

Figure I.3 Adrar wind power plant

I.5.2 Solar energy

The sun serves as an almost limitless source of energy, emitting radiation towards the Earth's surface that is approximately 8400 times the annual energy consumption of humanity. This equates to an instantaneous power reception of 1 peak kilowatt per square meter (kWp/m2), spanning the entire spectrum from ultraviolet to infrared. Deserts on our planet receive more solar energy in 6 hours than the total annual energy consumption of humanity.

The majority of solar energy applications are direct, as seen in agriculture through processes like photosynthesis or in various drying and heating applications. This energy is abundantly present across the Earth's surface, and despite significant attenuation as it traverses the atmosphere, a considerable amount still reaches the ground. In temperate zones, one can count on 1000 W/m2, and in areas with a lightly polluted atmosphere containing dust or water, it can go up to 1400 W/m^2 [6].

I.5.2.1 Solar potential in Algeria

According to its geographical location, Algeria holds one of the highest solar potential. Indeed, following an assessment by the satellites, the German Aerospace Center (DLR) concluded that Algeria has the largest solar potential in the Mediterranean basin: 169,440TWh/year. Sunshine duration on almost all the country over 2000 hours per year and can reach 3900 hours in the Highlands and the Sahara. The daily energy obtained on a horizontal surface is about 5 kWh on most of the national territory, about 1700 kWh / m² / year for the North and 2263 KWh / m² / year for the South [6]. The climatic conditions in Algeria are favorable for the development of solar energy due to the abundant sunshine throughout the year, especially in the Sahara region, Figure I.4 illustrates the solar irradiance map of Algeria [6].

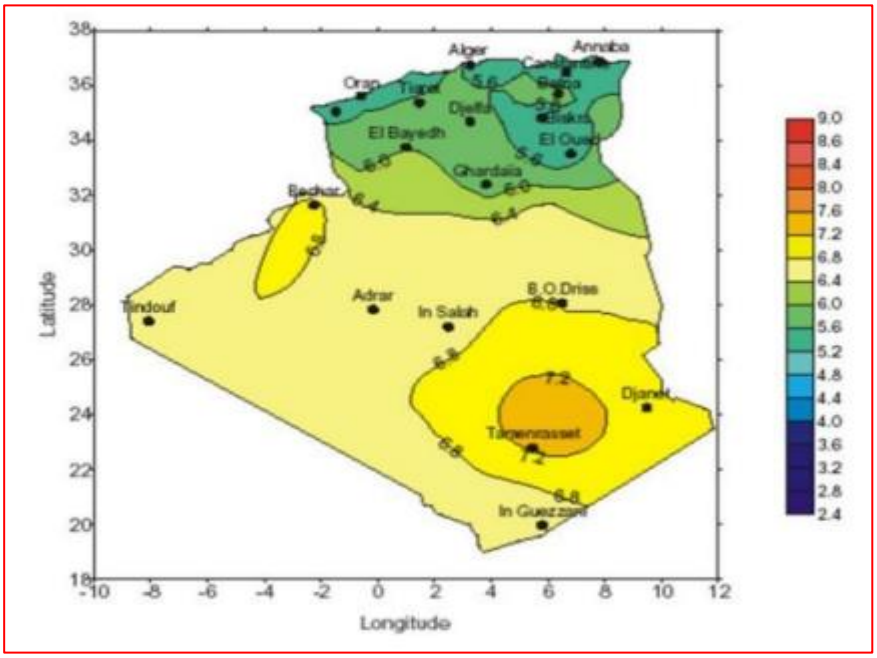

Figure I.4 Annual average intensity of daily solar radiation in various regions of Algeria (KW/hrs/m² per day) [7]

I.5.3 Hydraulic energy

Many civilizations have utilized the power of water, which represented one of the most important energy sources before the era of electricity. Nowadays, hydraulic energy is used in dams and is primarily used for electricity production, where hydropower is currently the leading renewable source of electricity. The installed hydroelectric capacity worldwide was estimated at 715 GW, accounting for approximately 19% of global electrical power. Nearly 15% of all installed electricity in Europe is of hydraulic origin.

Figure I.5 Dam intended for energy production

I.5.4 Biomass energy

Biomass is classified into four categories: dry biomass (wood, agricultural waste, etc.), biogas, renewable solid household waste, and wet biomass (bioethanol, biodiesel, vegetable oil, etc...). The heat generated by combustion warms a water reservoir, creating steam akin to a pressure cooker. This high-pressure steam is then released, propelling a turbine connected to a generator. It is this generator that enables electricity production. What makes biomass power plants particularly noteworthy is their ability to generate electricity using materials that are no longer needed [8].

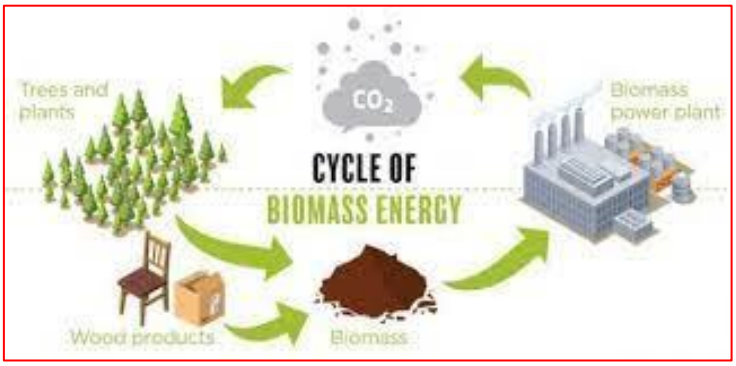

Figure I.6 cycle of biomass energy

I.5.5 Geothermal energy

Geothermal energy is the thermal energy extracted from the Earth's internal heat. Traditionally, geothermal energy is categorized into three types based on the temperature level available for exploitation:

- High-energy geothermal
- Low-energy geothermal
- Very low-energy geothermal

To tap into this underground energy source, cold water is directed below the Earth's surface. The cold water undergoes heating and is subsequently pumped back to the surface, where it can be utilized either for electricity generation in a power plant or directly as hot water for various domestic purposes, such as showers and radiators

Figure I.7 Geothermal energy

I.6 Advantages and disadvantages of renewable energy

I.6.1 Advantages of renewable energy

Renewable energy offers several advantages compared to fossil fuels. Here are some of the key benefits of utilizing alternative energy sources [9]:

- Renewable energy is sustainable and will not deplete over time.
- Alternative energy sources generally have lower maintenance needs.
- Using renewables can result in cost savings.
- Renewable energy provides various environmental benefits.
- Dependence on foreign energy sources can be reduced with renewables.
- Cleaner water and air are associated with the use of renewable energy.
- The renewable energy sector contributes to job creation.
- Adopting renewable energy can help minimize waste.

I.6.2 Disadvantages of renewable energies

While renewable energy offers numerous advantages, it is not always smooth sailing in the realm of sustainability. Here are some drawbacks of renewable energy when contrasted with traditional fuel sources:

- High initial costs are associated with renewable energy.
- Renewable energy can be intermittent, dependent on weather conditions.
- Storage capabilities for renewables are a concern.
- Geographic limitations exist for certain renewable energy sources.

• Renewables may not always be entirely carbon-free.

I.7 The Algerian future strategy for renewable energy 2011-2030

In 2011, a significant and promising program was launched in Algeria to develop and promote renewable energy. This program is set to continue for twenty years until 2030 and was adopted by the Algerian government on February 2, 2011, with the aim of developing and utilizing the available renewable energy sources in the country, such as solar and wind energy. The program also aims to achieve diversity in energy sources, extend the assumed lifespan of national fossil fuel reserves, achieve energy security for the country and meet environmental goals. As part of this program, a renewable energy fund was established under Executive Decree No. 11-423 in December 2011 to support and finance investment in the field of renewable energy. Three basic stages were outlined for the implementation of this program as follows [9]:

- The first phase (2011-2013): focused on developing pioneering (model) projects to select various available technologies;
- The second phase (2014-2015): characterized by the implementation of the program dissemination;
- The third phase (2016-2030): is dedicated to the wide-scale implementation of the program

The program will consist of installing up to 22,000 megawatts by 2030, which represents 40% of renewable energy generation capacity between 2011 and 2030. It is planned to use 12,000 megawatts of the project's energy to meet local electricity demand, while the remaining 10,000 megawatts will be directed for export over the next two decades.

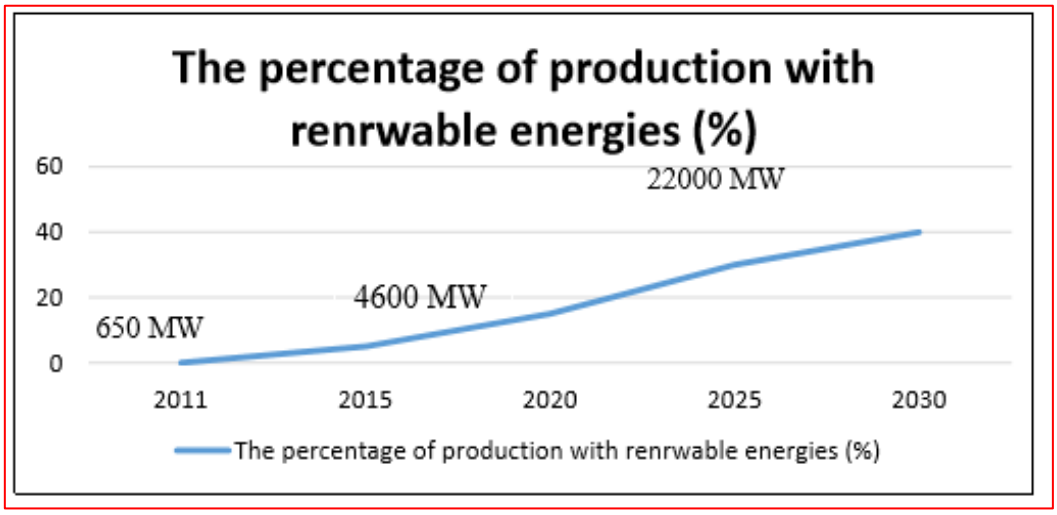

Figure I.8 Expected penetration rate of renewable energies in national production [10]

I.8 Renewable energy percentage in Algeria

Algeria is increasingly relying on renewable energy sources as part of its strategy to reduce carbon emissions and achieve sustainability. Photovoltaic solar constitutes the largest part of this mix at 61.7%, benefiting from the abundance of sunlight in the country. Wind energy comes in second at 22.8%, concentrated in areas with strong winds. And the solar thermal energy reserve 9.1%. Meanwhile, biomass power contributes 4.5% [11].

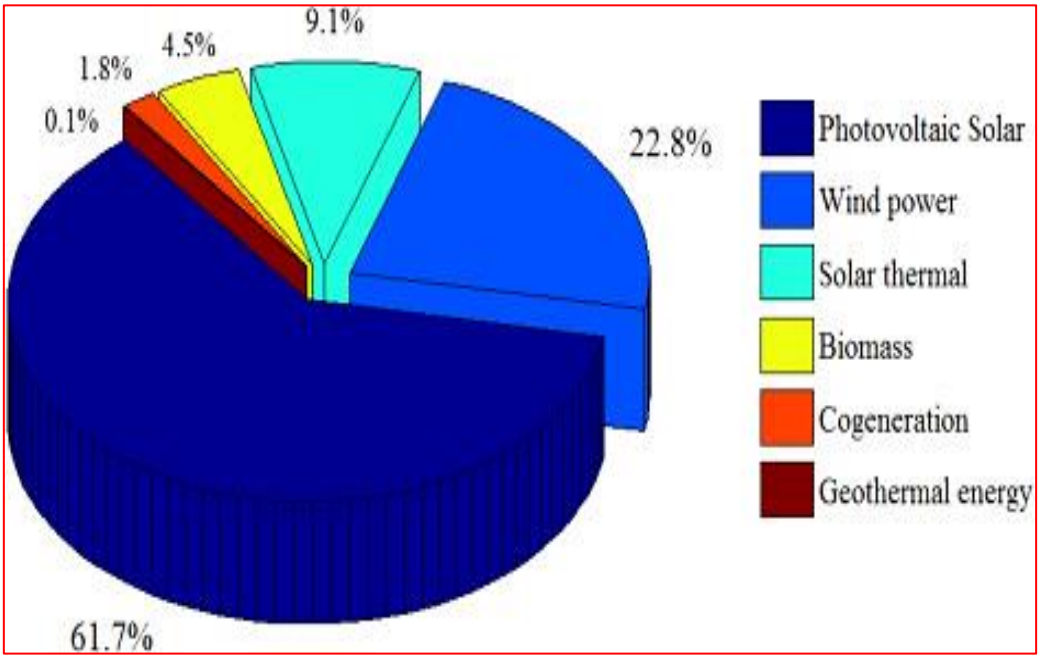

Figure I.9 Management strategy of energy resources in Algeria

I.8 Conclusion

In this section, we have provided a general overview of different renewable energy systems designed for electricity generation, including their technologies, structures, and operational principles. We have also discussed their pros and cons, emphasizing the prioritization of renewable energies in Algeria.

The next chapter is dedicated to the study of modeling a wind turbine.

CHAPITER II

STUDY AND MODELLING OF THE WIND TURBINE

II.1 Introduction

For a long time, wind energy has been a significant source of renewable energy. In recent years, the wind turbine industry has witnessed tremendous advancements in areas such as design, conversion technologies, and modeling. Understanding the types of wind turbines and the technology of converting wind energy into electrical power (WECS) is crucial for energy engineers and scientists in this field.

This chapter focuses on understanding the types of wind turbines and the developments in energy conversion technology, with an emphasis on modeling and reviewing Maximum Power Point Tracking (MPPT) methods.

In this study various types of wind turbines will be analyzed, including horizontal and vertical-axis forms, along with a review of power conversion techniques and necessary control mechanisms.

II.2 Wind turbines history

Wind turbines, which originated from the concept of windmills in ancient civilizations, made their modern debut in the late 19th century with the invention of the first electricity-generating wind turbine by Scottish engineer James Blyth in 1887. Since then, they have undergone significant technological advancements. Wind turbines are pivotal in electricity generation, particularly in the realm of renewable energy. By converting the kinetic energy of wind into electricity.

II.3 Types of wind turbines

There are two main types of wind turbines that differ essentially in their energy capture organ, namely the aero-turbine. Indeed, depending on the arrangement of the turbine with respect to the ground, a vertical axis or horizontal axis wind turbine is obtained [12].

a) Horizontal axis wind turbines

b) Vertical axis wind turbines

Figure II.1 Wind turbine technologies [13]

II.3.1 Vertical axis wind turbine

They were the first structures developed to produce electricity. Numerous technological variants have been tested, of which only two structures have reached the stage of industrialization, the Savonius rotor and the Darrieux rotor [12]. Nowadays, this type of wind turbine is rather marginal and its use is much less widespread. They have advantages and disadvantages that we can list as follows [12] [14].

- **Advantages:**

- The vertical design offers the advantage of placing the gearbox, generator, and control devices directly on the ground.

- Its vertical axis has a symmetry of revolution which allows it to function regardless of the wind direction without having to orient the rotor.

- Its design is simple, robust, and requires little maintenance.

- **Disadvantages:**

- They are less efficient than horizontal axis wind turbines.

- The vertical design of this type of wind turbine requires it to operate with wind close to the ground, therefore weaker due to being slowed down by the relief.

- Their installation on the ground requires the use of tie rods that must pass over the blades, thus occupying a larger surface area than tower wind turbines.

II.3.2 Horizontal axis wind turbines

These are currently the most widespread wind turbines, undoubtedly due to their remarkable advantages. They generally have two or three blades facing or downwind [12] [15].

- **Advantages:**

- A very small footprint compared to vertical axis wind turbines.
- This structure captures wind at a higher altitude, therefore stronger and more consistent than near the ground.
- The generator and control devices are in the nacelle at the top of the tower. Thus, it is not necessary to add a room for the equipment.

- **Disadvantages:**

- Very high construction cost.
- The equipment is located at the top of the tower, which hinders intervention in case of an incident.

After studying the nature of winds in Algeria, and considering their continuous change and variability, we decided in the study to use horizontal wind turbines; where these turbines are distinguished by their ability to harness wind currents from all directions, making them the optimal choice for generating energy efficiently and sustainably in this volatile atmospheric environment.

II.4 Wind energy conversion system WECS

II.4.1 Definition of WECS

WECS is a system that converts wind energy into another form of energy, such as electricity, that can be used to power homes and businesses [16].

II.4.2 WECS classification

Wind energy conversion systems are classified according to the type of rotational axis about which the turbine rotor blades rotate. The four main classifications of WECS are rotational axis, turbine, power control, and rotational speed control.

- **Rotational axis**

There are two types of rotational axis: horizontal and vertical [16].

1.*A horizontal axis wind turbine (HAWT)* is the most commonly used type. The rotor blades are mounted on a horizontal shaft perpendicular to the ground.

2.*A vertical axis wind turbine (VAWT)* has its rotor blades mounted on a vertical shaft parallel to the ground. VAWT is less common than HAWT because it is more expensive and complicated to build and is not as efficient in converting wind energy into electricity.

- **Turbine**

Turbines can also be classified by their electrical output. The size of the wind farm is determined by its production power. The current turbine system technology may be categorized into three groups based on the following [16]:

- Low Power turbines: These are turbine systems with a maximum output of 30 kW on average. These devices are used in distant areas to meet home electrical needs and charge batteries. They're also employed in emergencies to lessen reliance on primary power sources.
- Medium Power turbines: This category includes turbines with 30 to 300 kW outputs. They are, however, primarily utilized to provide electricity to houses in small communities. They are used with other renewable energy sources or power storage systems.
- High Power turbines: These are systems in which a considerable amount of power is produced. These are integrated into large-scale wind farms connected to the power systems that transmit electricity across towns

- **Power control**

The wind energy converted by the turbine must be managed appropriately to maintain a constant output of power. The two main ways to control power are active and reactive power control [16].

- Active power control is the most common type of power control, and it involves regulating the amount of wind that goes through the turbine blades. This is accomplished by using a pitch control mechanism, which regulates the angle of the blades.
- Reactive power control is less common, and it involves regulating the amount of electricity generated by the turbine. This is done using a generator, which converts mechanical energy into electrical energy.

- **Rotational speed control criteria**

The wind speed controls the speed of the turbine blades. The higher the wind speed, the faster the blades will spin. Two main ways to control the turbine's rotational speed are fixed speed and variable speed WECS [16].

1. Fixed speed WECS are the most common type, and they use a device called a governor to control the speed of the turbine. The governor is a mechanical device that is attached to the turbine blades. It prevents the blades from spinning too fast, damaging the turbine.
2. Variable speed WECS are less common, using an inverter device to control the turbine's speed. The inverter is an electronic device that converts direct current (DC) into alternating current (AC). It also regulates the speed of the turbine blades.

II.4.3 Components of WECS

A wind energy conversion system's major components are separated into two categories: mechanical and electrical [16].

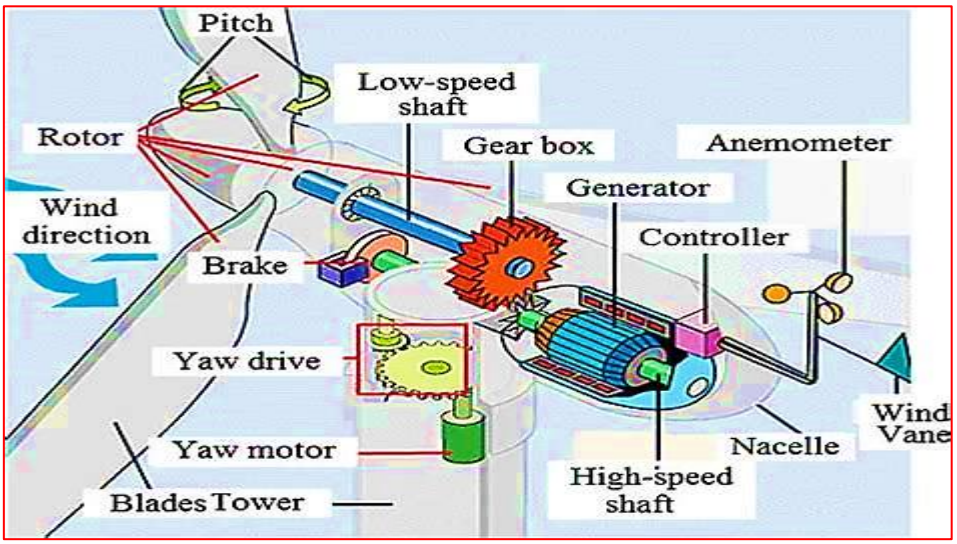

Figure II.2 Components of WECS

➢ **Mechanical components**

The mechanical components of a WECS include the rotor, the main shaft, gearbox, mechanical Brakes, nacelle, pitch and yaw drives, and wind measuring equipment.

- Rotor: It is the most important component of a WECS. It is a large wheel that has blades attached to it. The rotor is what captures the wind and turns it into mechanical energy.
- Main Shaft: The main shaft is the shaft attached to the rotor. It is made of steel or aluminum and connected to the gearbox.
- Gearbox: The gearbox is a device that increases the rotational speed of the rotor. It is made of gears, and it is located in the nacelle.
- Mechanical Breaks: Mechanical breaks are used to stop the rotor from spinning. They are located in the nacelle and activated when the wind speed is too high.

- Nacelle: The nacelle is the housing that contains all of the electrical and mechanical components of the WECS. It is located at the top of the turbine, and it is made of steel or aluminum.
- Pitch and Yaw Drives: Pitch and yaw drives are used to adjust the angle of the blades. They are located in the nacelle, and a computer operates them.
- Wind Measuring Equipment: Wind measuring equipment is used to measure wind speed and direction. It is located in the nacelle and consists of anemometers and wind vanes.

➢ **Electrical components**

The electrical components of a WECS include the generator, power converter, step-up transformer, and wind farm collection points or points of common coupling.

- Generator: A device that converts mechanical energy into electrical energy. It is located in the nacelle and is connected to the main shaft.
- Power Converter: The power converter is a device that converts DC into AC. It is located in the nacelle, connected to the generator.
- Step-up Transformer: The step-up transformer is a device that increases the voltage of the electricity. It is located in the nacelle, connected to the power converter.
- Wind Farm Collection Points or Point of Common Coupling: Are used to collect the electricity from the turbines. They are located at the turbine's base, and they are connected to the power converter.

II.5 Technology of wind turbine system

Constant-speed wind turbine system

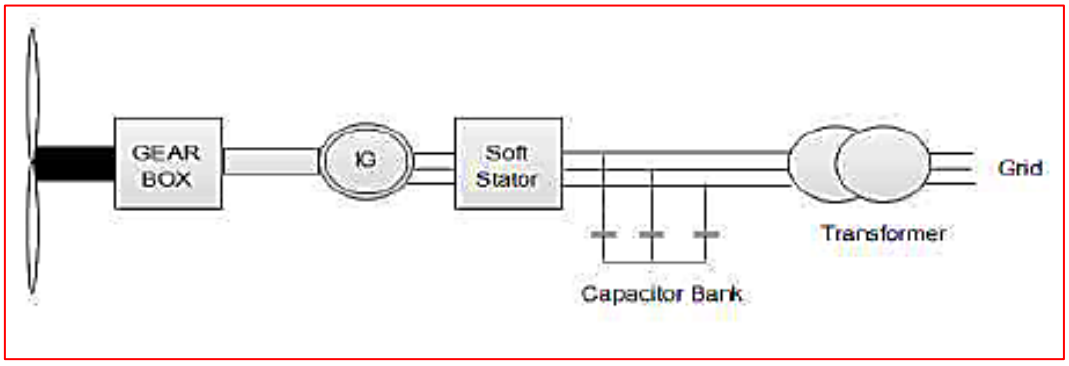

Figure II.3 Schematic Diagram for Fixed speed Wind Turbine

- **Variable-speed wind turbine system**

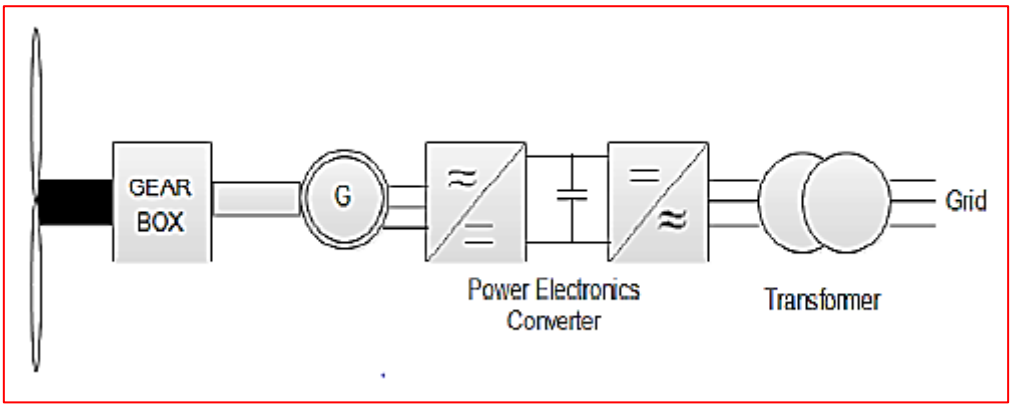

Figure II.4 Schematic Diagram for Variable-speed Wind Turbine

- **Variable-speed wind turbine with doubly-fed induction generator**

The diagram, as indicated in Figure II.5, involves a DFIG wind turbine. In this scheme the stator is directly connected to the grid and the rotor is connected to the grid through a converter. This scheme requires converter of lesser rating since the converter handles 20% -30% of total power. So power losses in the converter will be less, comparing to other various types of wind system. So cost of converter is less. Grid side converter is used to maintain dc-link voltage constant and rotor side converter is used to control power flow through rotor at different rotor speed [17].

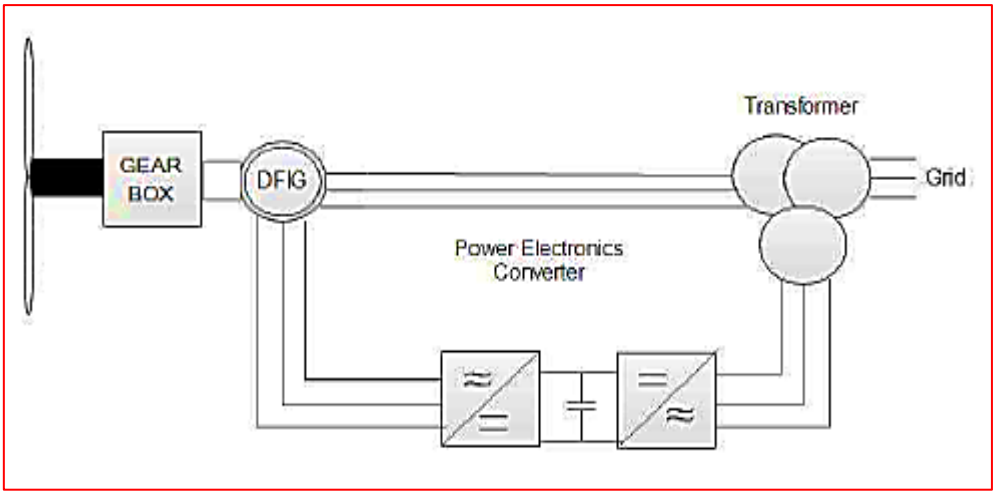

Figure II.5 Schematic diagram for Doubly-fed Wind Turbine

Doubly-fed induction generator systems for wind turbines

The scheme shown below is used for variable speed operation about thirty percent of synchronous speed .20-30% of the total power flowing through grid or vice versa is controlled by power electronic converter. The power factor of the overall system will be one.

The converters are controlled by PWM Pulse generators.

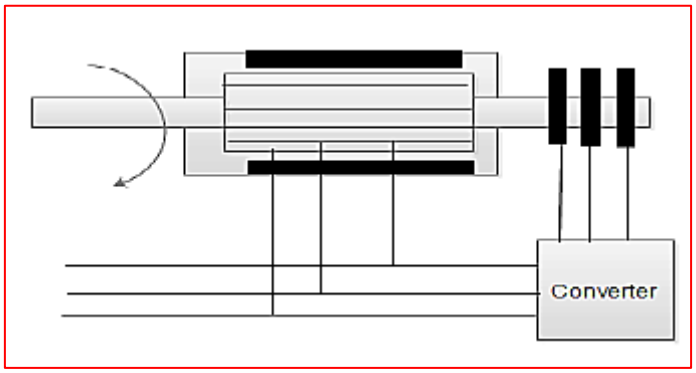

Figure II.6 Doubly-Fed Induction Generator Principle

The converters are connected in back-to-back fashion with a transformer to the grid that includes two converters. In between the two converters a dc capacitor is connected, to keep the voltage variances (or swell) in the link voltage to a minimum quantity.

II.6 Modeling and reproduction of wind variations

II.6.1 Wind definition

Wind is an air current that forms when air from a high-pressure area moves towards a low-pressure area. It is also defined as a velocity field of air mass movement and serves as the primary energy vector for a wind turbine system, thus constituting the primary energy source for electricity production calculations. The dynamic properties of wind are crucial for studying the entire energy conversion system.

II.6.2 Wind speed modeling

Wind cannot be represented solely by deterministic expressions. Modeling wind is not straightforward due to spatial variations ranging from kilometers to centimeters and temporal variations from seconds to months. The Van der Hoven spectrum exhibits three remarkable events (Figure II.7): Several energy peaks for low frequencies around a year (seasonal variation), 4 days (climate variation), and one day (daily variation), which are clearly associated with large-amplitude atmospheric motion [18].

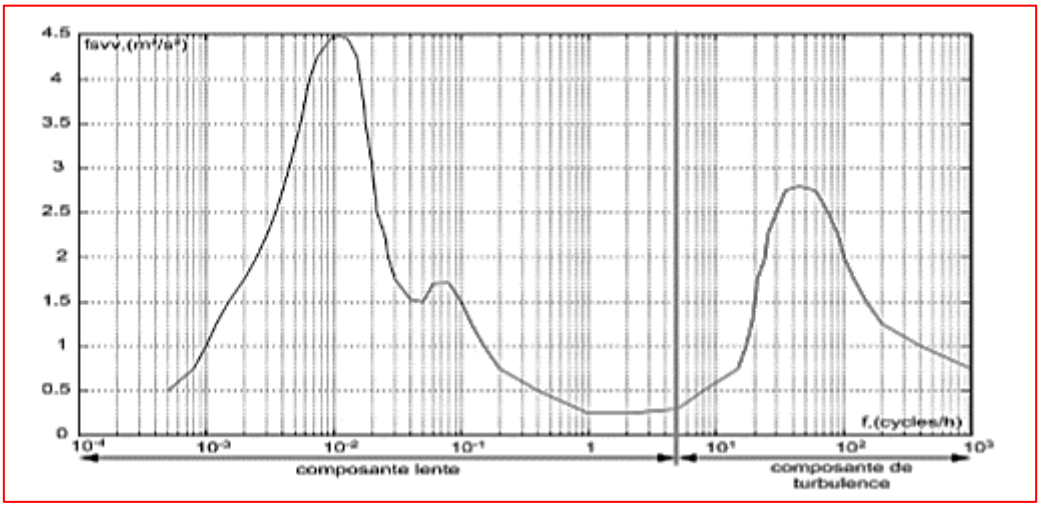

Figure II.7 Energy Spectrum of Atmospheric Motions according to Van der Hoven [19]

The discretization of the curve in the above figure into pulsations, along with the corresponding power, allows for the extraction of the amplitude of each spectral component associated with these pulsations.

$$A_i = \frac{2}{\pi}.\sqrt{S_i} \qquad \textbf{(II.1)}$$

Thus, the variation of wind speed $V_w(t)$ is expressed using the sum of harmonics corresponding to each pulsation W_i with a phase φ_i determined randomly.

$$V_w(t) = \sum_{i=1}^{N} A_i \,.\cos(\omega_i + \varphi_i) \qquad \textbf{(II.2)}$$

With N being the number of discrete values used for sampling.

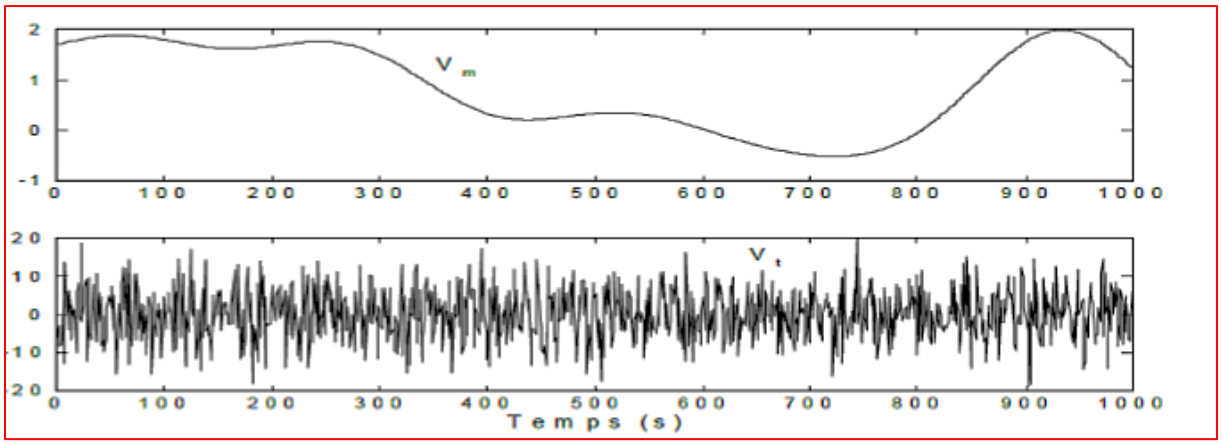

Figure II.8 Slow Component and Turbulence Component of Wind Speed [19]

Wind speed exhibits two components: a slow component corresponding to the average wind speed and a fast component known as turbulence that superimposes on this average speed. Figure II.8 depicts the evolution of these two components over 1000 seconds.
Thus, it can be observed that regardless of the average wind speed, the turbulence component possesses the same statistical properties [19].

Mathematically, wind speed is a three-dimensional vector. To perform various simulations of our system, we need to have a wind profile corresponding to what can be found at a wind site.

In this study, we represented the evolution of wind speed deterministically, by summing several harmonics described as follows:

$$V_w(t) = 5 + 0.05\sin(0.1047t) + 0.5\sin(0.2665t) + 0.25\sin(1.2930t) + 0.05\sin(3.6645t) \quad \textbf{(II.3)}$$

The temporal evolution obtained after simulating this equation is as follows:

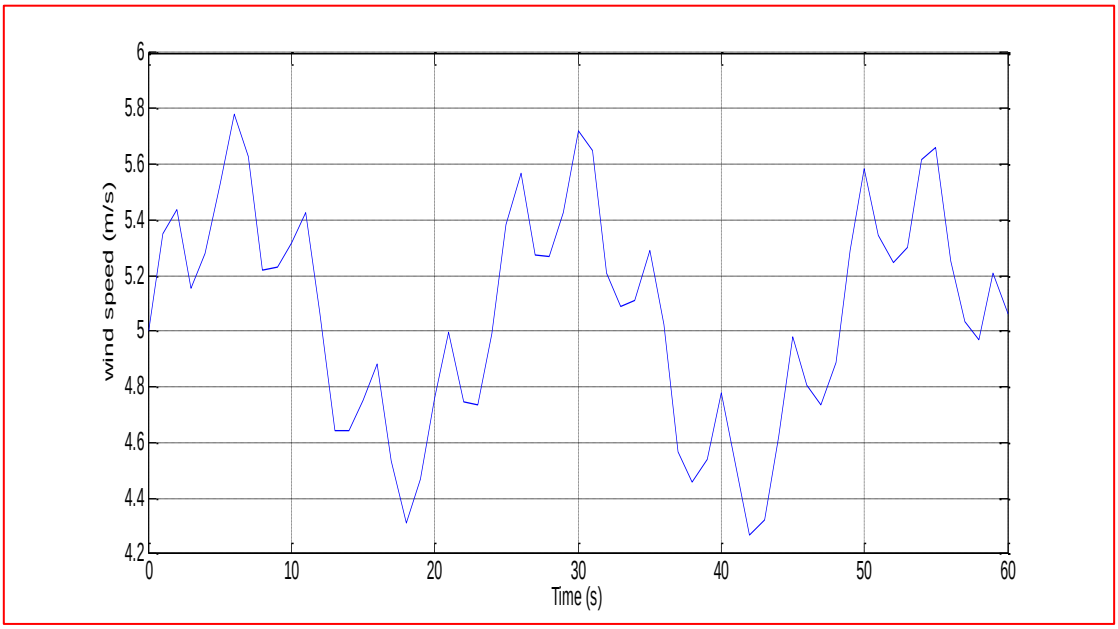

Figure II.9 Modeled Wind Profile

II.7 Modeling of the turbine

II.7.1 Simplifying assumptions for turbine modeling

Let's consider a wind turbine with three fixed blades of length *R* fixed on the turbine shaft, forming a mechanical block capable of rotating at a speed $\Omega_{turbine}$ thanks to the wind energy, which is also connected to a gearbox. In general, the turbine shaft is connected to a speed

multiplier, which in turn is connected to the generator shaft and drives it. This allows us to deduce that each part of this assembly is subject to three constraints: its own inertia, friction, and elastic stress, as illustrated in Figure II.10.

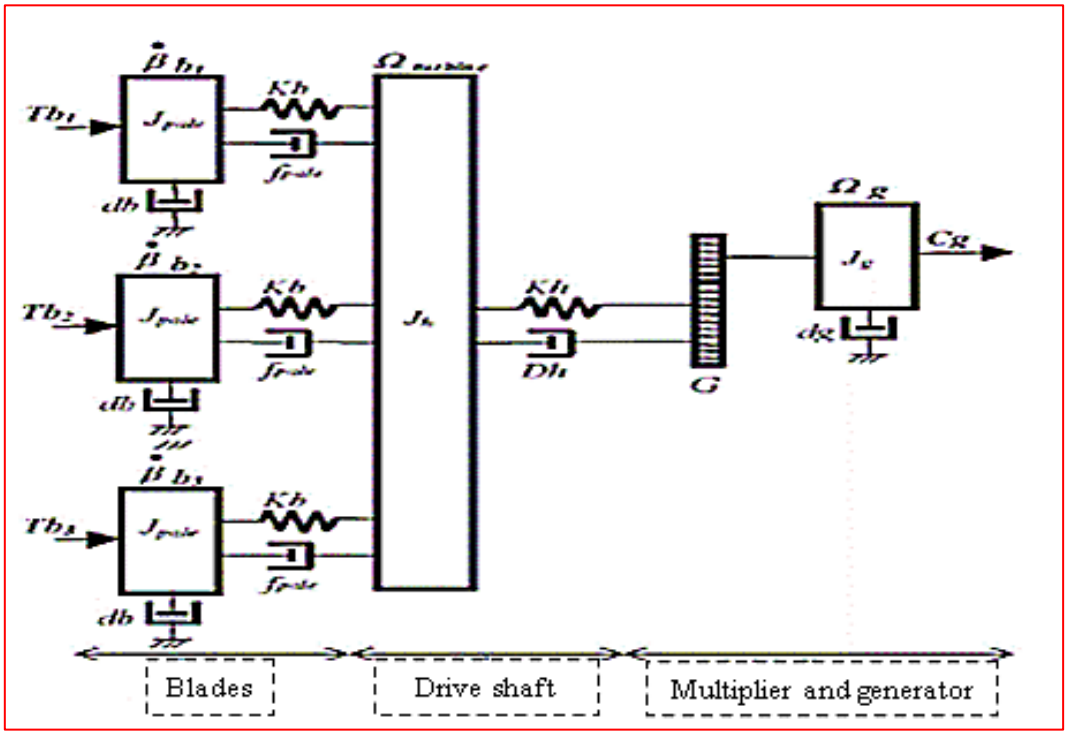

Figure II.10 Equivalent Mechanical Diagram of a Wind Turbine [20]

The three blades are considered to be of identical design and are characterized by:

- An inertia J_{blade}

- a friction coefficient f_{blade}

- elasticity K_b

These blades have the same friction coefficient f_{blade}, and the orientation speed of each blade is noted β_{b1}, β_{b2}, β_{b3}.Each blade receives a force T_{b1}, T_{b2}, T_{b3}which depends on the wind speed applied to it.

The drive shaft of the blades is characterized by:

- its inertia J_h

- its elasticity K_h

- its friction coefficient with respect to the multiplier D_h

The generator rotor also has its own characteristics:

- an inertia J_g

- a friction coefficient D_g

This rotor transmits a torque T_g to the electrical generator and rotates at a mechanical speed Ω_g. If we consider a uniform distribution of wind speed on all blades and thus an equality of all thrust forces, then we can consider the assembly of the three blades as a single mechanical system characterized by the sum of all mechanical characteristics. Similarly, since the turbine speed is low, friction losses are negligible compared to friction losses on the generator side. We thus obtain a mechanical model consisting of two rotating masses thanks to the aerodynamic torque T_{aer}, as explained in Figure II.11[21].

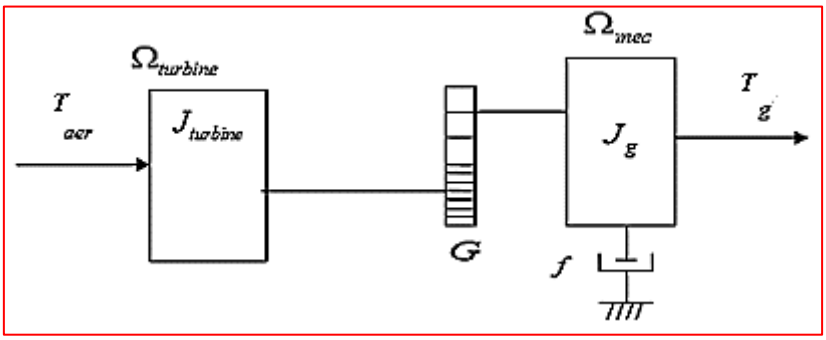

Figure II.11 Simplified Diagram of the Wind Turbine [21]

II.7.2 Mechanical equation of the wind turbine

II.7.2.1 Turbine modeling

Various types of power coefficient modeling can be found in the literature, often limited by input data and generally valid for a particular turbine: each turbine has a specific behavior [22].

For our study, we will use a 3 kW wind turbine. It is a horizontal-axis, three-blade model with a blade length of 4.5m and a speed multiplier ratio of 24 [22].

Formula (II.4) illustrates the evaluation of the power coefficient C_p, which depends on the aerodynamic characteristics of the turbine under study, as well as its operating conditions. The coefficient C_p is then expressed as a function of the speed ratio λ and the blade pitch angle β. The variations of C_p in our case are modeled by the following polynomial approximation:

$$C_p(\lambda) = -0.0003243\lambda^6 + 0.01174\lambda^5 - 0.1573\lambda^4 + 0.9072\lambda^3 - 1.942\lambda^2 + 1.713\lambda - 0.08196 \quad \textbf{(II.4)}$$

The speed ratio is defined as the ratio between the speed of the blades and the wind speed, as follows: (Figure II.12)

$$\lambda = \frac{\Omega_t R}{v_W} \quad \textbf{(II.5)}$$

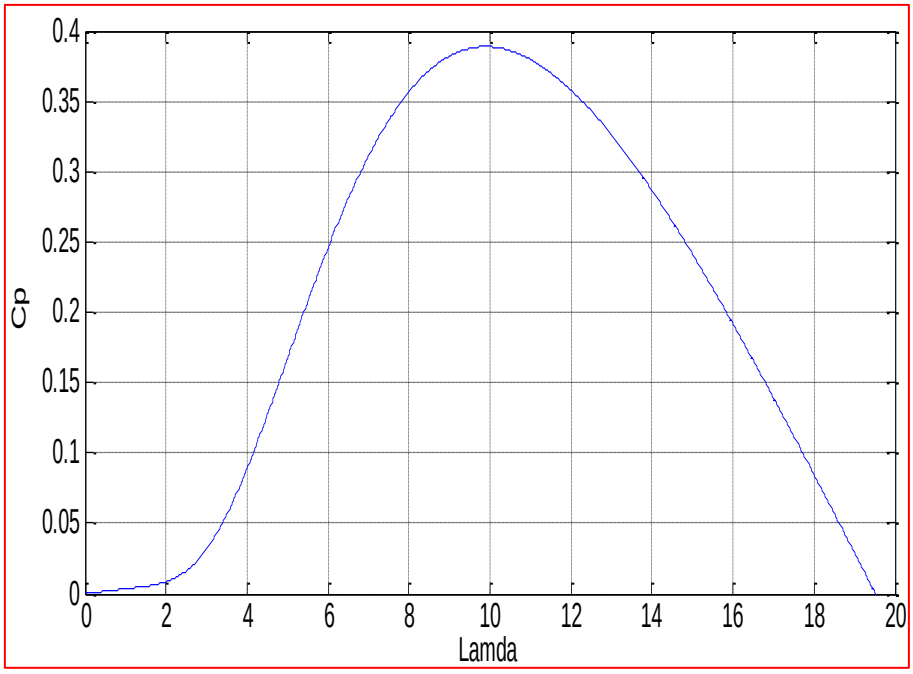

Figure II.12 Power coefficient as a function of turbine speed ratio (lamda)

The wind speed v_w applied to the wind turbine blades causes them to rotate and generates mechanical power on the turbine shaft, denoted as P, which is expressed by the formula:

$$P_t = \frac{1}{2} C_p(\lambda).\rho.S.v_w^3 \quad \textbf{(II.6)}$$

Given the rotational speed of the turbine and the available mechanical power, the available mechanical torque on the turbine shaft is expressed by the following formula:

$$C_t = \frac{P_t}{\Omega_t} = \frac{1}{2\lambda}\rho\pi R^3 v^2 C_p(\lambda,\beta) \quad \textbf{(II.7)}$$

The power coefficient Cp symbolizes the aerodynamic efficiency of the wind turbine. In the literature, several methods of modeling the power coefficient are available, and each turbine has its own behavior, conditioned by input data that are generally specific to a particular turbine. However, the shape of the curves remains constant.

The power coefficient used in our study is defined by the following expression:

$$C_p(\lambda,\beta) = C_1.C_2.\frac{1}{\lambda} - C_3.\beta - C_4.e^{\frac{-C_5}{\lambda}} + C_6.\lambda \quad \textbf{(II.8)}$$

With

$$\frac{1}{\lambda} = \frac{1}{\lambda+0.08\beta} - \frac{0.035}{\beta^3+1} \quad \textbf{(II.9)}$$

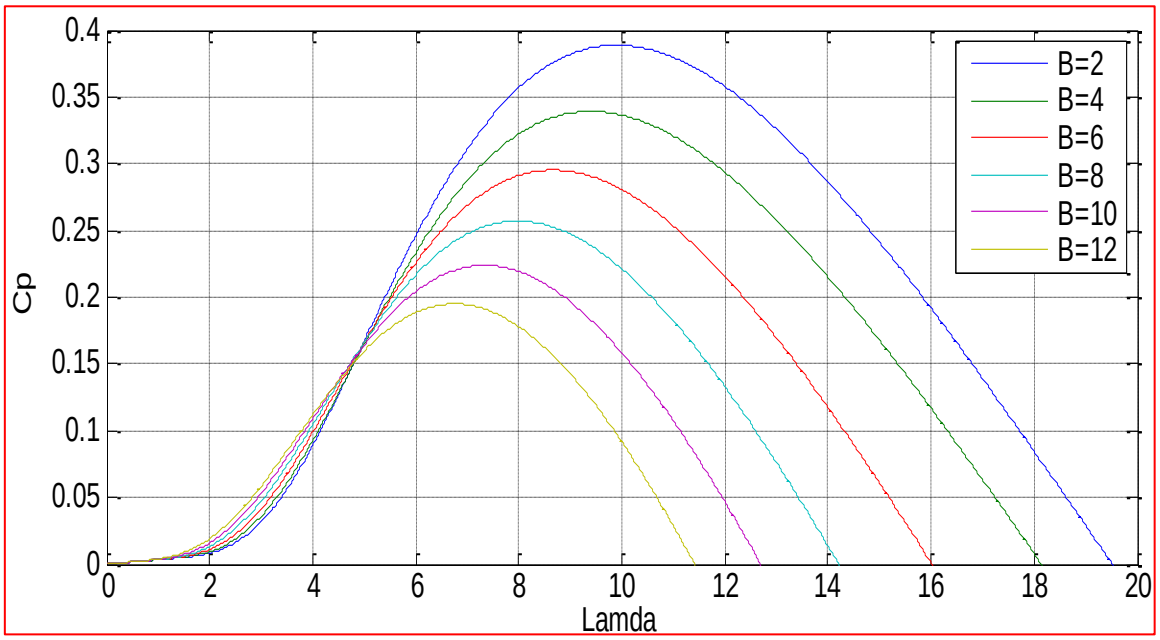

Figure II.13 Power coefficient as a function of turbine speed ratio λ for different Valeur of blade pitch angle β

II.7.2.2 Gearbox selection

The speed multiplier, which is positioned between the wind turbine and the generator, has the role of adapting the slow mechanical speed of the turbine Ω_m to the rapid rotation speed of the generator Ω_g. Assuming the multiplier is ideal (i.e., mechanical losses are negligible), this multiplier is mathematically modeled by the following equations [23]:

$$G = \frac{T_t}{T_g} \quad \textbf{(II.10)}$$

$$G = \frac{\Omega_g}{\Omega_t} \quad \textbf{(II.11)}$$

II.7.3 Mechanical shaft equations

In the previous study, we observed that the mechanical model of the wind turbine consists of two masses, the turbine, and the generator. These two masses can be summarized in the form of a single shaft (the generator shaft), while still accounting for the friction and inertia of the wind turbine to the wind generator rotor.

The mass of the wind turbine is represented on the turbine shaft in the form of an inertia $J_{turbine}$, which includes the mass of the blades and the mass of the turbine rotor. The proposed mechanical model considers the total inertia J_T, consisting of the turbine inertia transferred to the generator rotor and the inertia of the generator [19].

This same mechanical model will be characterized by the total friction coefficient F_T, which includes both the turbine friction transferred to the generator rotor and that of the generator. The equivalent mechanical model (single shaft) is illustrated in Figure II.14:

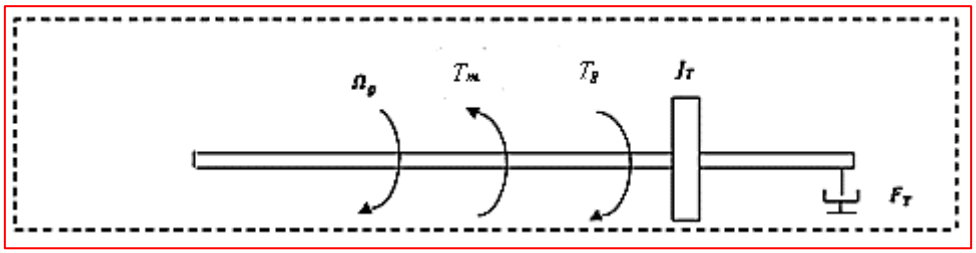

Figure II.14 Simplified Mechanical Model of Turbine

II.7.3.1 Mechanical equation on the generator shaft

The fundamental equation of dynamics for the mechanical system on the machine's mechanical shaft is as follows:

$$\left(\frac{J_t}{G^2} + J_m\right).\frac{d\Omega_m}{dt} + f_m\Omega_m = T_m - T_{em} \quad \textbf{(II.12)}$$

With:

- J_t: Moment of inertia of the turbine.
- J_m: Moment of inertia of the machine.
- f_m: Friction coefficient of the machine.
- T_m: Mechanical torque on the machine shaft.
- Ω_m: Machine rotation speed.
- T_{em}: Electromagnetic torque of the machine.

The simplified fundamental equation of dynamics of the system, which allows us to determine the evaluation of the mechanical speed from the available driving torque Tm on the generator rotor, is then written as follows [20]:

$$J_T.\frac{d\Omega_g}{dt} + f_T\Omega_G = T_g - T_{em} \quad \textbf{(II.13)}$$

✓ **Equation of J_T and F_T:**

The expression of the total equivalent inertia J_T of the wind system as seen from the generator rotor is composed of the turbine inertia J_T, which includes the three blades, the multiplication coefficient G, and the inertia of the generator J_m.

$$J_T = \left(\frac{J_t}{G} + J_m\right) \quad \textbf{(II.14)}$$

Similarly, the expression for the total friction coefficient F_T of the wind system consists of friction losses in the turbine and friction losses in the generator. Thus, we find that:

$$f_T = \left(\frac{f_t}{G^2} + f_m\right) \quad \textbf{(II.15)}$$

II.8 Method for finding the maximum power point (MPPT)

In this section, we will present three controls strategies for the wind turbine:

- Control without speed feedback
- Control with speed feedback using PI controller
- Control with speed feedback using fuzzy controller

In these strategies controls, we need to control the electromagnetic torque in order to follow the maximum efficiency. The system must find the maximum power, which is equivalent to searching for the optimal rotational speed. The diagram in the following figure illustrates the characteristic of the wind turbine for different variation speed plane.

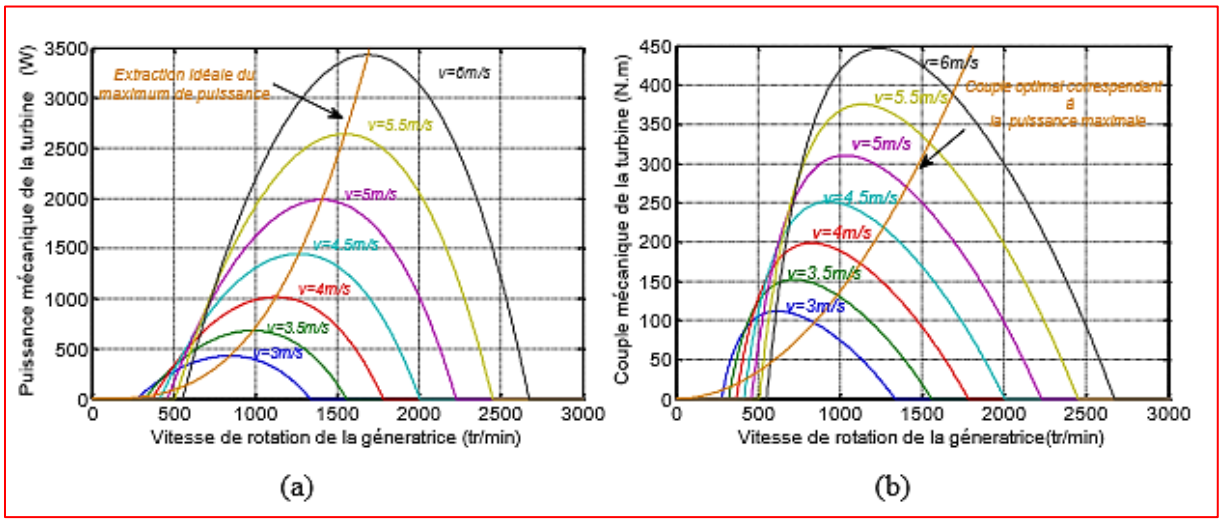

(a) Extraction of the maximum power from the wind turbine,

(b) Optimal turbine torque

Figure II.15 Extraction of the maximum power [21]

II.8.1 Maximum power point tracking (MPPT) without control

The method for maximizing power without speed feedback is illustrated in Figure (II.7). It is derived from the expressions of the aerodynamic and mechanical equations of the wind turbine at the operating point related to a maximum Cp. The use of wind turbine control without speed feedback has become a necessity for most manufacturers.

This method is based on the assumption that the wind speed, and consequently the rotational speed of the turbine, vary very little in steady-state conditions, which leads us to deduce that:

- The mechanical torque exerted on the shaft is considered zero $\boldsymbol{Tmec} = \mathbf{0}$.

- The resisting torque due to friction can be neglected $\mathbf{Tf} \approx \mathbf{0}$.

When the wind turbine operates at the optimal operating point, then:

$$\lambda_{opt} = \frac{R\Omega_{tur}}{V} \ , C_p = C_{p-max} \quad \textbf{(II.16)}$$

The dynamic behavior of the turbine is thus described by the static equation:

$$T_{opt} = T_g - T_{em} - T_f = T_g - T_{em} = 0 \quad \textbf{(II.17)}$$

The equation (II.17) gives:

$$T_{em} = T_g = T_{aer} = 0 \quad \textbf{(II.18)}$$

The reference electromagnetic torque is determined from an estimation of the aerodynamic torque:

$$T_{em-ref} = T_{aer-ref} \quad \textbf{(II.19)}$$

The estimated aerodynamic torque is determined by the expression:

$$T_{em-ref} = \frac{1}{2} C_p . \rho . s . \frac{1}{\Omega_{tur-est}} V_{estime}^3 \quad \textbf{(II.20)}$$

$\Omega_{Tur-est}$: is the estimated turbine speed, calculated from the measurement of the mechanical speed:

$$\Omega_{tur-est} = \Omega_{mec} \quad \textbf{(II.21)}$$

V_{estime}: is the estimated value of the wind speed, it can be given by the expression:

$$V_{estime} = \frac{\Omega_{tur-est} . R}{\lambda} \quad \textbf{(II.22)}$$

Using the formulas from (II.20) to (II.22), we obtain an overall expression for the reference electromagnetic torque:

$$T_{em-ref} = \frac{1}{2} \frac{C_p}{\lambda^3} . \rho . \pi . R^5 . \Omega_{mec}^2 \quad \textbf{(II.23)}$$

To maximize the extracted power, we associate the optimal value of λ, denoted λ_{opt}, with the maximum of the power coefficient C_{p-max}. The value of the reference electromagnetic torque is then adjusted to the following maximum value:

$$T_{em-ref} = \frac{1}{2} \frac{C_{p-max}}{\lambda_{opt}^3} . \rho . \pi . R^5 . \Omega_{mec}^2 \quad \textbf{(II.24)}$$

The block diagram of the turbine model is represented as follows:

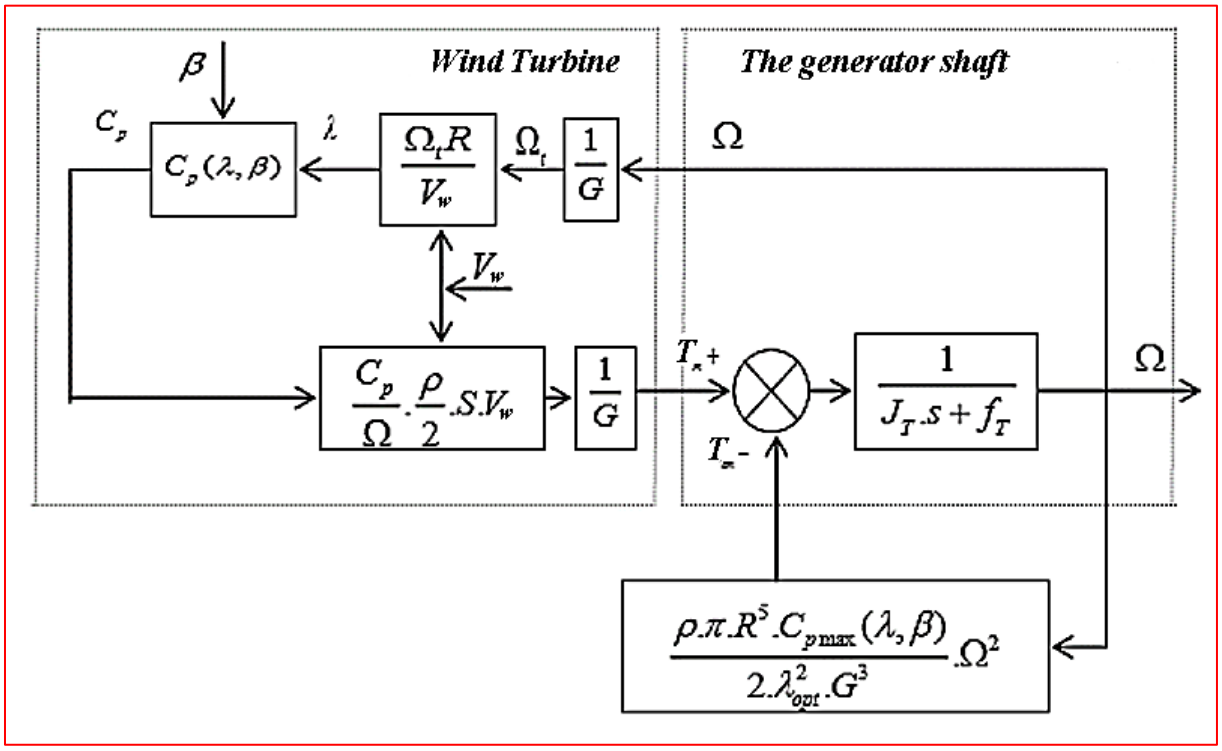

Figure II.16 Block diagram of the turbine with MPPT without control

II.8.2 Maximum power point tracking (MPPT) with speed control

This control strategy involves adjusting the torque on the turbine shaft to set its speed to a reference value. To achieve this, speed feedback control is utilized. The speed controller must accomplish two tasks:

- It must regulate the mechanical speed to its reference value.
- It must mitigate the effect of wind torque, which acts as a disturbance input.

In this section, we have proposed two types of controllers: PI controllers and a fuzzy controller, to achieve this objective.

II.8.2.1 Using PI controller

This control approach requires the use of a PI controller for speed regulation. We conducted simulations of the turbine using the equations provided earlier. The simulation conditions are as follows:

- Cp−max = 0,46: This is the maximum power coefficient.
- λ= 8,22: This is the maximum relative speed.

The simulation setup should enable speed control to maintain the maximum values of Cp an λ regardless of wind speed. For this purpose, we will use a speed controller, specifically a PI controller.

The block diagram of the turbine model is depicted in Figure (II.17).

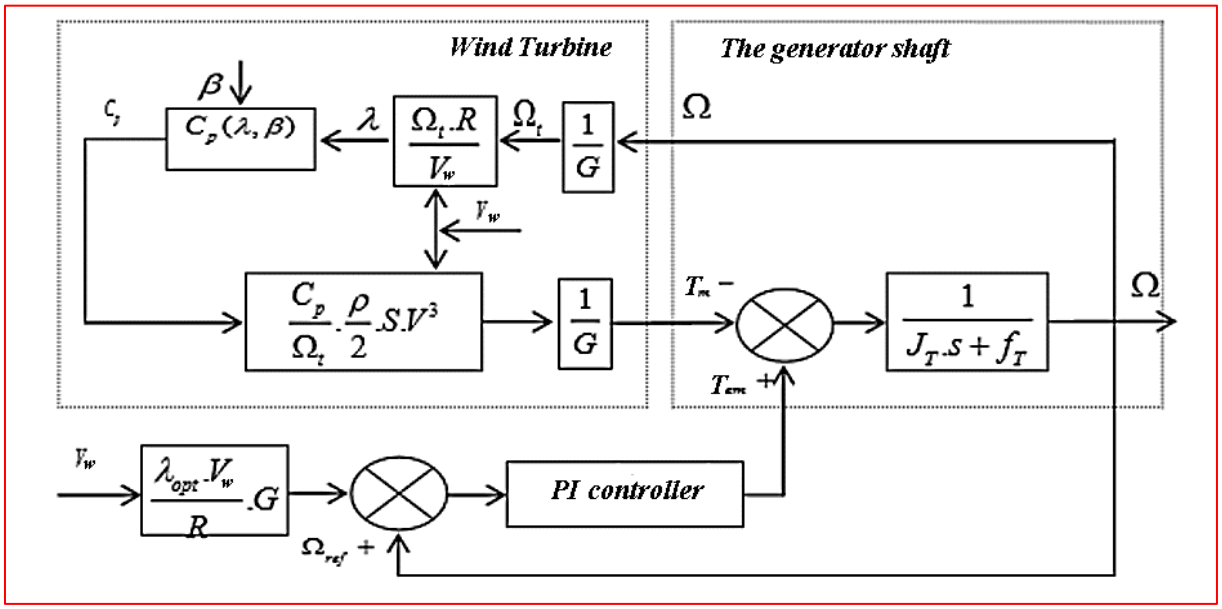

Figure II.17 Block diagram of the turbine with MPPT using a PI controller

- **PI controller**

Effect of the controller:

- Increase in phase margin (as indicated by the name of the controller).
- Increase in bandwidth (increase in speed c with decreases in tr).
- Imposed steady-state errors.
- Increase in stability margin -----> derivative effect.

- **Calculation of the turbine speed controller:**

The functional diagram of the speed control is given by:

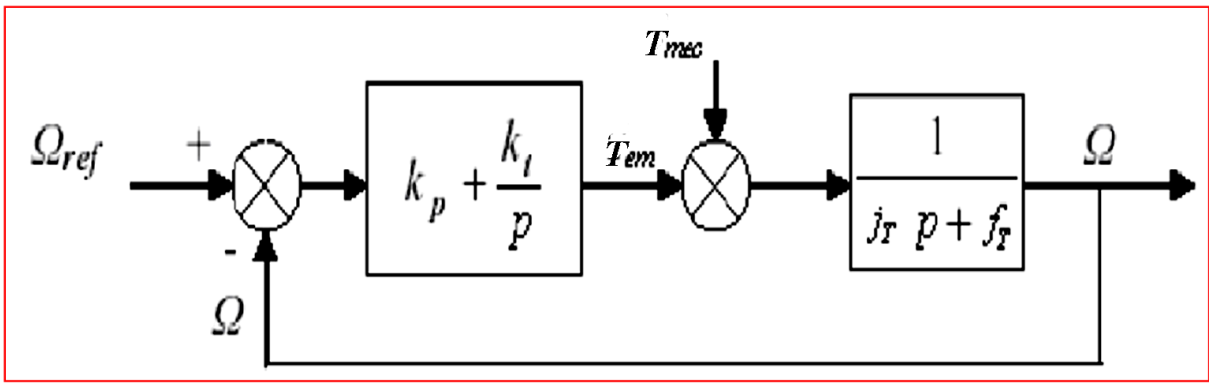

Figure II.18 Speed Regulation

The reference electromagnetic torque is obtained through the action of a PI controller on the difference between the reference speed and the rotational speed. The transfer function describing this action is given by:

$$T_{em-ref} = C(P)(\Omega_{tur-ref}(P) - \Omega_{mec}(P)) \quad \textbf{(II.25)}$$

$$T_{em-ref} = (K_p + \frac{K_i}{P})(\Omega_{tur-ref}(P) - \Omega_{mec}(P)) \quad \textbf{(II.26)}$$

Kp: The proportional gain.

Ki: The integral gain.

Since the studied system is linear, we can write, by virtue of the superposition theorem, the transfer function in the following form:

$$\Omega_{mec}(p) = F(p).\Omega_{ref}(p) - P(p).T_{mec}(p) \quad \textbf{(II.27)}$$

$$F(p) = \frac{p}{j.P^2+(f+K_p)P+K_i} \quad \textbf{(II.28)}$$

$$P(p) = \frac{K_p p+K_i}{j.P^2+(f+K_p)P+K_i} \quad \textbf{(II.29)}$$

We assume that the disturbance is zero:

$$T_{mec} = 0 \quad \textbf{(II.30)}$$

The transfer function will then be written as follows:

$$\Omega_{mec} = F(p).\Omega_{ref}(p) \quad \textbf{(II.31)}$$

The transfer function has a second-order dynamics. By identifying it with the canonical form of the second order, the characteristic equation can be represented as follows:

$$\frac{1}{\omega_0^2}P^2 + \left(\frac{2\xi}{\omega_0}\right)P + 1 \quad \textbf{(II.32)}$$

Then,

$$\frac{J_T}{K_i} = \frac{1}{\omega_0^2} \quad \textbf{(II.33)}$$

$$\frac{f+K_P}{K_i} = \frac{2\xi}{\omega_0} \quad \textbf{(II.34)}$$

Then,

$$K_i = J_t.\omega_0^2 \quad \textbf{(II.35)}$$

$$K_p = \frac{2.\xi K_i}{\omega_0} - f_t \quad \textbf{(II.36)}$$

ξ: Damping coefficient.

To obtain the optimal response, we choose the damping coefficient ξ=0.7. The 5% settling time is given by:

$$t_T = \frac{3}{\xi\omega_0} \quad \textbf{(II.37)}$$

We take half of the time constant τ_m to ensure the speed of the controller, with:

$$\tau_m = \frac{j_t}{f_t} \quad \textbf{(II.38)}$$

τ_m: Time constant of the system to be controlled.

Then,

$$\omega_0 = \frac{3}{\xi(\tau_m/2)} \quad \textbf{(II.39)}$$

Finally, using the pole placement method, we can ultimately deduce the values of Ki and Kp.

II.8.2.2 Using FUZZY controller

This control requires the use of a fuzzy controller for speed control. Therefore, we proceeded with the simulation of the turbine by replacing only the PI controller with a fuzzy controller, while keeping the simulation conditions the same:

- Cp−max = 0,46: This is the maximum power coefficient.
- λ= 8,22: This is the maximum relative speed.

The block diagram of the turbine model is represented in Figure (II.19).

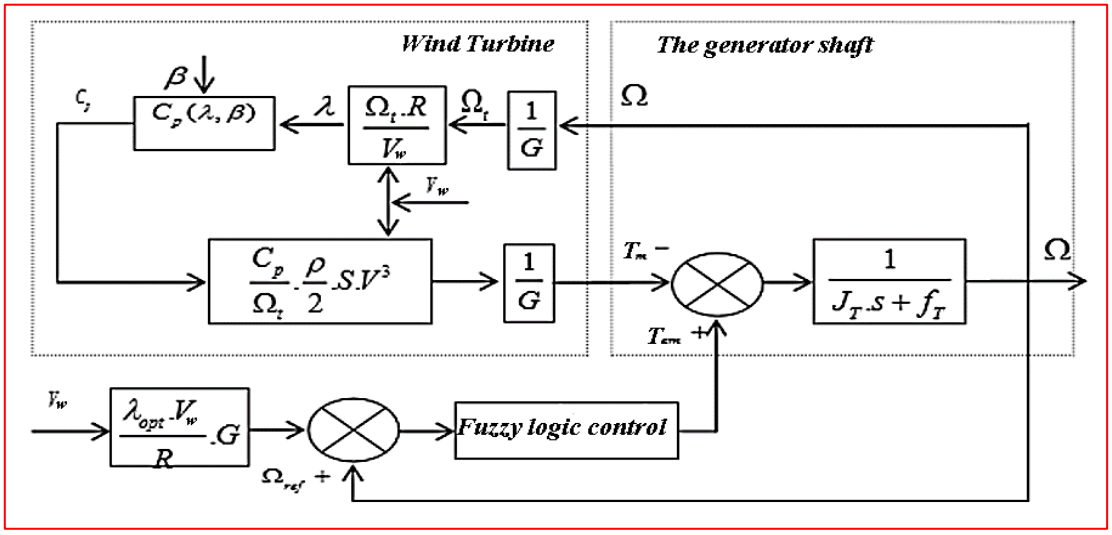

Figure II.19 Block diagram of the turbine with MPPT based on a fuzzy controller

Fuzzy controller

Until now, conventional controllers remain widely used in industrial applications. About 90% of industrial controllers are PI and PID controllers [24]. The remaining portion consists of dedicated control systems based on various advanced control techniques. The simplicity of the PI controller, its ease of operation, its good performance under certain conditions, and its cost are the main advantages of its use. To address regulation problems in transient regimes, in the face of system parameter variations, it is known that the fuzzy controller provides effective solutions. Particularly in the case of the presence of nonlinear dynamics in the system. In this context, the different structures of developed fuzzy controllers are represented.

The fuzzy logic controller is therefore composed of four basic elements:

- Fuzzification
- Fuzzy inference engine
- Knowledge base (rules)
- Defuzzification

Application of fuzzy speed controllers

The basic scheme of the fuzzy controller relies on the structure of an incremental controller (Figure II.19). Observing the process shows that the significant quantities for control are the speed error and its variation. Therefore, for the inputs of the fuzzy controller, these two characteristic quantities denoted as e and Δe are adopted. The output of the controller will be the speed increment Ω_{mec} It is sufficient to integrate this quantity to obtain the reference speed Ω_{-ref}.

The two inputs of the fuzzy controller are the speed error and its variation.

The speed error denoted as e is defined by:

$$e = \Omega_{-ref} - \Omega_{mec} \quad \textbf{(II.40)}$$

The variation of the speed error, denoted as Δe, is defined by:

$$\Delta e = (t + \Delta t) - e(t) = e(k+1) - e(k) \quad \textbf{(II.41)}$$

In the input and output of the fuzzy controller, we find gains called "adaptation gains" or normalization gains defined by:

$$\begin{cases} E = K_e e \\ \Delta E = K_{\Delta e} \Delta e \\ \Delta U = K_{\Delta u} \Delta u \end{cases} \quad \textbf{(II.42)}$$

The output of the controller corresponds to the control variation denoted as Δu.

Fuzzification:

We introduce, for the input and output variables of the fuzzy logic controller (FLC), seven sets represented by triangular-shaped membership functions. Except for the endpoints where trapezoidal shapes are used.

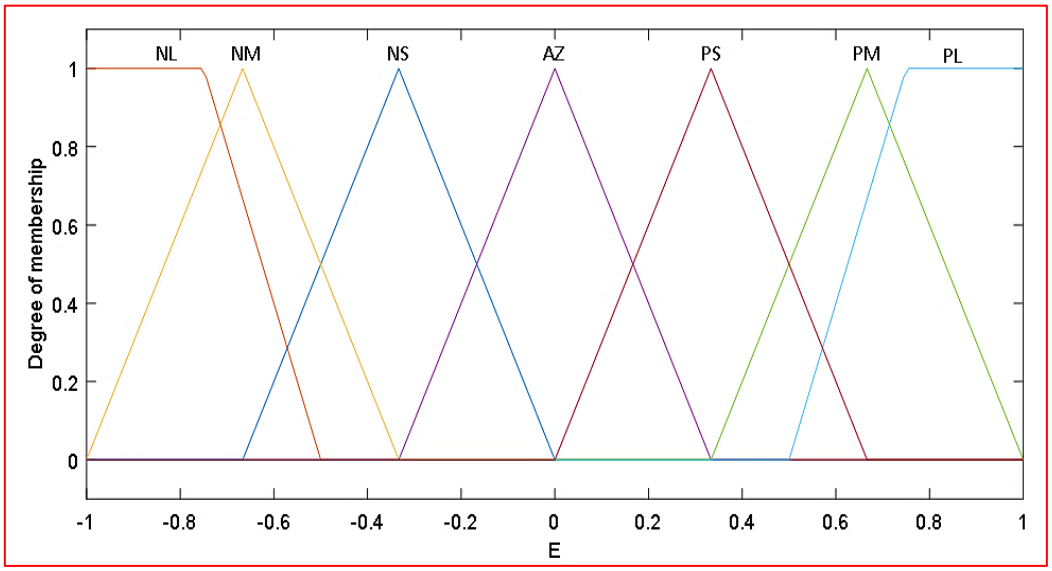

a) Error

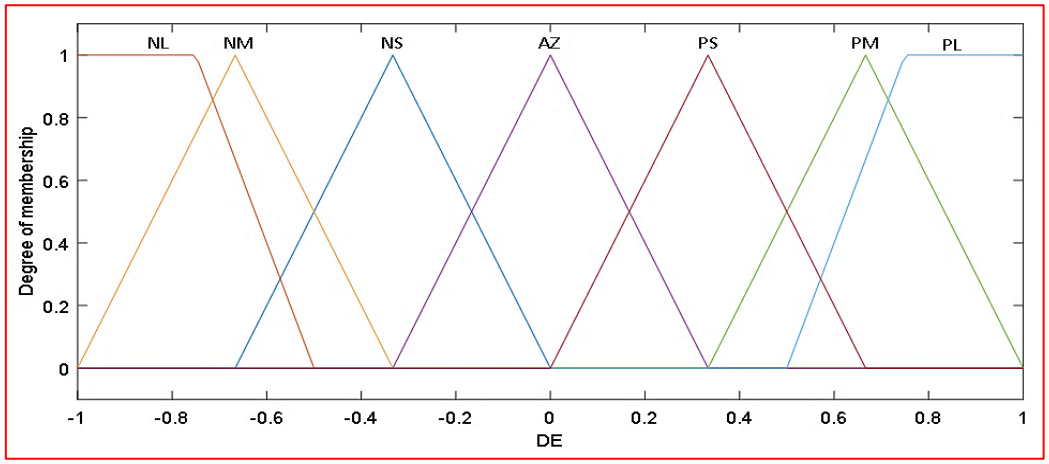

b) Error derivative

Figure II.20 Membership functions of the input's variables

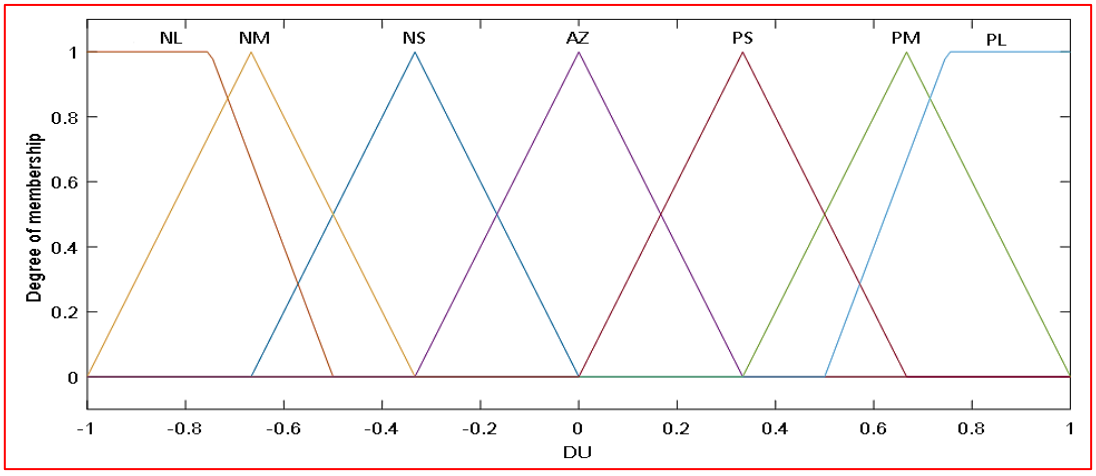

Figure II.21 Membership functions of the output variables

- **Rule base**

The rule base represents the control strategy and the desired goal through linguistic control rules [24]. It allows determining the decision or action at the output of the fuzzy controller and qualitatively expressing the relationship between the input variables and the output variable. From the study of the system behavior, we can establish control rules that relate the output to the inputs. As mentioned, each of the two linguistic inputs of the fuzzy controller has seven fuzzy sets, resulting in a set of 49 fuzzy rules. These rules are represented in a matrix called "inference matrix" (Table II.1).

Table II.1 Inference Matrix

DE \ E	**NL**	**NM**	**NS**	**AZ**	**PS**	**PM**	**PL**
NL	NL	NM	NL	NL	NM	NS	AZ
NM	NL	NM	NL	NM	NS	AZ	PS
NS	NL	NS	NM	NS	AZ	PS	PM
AZ	NL	NS	NS	AZ	PS	PM	PL
PS	NM	NM	AZ	PS	PM	PL	PL
PM	NS	AZ	PS	PM	PL	PL	PL
PL	AZ	PS	PM	PL	PL	PL	PL

According to this matrix, we can define the 49 rules, for example:

Rule 1: If E is NL and DE is NL then U is NL

- **Inference mechanism**

For the numerical processing of inferences related to the fuzzy controller, we have adopted the "MAX-MIN" method of Mamdani:

- AND operator: minimum formation,
- OR operator: maximum formation,
- IMPLICATION operator: minimum formation,
- Aggregation: maximum formation.

- **Defuzzification**

The defuzzification step is the final step in designing a fuzzy controller. When the fuzzy output is computed, it needs to be transformed into a numerical value. There are several methods

to perform this transformation. The most commonly used method is the centroid method, which we have adopted in our work.

II.9 Simulation and discussion results

We will illustrate the simulation results of wind turbine control with and without control speed feedback.

II.9.1 Simulation results for MPPT without control

This simulation section involves keeping the same wind profile (variable wind speed). The results obtained after simulation are illustrated in the following figures. According to these figures, it can be observed that the turbine shows good adaptation to variations in wind speed. The simulation without speed feedback control shows a clear improvement compared to the open-loop simulation.

*Figure II.22 shows the variable wind speed as a function of time:

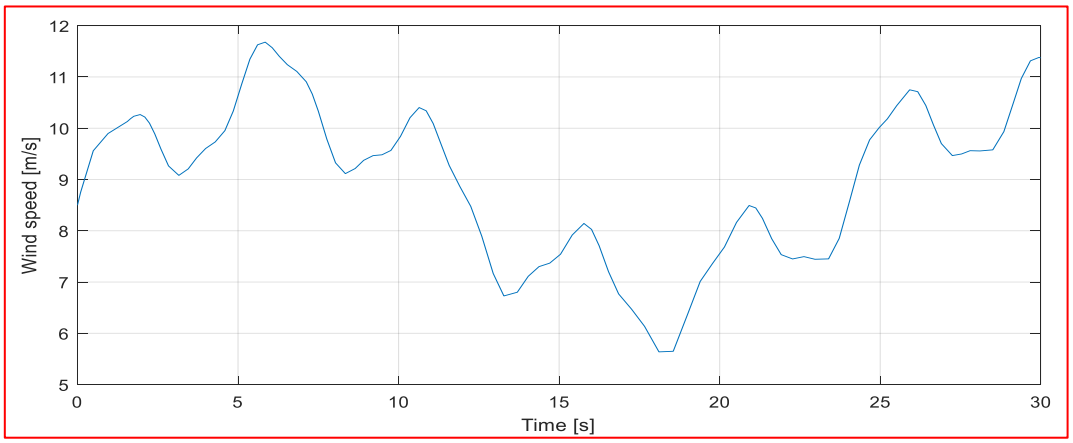

Figure II.22 wind speed

*Figure II.23 shows the evolution of the power coefficient Cp as a function of time for variable wind speed. The Cp coefficient always takes on a variable form, fluctuating between the value Cp = 0.48 and not reaching the theoretical maximum value given by Betz (0.59), which clearly demonstrates the influence of the wind profile on the turbine's Cp coefficient.

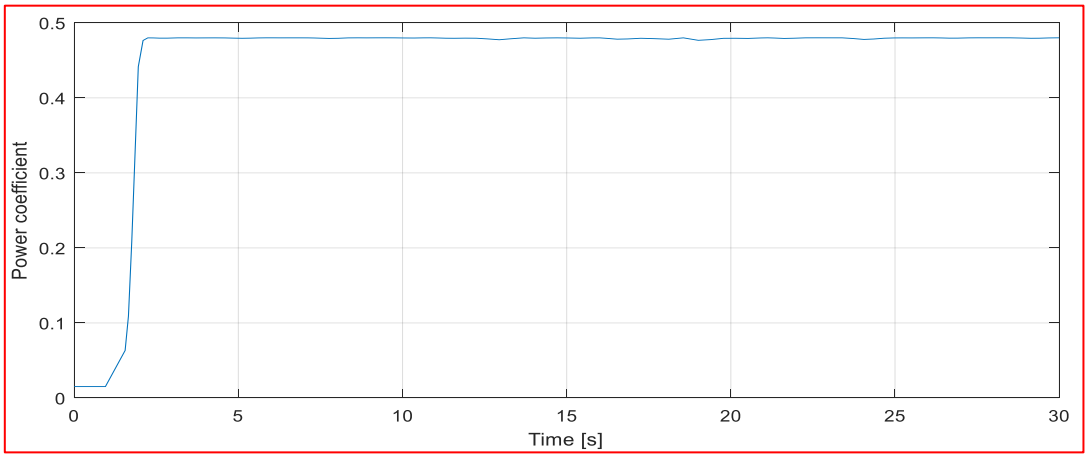

Figure II.23 Power coefficient

*Figure II.24 shows the evolution of the coefficient λ as a function of time for variable wind speed; the curve's shape varies and takes a value around λ= 8, clearly demonstrating the influence of the wind profile on the turbine's λ coefficient.

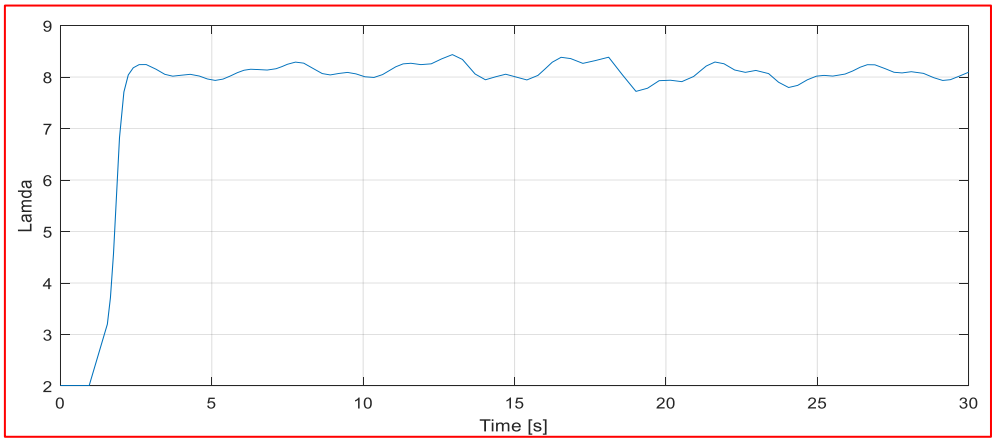

Figure II.24 Relative speed λ without control

*The relative speed λ and the power coefficient C_p are close to their optimal values, with minimal error relative to these values. Thus, for the rotation speed of the machine, it is observed that it also follows the shape of the wind speed. It can be noted that this machine speed varies between (85-177) rad/s for a variable wind profile, as shown in Figure II.25.

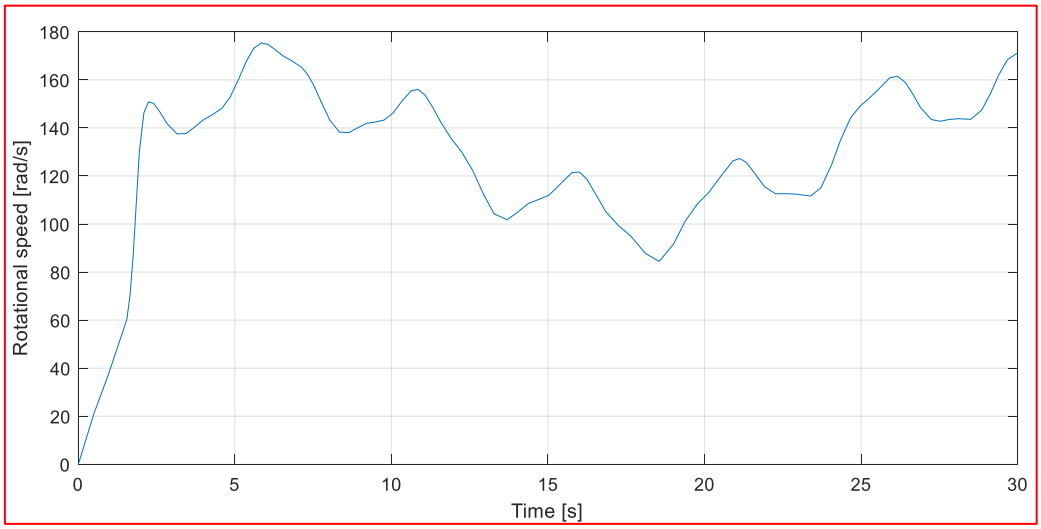

Figure II.25 Machine rotation speed

*Figure II.26 shows the evolution of the mechanical torque of the turbine as a function of time for variable wind speed. The curve's shape consistently fluctuates. Clearly indicating the disturbance caused by the wind profile on the mechanical torque of the turbine which generates undesirable vibrations in the operation of the system.

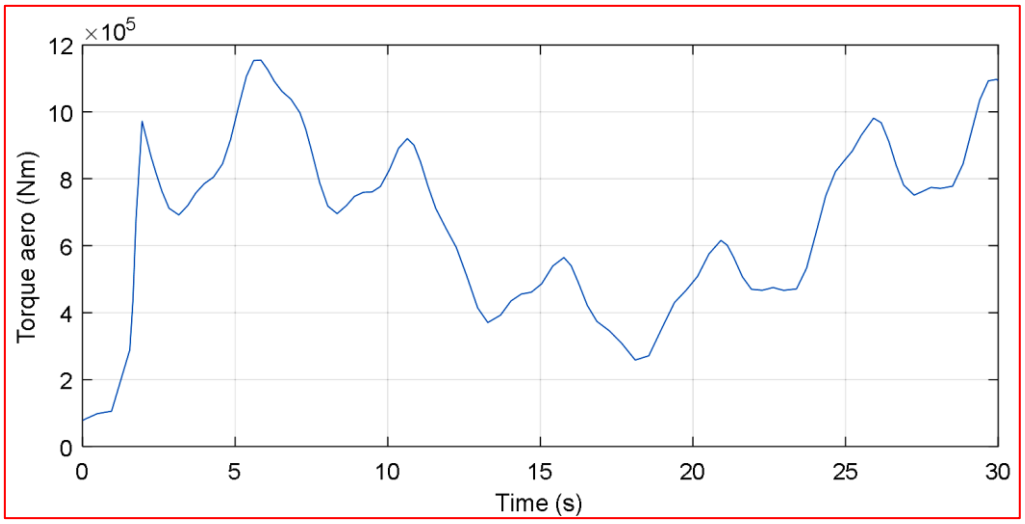

Figure II.26 turbine torque

II.9.2 Simulation results for MPPT with speed feedback

1st Case: In the use of a PI controller

In this part of the simulation with feedback control, the use of a controller allows us to approach the optimal and maximum values of wind turbine operation as closely as possible.

*Figure II.27 illustrates the evolution of the power coefficient Cp and the relative speed λ, which approach their optimal values of 0.48 and 8.1, respectively. Controlling these two

parameters will influence all other controlled variables (torque, rotation speed), which will also approach their ideal values.

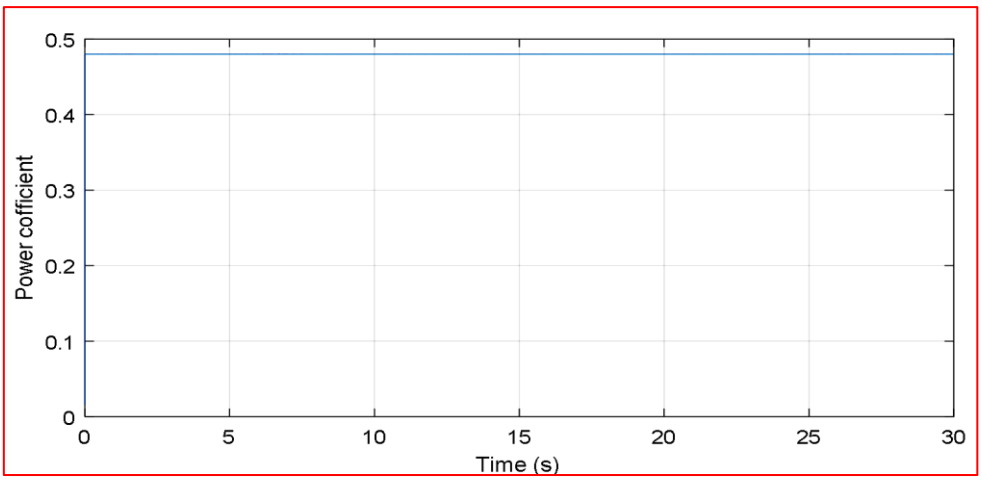

Figure II.27 Power coefficient (C_P) using PI controller

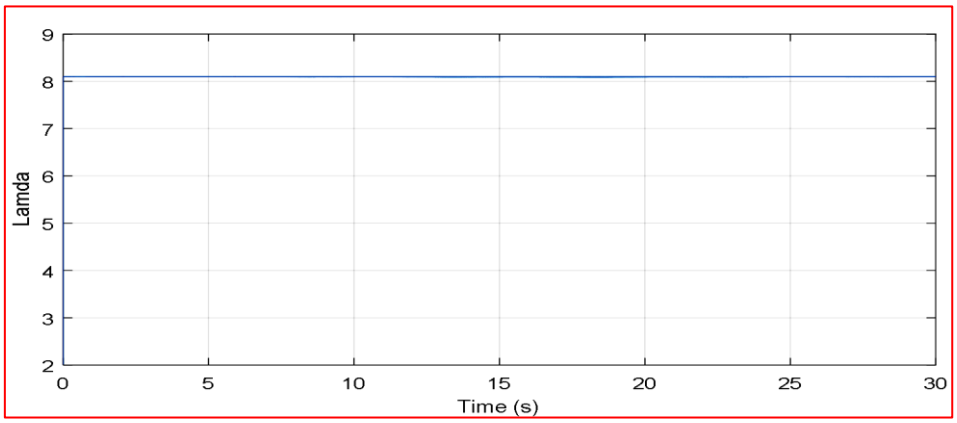

Figure II.28 Relative speed λ using PI controller

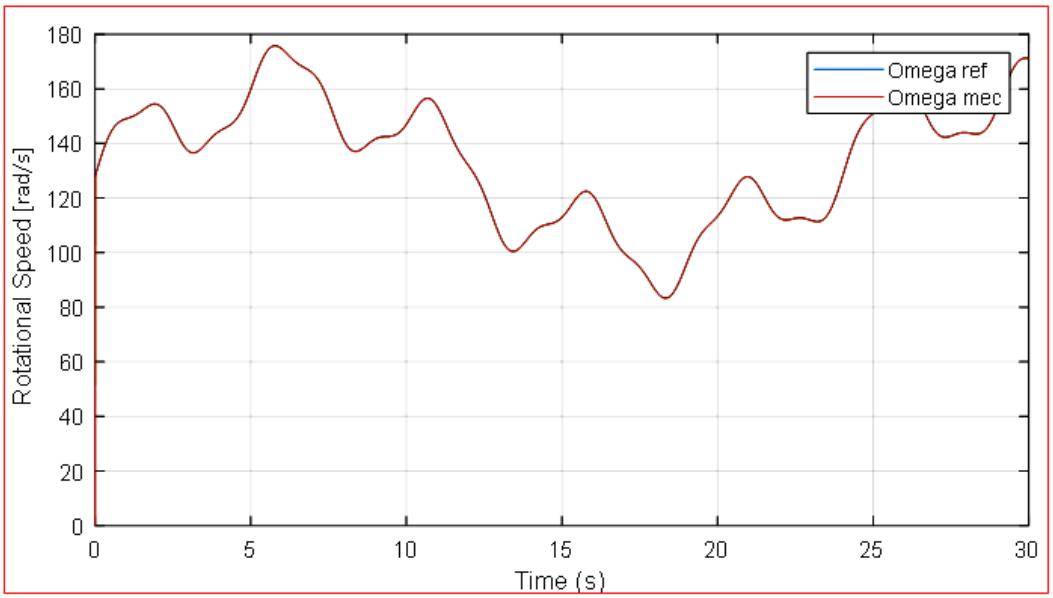

Figure II.29 rotational speed using PI controller

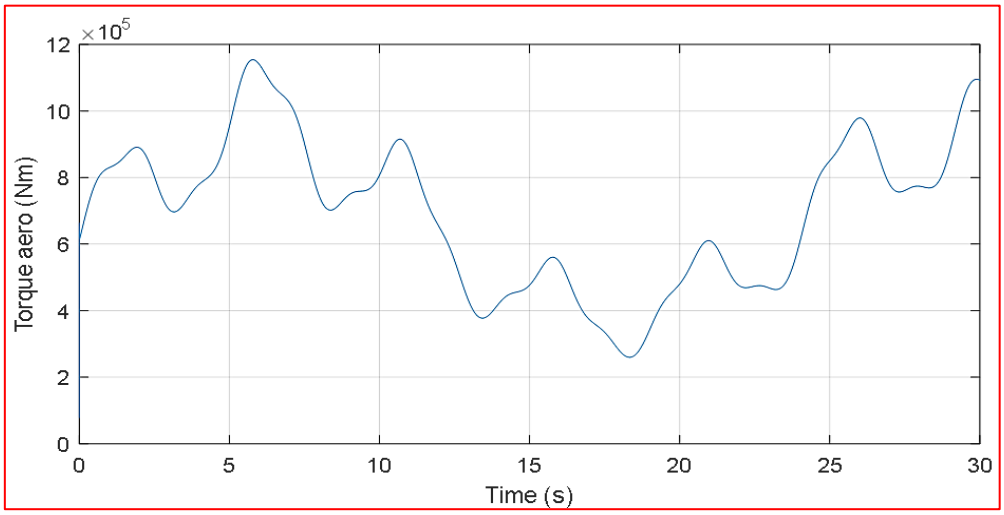

Figure II.30 torque aerodynamic using PI controller

*For a various wind profile applied to the turbine blades, we observe that the mechanical speed of wind turbine follows perfectly its reference. The speed ratio (**λ**) varies slightly around its optimal value. The power coefficient (Cp) remains below the value of Cpmax.

2nd Case: In the use of a fuzzy logic controller

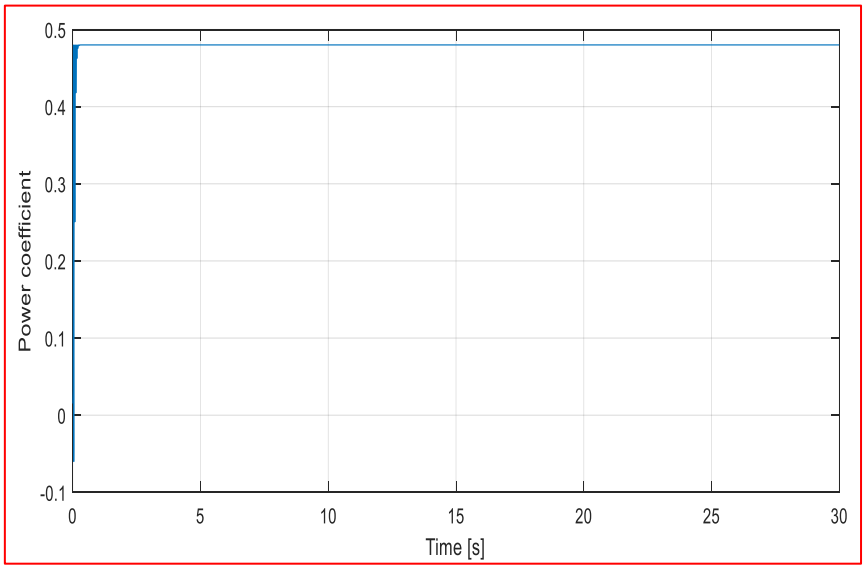

Figure II.31 Power coefficient (CP) using fuzzy logic controller

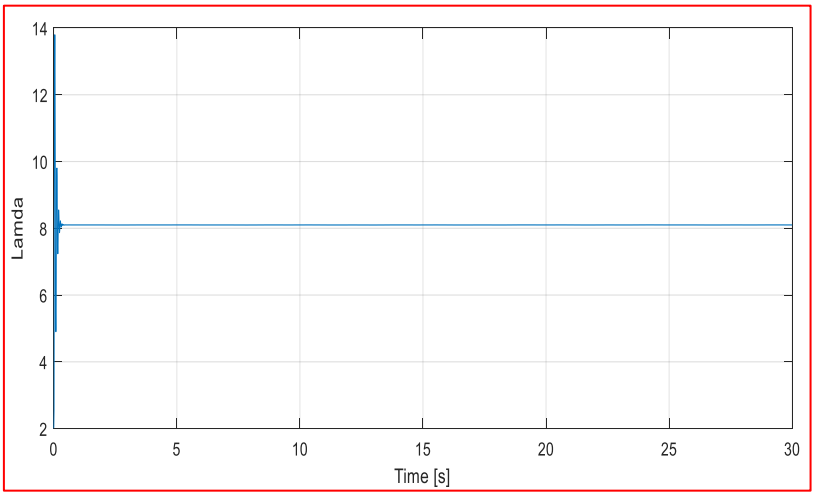

Figure II.32 Relative speed λ using fuzzy logic controller

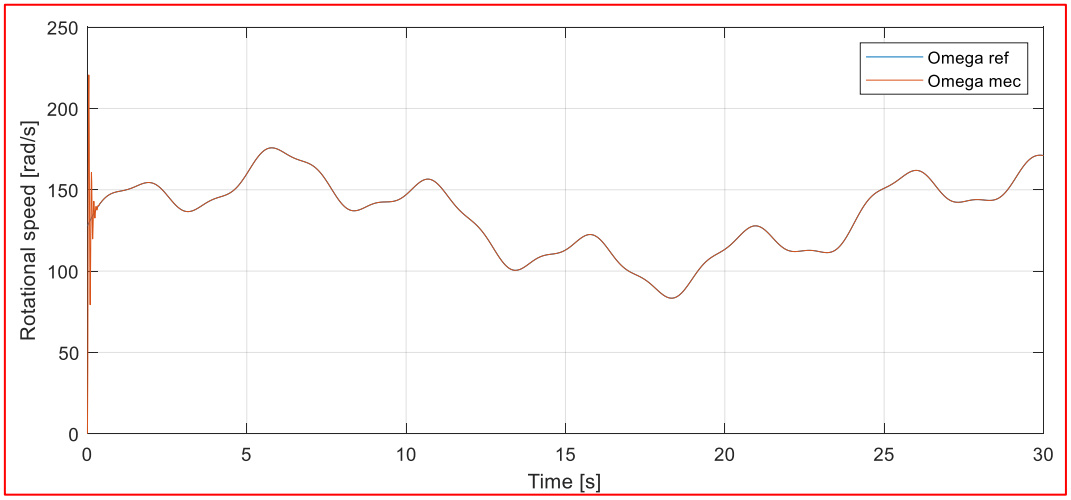

Figure II.33 rotational speed using fuzzy logic controller

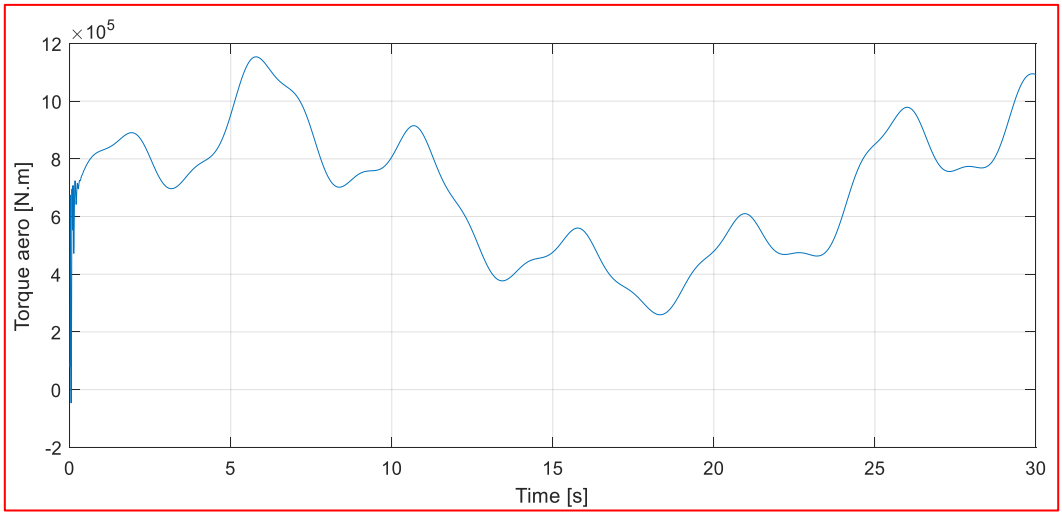

Figure II.34 torque aerodynamic using fuzzy logic controller

In this case, we can see for the various wind profile applied to the turbine blades, we observe that the mechanical speed of wind turbine follows perfectly its reference. The speed

ratio (**λ**) varies slightly around its optimal value. The power coefficient (Cp) remains below the value of Cpmax.

II.9.3 Comparison results

Firstly, we notice that the simulation results without feedback speed show a very small relative deviation from the optimal value, indicating that the MPPT method with feedback allows us to control of generator speed better compared to the MPPT method without feedback.

In contrast, the control method with speed feedback using a PI controller compares the initial value to its reference value and aims to eliminate any possible error to ensure the system operates properly. However, the control method using a Fuzzy Logic Controller (FLC) shows a significant improvement in the performance system.

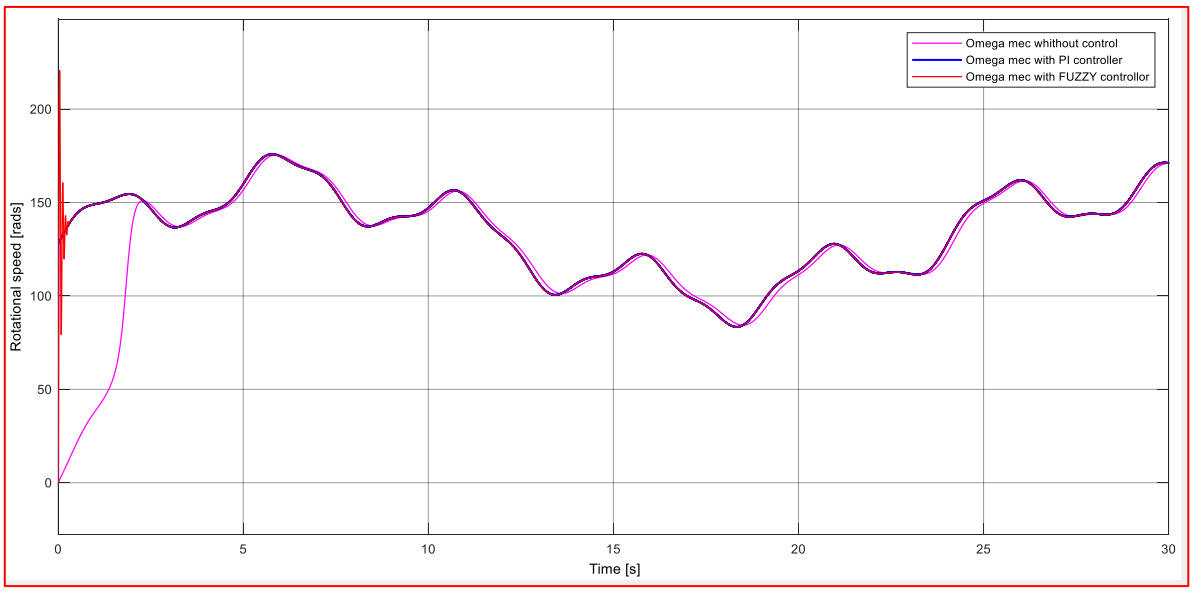

Figure II.35 comparative speed results

II.10 Conclusion

In this chapter, firstly, we modeling wind dynamics to capture detailed variations for the entire mechanical system including the gearbox, enabling connection with the generator. Then, we illustrated various control methods for the wind turbine control that's without speed feedback, control with speed feedback using PI controller and control with speed feedback using fuzzy controller with his diverse simulations to optimize its operation. Finally, we dedicated this section to the simulation and presentation of results conducted using Matlab/Simulink.

We concluded that the MPPT with speed control is the most reliable method as it allows us to closely approach of the turbine power reference and thus extract the maximum power from the wind. In the next chapter, we will study the modeling and simulation of doubly fed induction generator (DFIG) using in wind turbine conversion system.

CHAPTER III

MODELING AND SIMULATION OF THE DOUBLY-FED INDUCTION MACHINE

III.1 Introduction

With the advent of modern technology in the field of electrical engineering, modeling and simulation of electrical machines stand out as one of the most important tools for understanding and improving their performance. The Doubly-Fed Induction Machine (DFIM) emerges as a significant development in the field of electrical power generation, combining the advantages of traditional rotating machines with modern technology to enhance the efficiency and flexibility of power generation systems.

This chapter aims to explore and understand the operation and performance of the asynchronous doubly-fed machine through a focus on the modeling and simulation process. We will then proceed to the modeling process, applying appropriate mathematical and engineering models to accurately represent the behavior of the asynchronous doubly-fed machine. This will include studying factors influencing the machine's performance such as load, feed, and various operating conditions.

Finally, we will utilize the models created in the simulation process to evaluate the machine's performance under different conditions and analyze its efficiency and flexibility.

III.2 Electrical machine types

III.2.1 Synchronous machine

Synchronous generators, utilized in various electricity generation methods like thermal, hydraulic, and nuclear power plants, offer advantages over asynchronous ones due to their absence of reactive magnetization current [25]. They can be magnetically fielded using magnets or conventional excitation winding, and with ample poles, they are suitable for direct drive applications, eliminating the need for gearboxes. Despite higher costs for wind energy applications compared to induction generators, synchronous generators facilitate variable-speed operation and are often indirectly connected to the grid through static converters. Permanent magnet generators are simpler and more cost-effective for smaller-scale units, but beyond approximately 20 kW, synchronous generators become more expensive and complex [26].

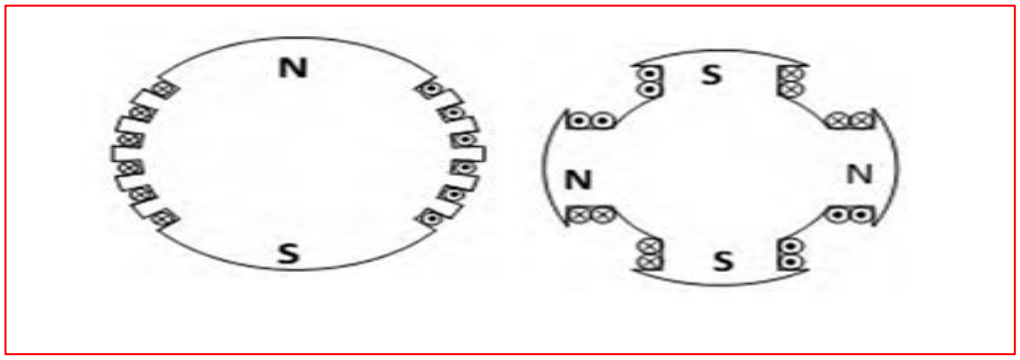

a) Smooth Pole Rotor p=1(2 poles) **b)** Rotor with salient poles p=2(4 poles)

Figure III.1 Rotor with Smooth and salient poles

III.2.2 Asynchronous machine

We will present an incomplete list of wind energy conversion systems that utilize the asynchronous machine. These systems are categorized into two primary groups: those linked to the grid and those functioning in remote locations. The stator is constructed similarly to that of the synchronous machine, and the rotor incorporates either a short-circuited squirrel cage or a system of three-phase windings (if the stator is also three-phase) [26] [27].

a. Squirrel cage asynchronous machine

The asynchronous machine with a squirrel cage design, when equipped with a frequency converter, enables variable speed operation, albeit at a considerable cost [27].

This configuration is less competitive compared to the doubly-fed asynchronous machine due to its fixed number of pole pairs, limiting its speed range to less than 2% slip. Operation beyond this range can lead to increased stator currents and potential damage.

Additionally, the machine consumes reactive power, impacting the grid's power factor, which can be mitigated by adding capacitors or using a frequency converter, albeit at an increased expense. However, converters are dimensioned for the entire power exchange between the machine and the grid, incurring significant costs, losses of up to 3% of nominal power, and introducing disturbances that affect energy efficiency and quality [28].

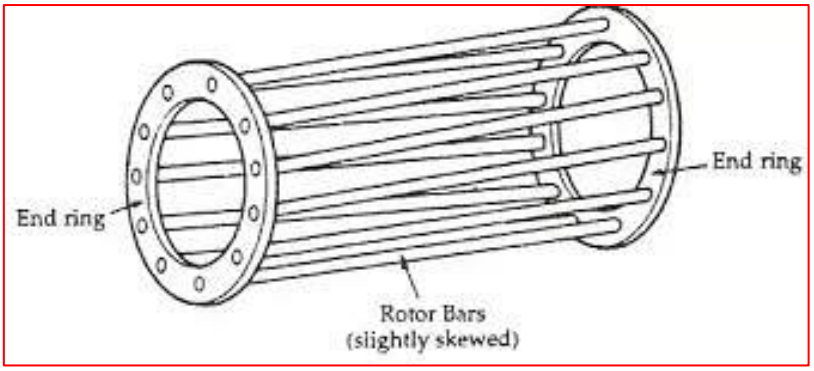

Figure III.2 Squirrel cage rotor

b. Double-stator asynchronous machine

To improve the effectiveness of the earlier system, certain manufacturers opt for a setup utilizing a double-stator asynchronous machine, illustrated in Figure III.3. Lower speeds are associated with a greater number of pole pairs, while higher speeds are linked to a high-power stator and consequently fewer pole pairs, especially during high wind speeds. Switches are employed for grid connection when facing elevated wind speeds [29].

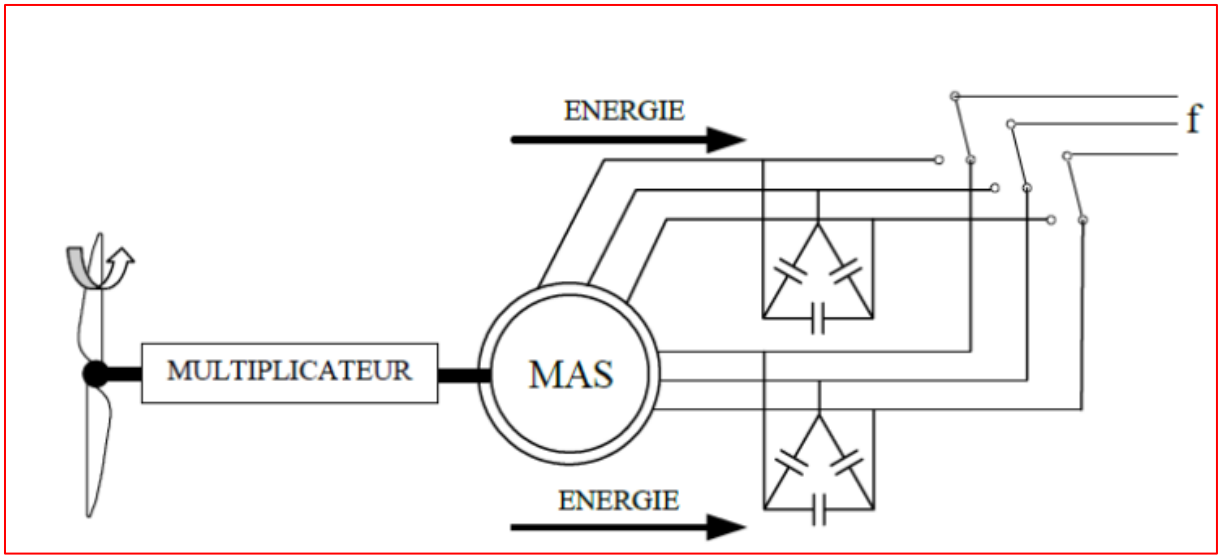

Figure III.3 Double-stator asynchronous machine [26]

C. Doubly-fed asynchronous machine

The present body of literature confirms the substantial attention currently directed towards the doubly-fed machine, which finds application in diverse areas. It is utilized both as a generator in wind energy systems and as a motor for specific industrial purposes, including rolling processes, railway traction, and maritime propulsion [30].

Using DFIM for Wind Energy Converter systems (WECs) offers several advantages. These include enhanced modeling accuracy, improved performance prediction, and the development of advanced control strategies. These benefits support informed decision-making and optimization of WEC designs, leading to more efficient and reliable wind energy conversion systems.

Based on these benefits, we have chosen to continue our study using the Doubly-Fed Induction Machine (DFIM).

III.3 Doubly-fed induction machine

III.3.1 Operation of the doubly-fed induction machine (DFIM)

The DFIM is equipped with a three-phase stator that closely resembles that of a traditional asynchronous machine, commonly referred to as a squirrel-cage induction motor. Its rotor

comprises a three-phase winding accessible through three rings equipped with sliding contacts (brushes). The machine's robustness experiences a slight reduction compared to a conventional asynchronous machine, attributable to the presence of this ring/brush system.

Once the stator of the machine is connected to the electrical grid, a magnetic flux emerges within the stator. This flux is influenced by the reluctance of the magnetic circuit, the number of pole pairs in the winding, and the stator current. During rotation, the magnetic flux generated by the stator induces electromotive forces (EMFs) in the rotor windings [31].

III.3.2 Advantages and disadvantages of the DFIM

- **Advantages**

- The static converters utilized have the following characteristics:
- Reduced size.
- Lower cost.
- Consequently, a lighter cooling system is required [32].
- Accessibility to the rotor enables control over electrical parameters such as current and voltage, providing significant flexibility and precision in managing flux and electromagnetic torque.
- Bidirectional transfer of rotor power [33].
- Measurement of currents at both the stator and rotor, in contrast to the cage machine, allowing for greater flexibility and precision in controlling flux and electromagnetic torque.
- Capability to operate at a constant torque beyond the rated speed [26].
- The DFIM combines the benefits of both synchronous and asynchronous machines, including:
- Operation at variable rotational speeds.
- Decoupled regulation of active and reactive powers [33].

- **Disadvantages**

- Deployment of a higher number of static converters compared to a traditional machine.
- Larger physical size compared to a typical asynchronous machine, often elongated due to the presence of brushes [26].
- The overall cost of the machine is higher compared to other types of electrical machines.

III.4 Modeling the doubly-fed induction machine

involves conducting its modeling before delving into the vector control aspect. This process enables comprehension of its physical operational principles and the development of an action model. This model facilitates the calculation of controllers for implementing vector control and simulating the DFIM in both dynamic and steady-state conditions [25].

III.4.1 Simplifying assumptions

The model is based on the following classical simplifying assumptions:

- Constant air gap.
- Neglect of the notch effect.
- Sinusoidal spatial distribution of magnetic air-gap forces.
- Effects of skin effect and non-consideration of heating not taken into account.
- Non-saturated magnetic circuit with constant permeability.
- No homopolar regime as the neutral is not connected.

These choices imply, among other things, that the cumulative magnetic fluxes, the self-inductances, and the mutual inductances between the stator and rotor windings exhibit a sinusoidal variation based on the electrical angle of their magnetic axes.

The overall configuration of the doubly-fed asynchronous machine comprises six windings in the electrical domain. The stator axes are displaced from each other by an angle of (2/3), mirroring the offset of the rotor axes. The angle θ signifies the angular displacement between the axis of the reference rotor phase (r_b) and the fixed axis of the reference stator phase (s_b). The rotor axes, revolving at a rate of (ω_r) relative to the fixed stator axes, are depicted in Figure III.4.

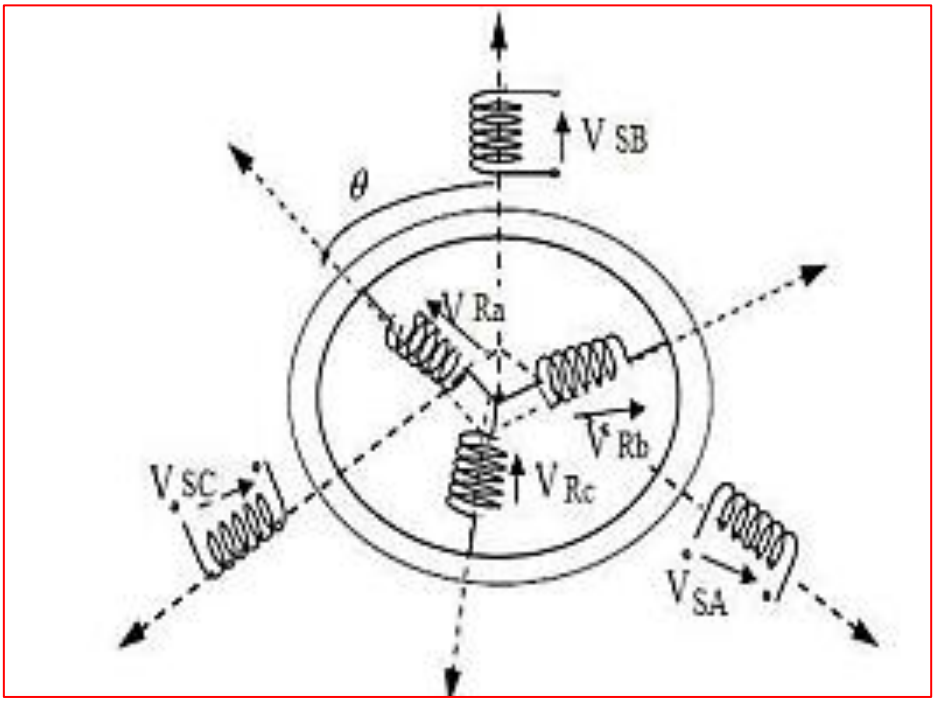

Figure III.4 Representation of the doubly-fed asynchronous machine (DFIM) in the three-phase system

III.4.2 Representation of the DFIM in the three-phase system (a, b, c)

The general equations of the doubly-fed asynchronous machine in a three-phase reference frame [34].

- **Electrical equations**

By applying Faraday's law to each winding, we can write:

$$\frac{d\varphi}{dt} = V - R_i \quad \textbf{(III.1)}$$

When applying this relationship to the three-phase winding of the stator and rotor, we obtain [25]:

- for the stator

$$\begin{cases} V_{sa} = R_s I_{sa} + \frac{d\varphi_{sa}}{dt} \\ V_{sb} = R_s I_{sb} + \frac{d\varphi_{sb}}{dt} \\ V_{sc} = R_s I_{sc} + \frac{d\varphi_{sc}}{dt} \end{cases} \quad \textbf{(III.2)}$$

- for the rotor

$$\begin{cases} V_{ra} = R_r I_{ra} + \frac{d\varphi_{ra}}{dt} \\ V_{rb} = R_r I_{rb} + \frac{d\varphi_{rb}}{dt} \\ V_{rc} = R_r I_{rc} + \frac{d\varphi_{rc}}{dt} \end{cases} \quad \textbf{(III.3)}$$

In matrix form

$$\begin{cases} [V_s] = [R_s][I_s] + \frac{d}{dt}[\varphi_s] \\ [V_r] = [R_r][I_r] + \frac{d}{dt}[\varphi_r] \end{cases} \quad \textbf{(III.4)}$$

With

$$[R_s] = \begin{bmatrix} R_s & 0 & 0 \\ 0 & R_s & 0 \\ 0 & 0 & R_s \end{bmatrix} ; [R_r] = \begin{bmatrix} R_r & 0 & 0 \\ 0 & R_r & 0 \\ 0 & 0 & R_r \end{bmatrix} \quad \textbf{(III.5)}$$

- **Magnetic equations**

The magnetic equations are given by the following expressions:

$$\begin{bmatrix} \varphi_s \\ \varphi_r \end{bmatrix} = \begin{bmatrix} [L_s] & [M_{sr}] \\ [M_{rs}] & [L_r] \end{bmatrix} \begin{bmatrix} I_s \\ I_r \end{bmatrix} \quad \textbf{(III.6)}$$

As follows

$$[\varphi_s] = \begin{bmatrix} \varphi_{sa} \\ \varphi_{sb} \\ \varphi_{sc} \end{bmatrix} ; [\varphi_r] = \begin{bmatrix} \varphi_{ra} \\ \varphi_{rb} \\ \varphi_{rc} \end{bmatrix} \quad \textbf{(III.7)}$$

$$[I_s] = \begin{bmatrix} I_{sa} \\ I_{sb} \\ I_{sc} \end{bmatrix} ; [I_r] = \begin{bmatrix} I_{ra} \\ I_{rb} \\ I_{rc} \end{bmatrix} \quad \textbf{(III.8)}$$

$$[L_s] = \begin{bmatrix} l_s & M_s & M_s \\ M_s & l_s & M_s \\ M_s & M_s & l_s \end{bmatrix} ; \ [R_r] = \begin{bmatrix} l_r & M_r & M_r \\ M_r & l_r & M_r \\ M_r & M_r & l_r \end{bmatrix} \quad \textbf{(III.9)}$$

$$[M_{rs}]^t = [M_{sr}] = [M] = M_{sr} * \begin{bmatrix} \cos\theta & \cos(\theta - 4\pi/3) & \cos(\theta - 2\pi/3) \\ \cos(\theta - 2\pi/3) & \cos\theta & \cos(\theta - 4\pi/3) \\ \cos(\theta - 4\pi/3) & \cos(\theta - 2\pi/3) & \cos\theta \end{bmatrix}$$

(III.10)

With

Is, Ir: Self-inductance of a statoric and rotoric phase

Ms, Mr: Mutual inductance between stator and rotor phases.

$[Ls]$: Stator inductance matrix.

$[Lr]$: Rotor inductance matrix.

$[Msr]$: Matrix of mutual inductances for stator-rotor coupling.

$[Mrs]$: Matrix of mutual inductances for rotor-stator coupling.

θ: Angle representing the orientation of the rotor phase axis relative to the fixed axis of the stator phase.

•Mechanical equations

The mechanical equation reflecting the rotational movement of the electric motor shaft is given by the electromagnetic torque [35].

$$T_{em} = \frac{1}{2}[I_s]^t \left\{\frac{d}{d\theta}[L]\right\}[I_r] \quad \textbf{(III.11)}$$

With

$$[L] = \begin{bmatrix} [L_S] & [M] \\ [M] & [L_R] \end{bmatrix} \quad \textbf{(III.12)}$$

And

$$[I] = [I_{sa}\ I_{sb}\ I_{sc}\ I_{ra}\ I_{rb}\ I_{rc}]^t = \begin{bmatrix} I_s \\ I_r \end{bmatrix} \quad \textbf{(III.13)}$$

The matrices $[Ls]$and $[Lr]$ only contain constant terms as the angle θ varies. This allows simplification of the torque expression to be:

$$[T_{em}] = \frac{1}{2}[I_s]^t \left\{\frac{d}{d\theta}[M]\right\}[I_r] \quad \textbf{(III.14)}$$

One can also express the electromagnetic torque as a function of the resisting torque Cr created by the mechanical load of the motor, the moment of inertia of all rotating parts, and the viscous friction coefficient F:

$$T_e = j\frac{d\Omega}{dt} + f\Omega - T_r \quad \textbf{(III.15)}$$

III.4.3 Three-phase to two-phase transition (park transformation)

The Park transformation involves applying a variable change to currents, voltages, and fluxes, which includes the angle between the axis of a stator phase (Va) and the axis system (d, q). It is defined by [36]:

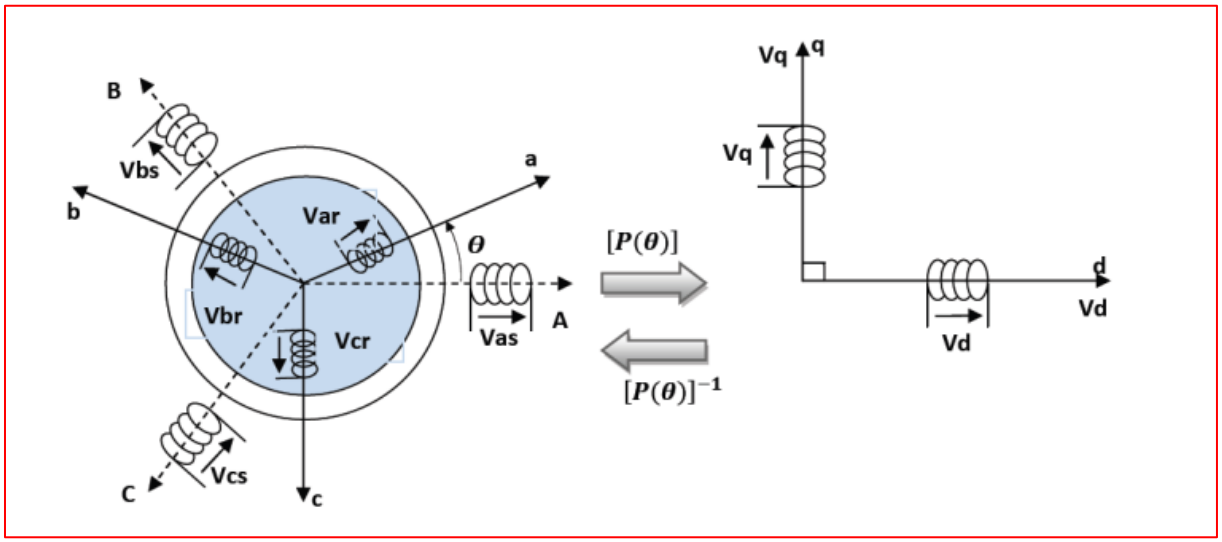

Figure III.5 Transition from three-phase to two-phase and vice versa

$$[P(\theta)] = \sqrt{\frac{2}{3}}\begin{bmatrix} \cos\theta & \cos(\theta - 2\pi/3) & \cos(\theta - 4\pi/3) \\ -\sin\theta & -\sin(\theta - 2\pi/3) & -\sin(\theta - 4\pi/3) \\ \frac{1}{\sqrt{2}} & \frac{1}{\sqrt{2}} & \frac{1}{\sqrt{2}} \end{bmatrix} \quad \textbf{(III.16)}$$

$$[P(\theta)]^t = \sqrt{\frac{2}{3}}\begin{bmatrix} \cos\theta & -\sin\theta & 1 \\ \cos(\theta - 2\pi/3) & -\sin(\theta - 2\pi/3) & 1 \\ \cos(\theta - 4\pi/3) & -\sin(\theta - 4\pi/3) & 1 \end{bmatrix} \quad \textbf{(III.17)}$$

III.4.4 Application of the park transformation

By applying the Park transformation to the equations of the doubly fed asynchronous machine in any reference frame (equations (III.2), (III.3)), the machine model is obtained, taking into account the homopolar components, in the following form [36]:

$$[P(\theta)]^{-1}[V_{dq0}] = [R][P(\theta)]^{-1}[i_{dq0}] + \frac{d}{dt}\left[[P(\theta)] - 1[\varphi_{dq0}]\right] \quad \textbf{(III.18)}$$

$$[P(\theta)][V_{dq0}] = [R][i_{dq0}] + \left[\frac{d}{dt}[P(\theta)] - 1[\varphi_{dq0}]\right] \quad \textbf{(III.19)}$$

$$[P(\theta)]\left[\frac{d}{dt}[P(\theta)]^{-1}\right] = \begin{bmatrix} 0 & -1 & 0 \\ 1 & 0 & 0 \\ 0 & 0 & 0 \end{bmatrix}\left[\frac{d\theta}{dt}\right] \quad \textbf{(III.20)}$$

Such as

$\theta = \theta s$ for stator quantities

$\theta = \theta s - \theta r$ for rotor quantities

By substituting equation (III.20) into equation (III.19), the following equivalent biphasic model is obtained [36].

$$\begin{cases} V_d = R_{id} + \frac{d\varphi_d}{dt} - \frac{d\theta}{dt}\varphi_q \\ V_q = R_{iq} + \frac{d\varphi_q}{dt} - \frac{d\theta}{dt}\varphi_d \\ V_0 = R_{i0} + \frac{d\varphi_0}{dt} \end{cases} \quad \textbf{(III.21)}$$

III.4.5 Representation of DFIM in a two-phase (dq) reference frame

By multiplying the systems of equations (III.4) by the park matrix, the result is obtained [33] [36] [37].

•Electrical equations

$$\begin{cases} V_{sd} = R_s I_{sd} + \frac{d\varphi_{sd}}{dt} - \omega_s \varphi_{sq} \\ V_{sq} = R_s I_{sq} + \frac{d\varphi_{qs}}{dt} + \omega_s \varphi_{sd} \\ V_{rd} = R_r I_{rd} + \frac{d\varphi_{rd}}{dt} - (\omega_s - \omega)\varphi_{rq} \\ V_{rq} = R_r I_{rq} + \frac{d\varphi_{rq}}{dt} + (\omega_s - \omega)\varphi_{rd} \end{cases} \quad \textbf{(III.22)}$$

•Magnetic equations

The stator and rotor fluxes

$$\begin{cases} \varphi_{sd} = L_s I_{sd} + M I_{rd} \\ \varphi_{sq} = L_s I_{sq} + M I_{rq} \\ \varphi_{rd} = L_s I_{rd} + M I_{sd} \\ \varphi_{rq} = L_s I_{rq} + M I_{sq} \end{cases} \quad \textbf{(III.23)}$$

The Park angles related to stator and rotor magnitudes are interconnected, as illustrated in Figure III.6, through the relationship [36]:

$\theta s = \theta e + \theta r$ **(III.24)**

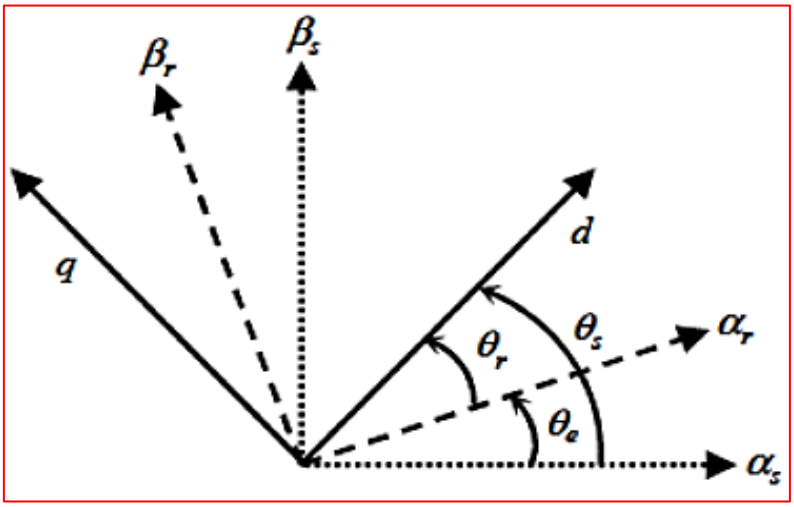

Figure III.6 Park angles of stator and rotor magnitudes

•Mechanical equation

$$\boldsymbol{T_{em} = \frac{P_m}{\Omega_s} \;;\Omega_s = \frac{\omega_s}{p} \;;T_{em} = p\frac{P_M}{\omega_s}} \quad \textbf{(III.25)}$$

The electromagnetic torque Cemcan be expressed, based on stator fluxes and currents, as follows

$$\boldsymbol{T_{em} = p(\varphi_{sd} I_{sd} - \varphi_{sq} I_{sd})} \quad \textbf{(III.26)}$$

By substituting the flows with their expressions provided by relations (III.23), it is possible to establish alternative expressions for the pair

$$\boldsymbol{T_{em} = p(\varphi_{rd} I_{rq} - \varphi_{rq} I_{rd})} \quad \textbf{(III.27)}$$

$$\boldsymbol{T_{em} = pM(I_{sq} I_{rd} - I_{sd} I_{rq})} \quad \textbf{(III.28)}$$

$$\boldsymbol{T_{em} = p\frac{M}{L_r}(\varphi_{sq} I_{rd} - \varphi_{sd} I_{rq})} \quad \textbf{(III.29)}$$

$$\boldsymbol{T_{em} = p\frac{M}{L_r}(\varphi_{rd} I_{sq} - \varphi_{rq} I_{sd})} \quad \textbf{(III.30)}$$

By applying the fundamental relationships of dynamics to the machine, the mechanical equation is expressed as [37]

$$\boldsymbol{\frac{J}{p}\frac{d(\omega_r)}{dt} = T_e - T_r - T_f} \quad \textbf{(III.31)}$$

J : Inertia moment of rotating parts (of the engine with the load).

Te: Resistant torque.

Tf: Friction torque.

$$\boldsymbol{T_e = J\frac{d\Omega}{dt} + f\Omega - T_r} \quad \textbf{(III.32)}$$

III.4.6 Machine state representation

The manner in which the DFIM is represented in terms of state relies on the chosen reference frame and state variables for the electrical equations. These equations are formulated within the (d, q) reference frame, deemed the most comprehensive solution.

The selection of state variables is contingent on the specific goals, whether for control or observation. In our scenario, we opt for the subsequent state vector [37]

$[I_{sd}, I_{sq}, \varphi_{rd}, \varphi_{rq}]^T$.

Expressing the control model of the machine takes the form of a system of state equations

$$\begin{cases} \boldsymbol{\frac{dx}{dt} = AX + BU} \\ \boldsymbol{Y = CX} \end{cases} \quad \textbf{(III.33)}$$

With

X: state vector of the system.

A: state matrix of the system.

B: control matrix.

U: control vector $[V_{sd}\ V_{sq}\ V_{rd}\ V_{rq}]^T$

Y: output vector.

C: observation matrix.

The equations for rotor currents are deduced from the rotor flux equations (III.23) [36] [37].

$$\begin{cases} \boldsymbol{I_{rd} = \frac{1}{L_r}\varphi_{rd} - \frac{M}{L_r}I_{sd}} \\ \boldsymbol{I_{rq} = \frac{1}{L_r}\varphi_{rq} - \frac{M}{L_r}I_{sq}} \end{cases} \quad \textbf{(III.34)}$$

By replacing the rotor currents in the stator flux equations (III.23), we obtain:

$$\begin{cases} \boldsymbol{\varphi_{sd} = L_s\sigma I_{sd} + \frac{M}{L_r}\varphi_{rd}} \\ \boldsymbol{\varphi_{sq} = L_s\sigma I_{sq} + \frac{M}{L_r}\varphi_{rq}} \end{cases} \quad \textbf{(III.35)}$$

With

$$\boldsymbol{\sigma = \left(1 - \frac{M^2}{L_s L_r}\right)} \quad \textbf{(III.36)}$$

By replacing $\boldsymbol{\varphi_{sd}}$ and $\boldsymbol{\varphi_{sq}}$ in terms of $\boldsymbol{I_{rd}}$ and $\boldsymbol{I_{rq}}$ in the equations of stator voltages (III.22), we obtain the following equations:

$$\begin{cases} \boldsymbol{V_{sd} = R_s.I_{sd} + L_s\sigma\frac{I_{sd}}{dt} + \frac{M}{L_r}\frac{d\varphi_{rd}}{dt} - \omega_s\left(L_s\sigma I_{sq} + \frac{M}{L_r}\varphi_{rq}\right)} \\ \boldsymbol{V_{sq} = R_s.I_{sq} + L_s\sigma\frac{I_{sq}}{dt} + \frac{M}{L_r}\frac{d\varphi_{rq}}{dt} - \omega_s\left(L_s\sigma I_{sd} + \frac{M}{L_r}\varphi_{rd}\right)} \end{cases} \quad \textbf{(III.37)}$$

The derivative of rotor flux is determined from the rotor voltage equations (III.22):

$$\begin{cases} \boldsymbol{\frac{d\varphi_{rd}}{dt} = V_{rd} - R_r I_{rd} + (\omega_s - \omega_r)\varphi_{rq}} \\ \boldsymbol{\frac{d\varphi_{rq}}{dt} = V_{rq} - R_r I_{rq} + (\omega_s - \omega_r)\varphi_{rd}} \end{cases} \quad \textbf{(III.38)}$$

We replace the two rotor currents (III.34) in the equations of the rotor flux derivatives (III.38), we find

$$\begin{cases} \boldsymbol{\frac{d\varphi_{rd}}{dt} = V_{rd} - \frac{R_r}{L_r}\varphi_{rd} + \frac{MR_r}{L_r}I_{sd} + (\omega_s - \omega_r)\varphi_{rq}} \\ \boldsymbol{\frac{d\varphi_{rq}}{dt} = V_{rq} - \frac{R_r}{L_r}\varphi_{rq} + \frac{MR_r}{L_r}I_{sq} - (\omega_s - \omega_r)\varphi_{rd}} \end{cases} \quad \textbf{(III.39)}$$

We substitute the last equation into the stator voltage equation system (III.37) and find:

$$\begin{cases} \boldsymbol{\frac{I_{sd}}{dt} = -\gamma I_{sd} + \omega_s I_{sq} + \frac{k}{T_r}\varphi_{rd} + k\omega_r\varphi_{rq} + \frac{1}{L_s\sigma}V_{sd} - KV_{rd}} \\ \boldsymbol{\frac{I_{sq}}{dt} = -\gamma I_{sq} - \omega_s I_{sd} + \frac{k}{T_r}\varphi_{rq} - k\omega_r\varphi_{rd} + \frac{1}{L_s\sigma}V_{sq} - KV_{rq}} \end{cases} \quad \textbf{(III.40)}$$

And

$$\begin{cases} \frac{d\varphi_{rd}}{dt} = \frac{M}{T_r} I_{sd} - \frac{1}{T_r}\varphi_{rd} + (\omega_s - \omega_r)\varphi_{rq} + V_{rd} \\ \frac{d\varphi_{rq}}{dt} = \frac{M}{T_r} I_{sq} - \frac{1}{T_r}\varphi_{rq} - (\omega_s - \omega_r)\varphi_{rd} + V_{rq} \end{cases} \quad \textbf{(III.41)}$$

So

$$A = \begin{bmatrix} -\gamma & \omega_s & \frac{K}{T_r} & \omega_r \\ -\omega_s & -\gamma & -\omega_r K & \frac{K}{T_r} \\ \frac{M}{T_r} & 0 & -\frac{1}{T_r} & \omega_{sl} \\ 0 & \frac{M}{T_r} & -\omega_{sl} & -\frac{1}{T_r} \end{bmatrix} \quad \textbf{(III.42)}$$

And

$$B = \begin{bmatrix} \frac{1}{L_s\sigma} & 0 & -K & 0 \\ 0 & \frac{1}{L_s\sigma} & 0 & -K \\ 0 & 0 & K & 0 \\ 0 & 0 & 0 & K \end{bmatrix} \quad \textbf{(III.43)}$$

With

$$\begin{cases} \frac{R_s}{L_s} = \frac{1}{T_s} \\ \frac{R_r}{L_r} = \frac{1}{T_r} \\ K = \frac{M}{L_r L_s \sigma} \\ \gamma = \left(\frac{1}{T_s\sigma} + \frac{MK}{T_r}\right) \end{cases} \quad \textbf{(III.44)}$$

The mechanical equation governing the rotating part of the machine is given by [36] [37]:

$$T_{em} = -\frac{3}{2} p . \frac{M}{L_r} \left(\varphi_{rd} . I_{sd} - \varphi_{rq} . I_{sd}\right) \quad \textbf{(III.44)}$$

III.5 Simulation and interpretation of results

Now, we attempt to validate the model of the doubly fed induction machine (DFIM) described by the equations derived using the Park transformation related to the rotating field mentioned earlier. The system parameters of DFIM are presented in table III.1.

Table III.1 The simulation parameters of the DFIM

Parameters	Values
Nominal power	Pn=19 kw
Stator voltage	Vs=400 V
Stator resistance	Rs=1.2Ω
Rotor resistance	Rr=1.8Ω
Stator inductance	Ls=0.1554H

Rotor inductance	Lr=0.1568H
Mutuel inductance	M= 0.15H

The figure III.7 presents the block diagram of DFIM in Matlab/Simulink.

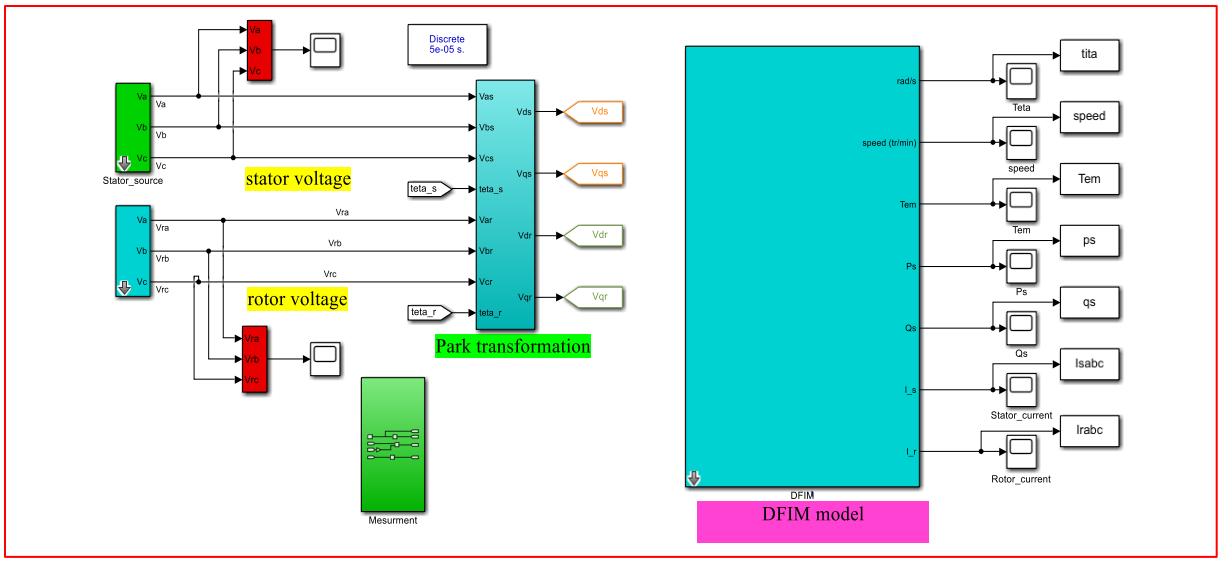

Figure III.7 Block diagram of the studied system in Matlab/Simulink

The study of the DFIM has been validated through numerical simulation using MATLAB/Simulink software. To perform regulation tests, the system was subjected to step changes in electromechanical torque. From 0 Nm to 100 Nm at t=3s. Figures blew present different simulation results of the DFIM.

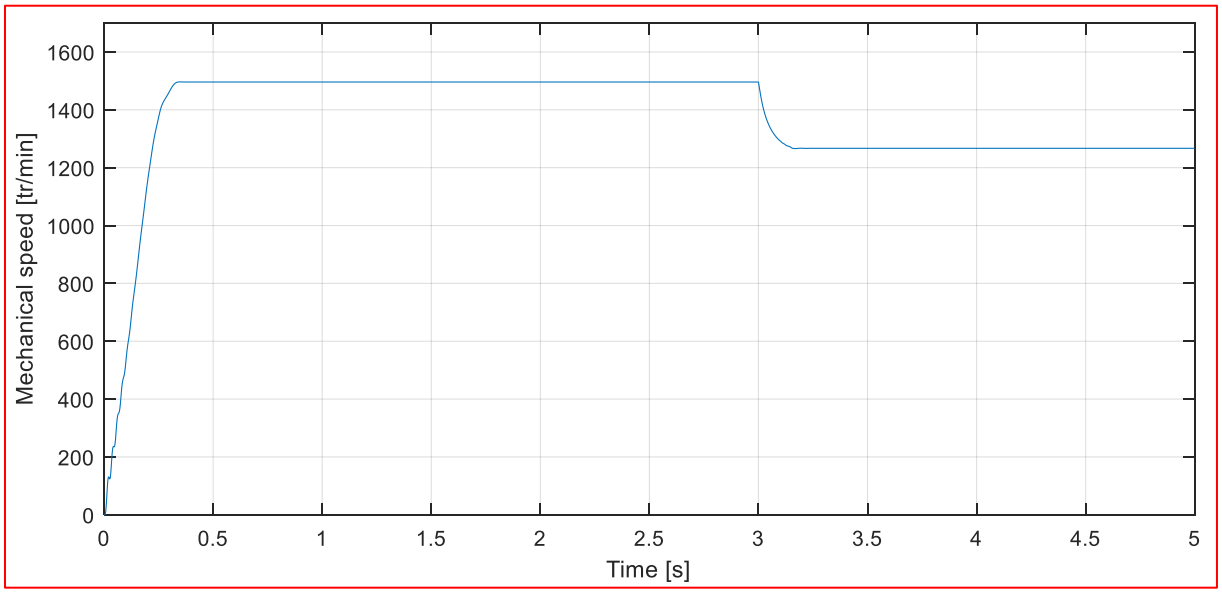

Figure III.8 Mechanical speed

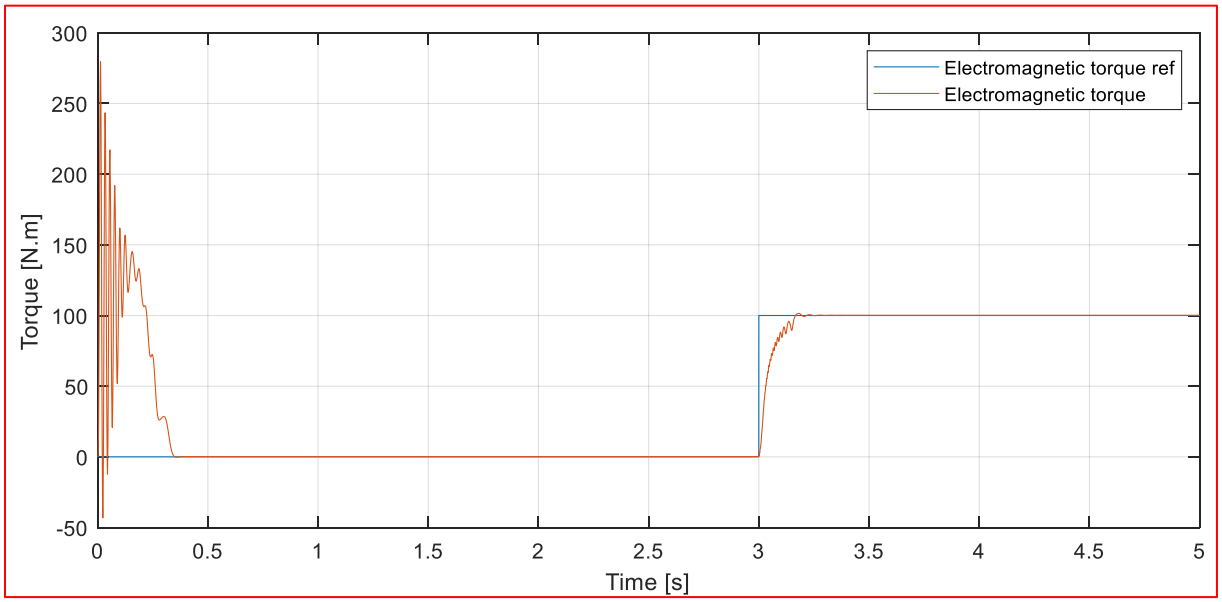

Figure III.9 Electromagnetic torque with reference

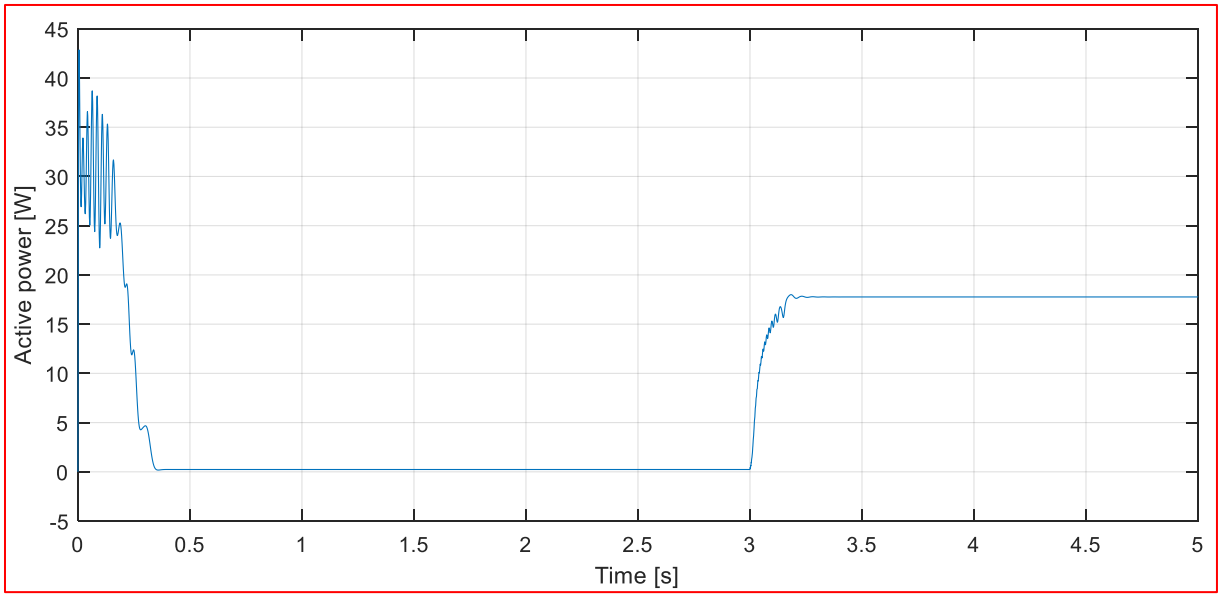

Figure III.10 Stator Active power

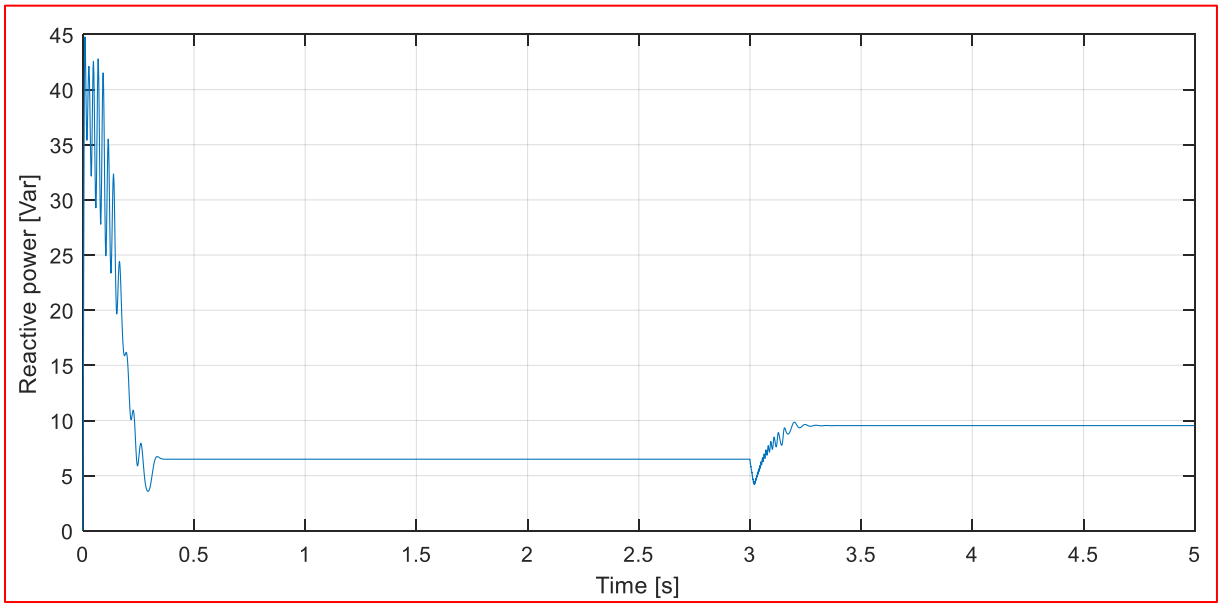

Figure III.11 Stator reactive power

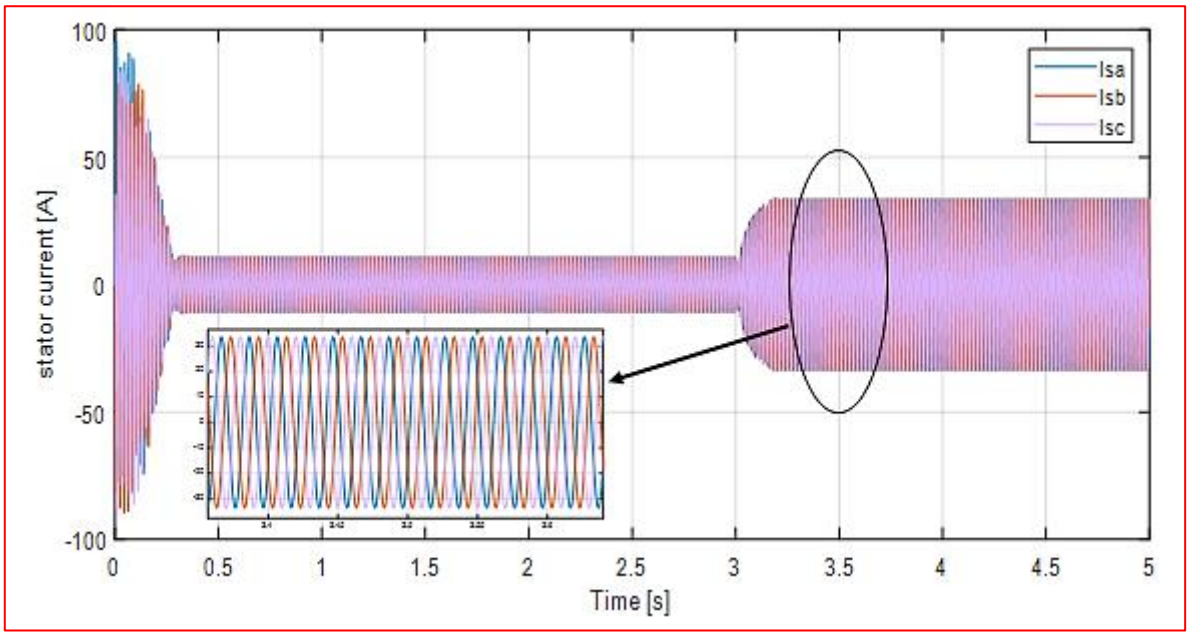

Figure III.12 Stator currents

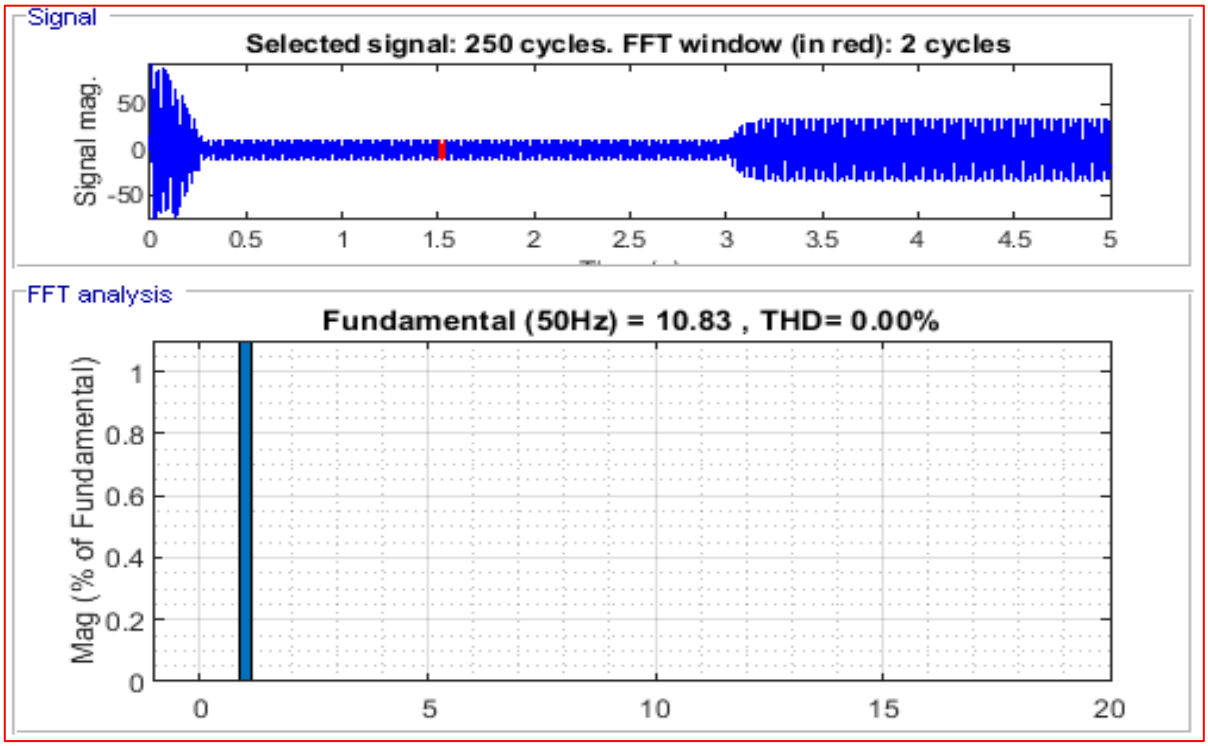

Figure III.13 Spectrum harmonic analysis of stator currents

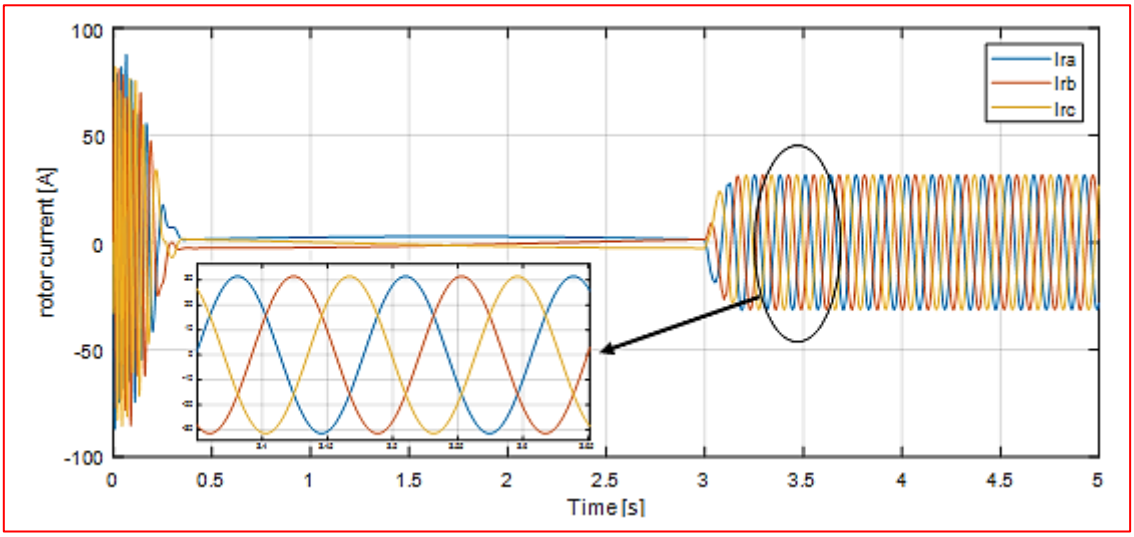

Figure III.14 Rotor currents

The Figure III.12 and III.13 shows the stator current and its spectrum harmonic analysis, we can see in these figures that the waveform of currents is purely sinusoidal and it THD is egal to zero.

The Figure III.14 present the rotor current are sinusoidal, figure III.9 show the electromagnetic torque with its reference that is charged to 100Nm at 3s, we observe in this case that the electromagnetic torque flow up perfectly its reference, finally figure 8 present the speed rotor, we can see that the speed is dynamic stable.

III.6 Conclusion

In this chapter, we have studied the modeling and simulation of the doubly-fed asynchronous machine, we have found that the model of the doubly-fed asynchronous machine is a system of differential equations. To simplify the machine model, we have established the machine model in a two-phase (d, q) axis system linked to the rotating field using the Park transformation. Simulation results are presented and interpreted. The next chapter will focus on control of the DFIG using direct power control.

CHAPTER VI

DPC FUZZY LOGIC CONTROL OF A WIND ENERGY CONVERSION SYSTEM BASED ON DFIG CONNECTED TO GRID

IV.1 Introduction

Doubly fed induction generators (DFIG) are extendedly used in modern wind power generation systems due to their variable speed operation [38], Classical control of grid-connected DFIG is usually based on the orientation of the stator voltage oriented, stator-flux (SFO), or vector control (VC) [39]. Control of instantaneous stator active and reactive powers is then achieved by regulating the decoupled rotor currents, using proportional-integral (PI) controllers. One main drawback for this control scheme is that the performance highly relies on the tuning of the PI parameters and accurate machine parameters such as stator and rotor inductances and resistances [40].

The progress of power electronics related to the onset of rapid switches and the development of digital technologies have enabled the control of power full with of high efficient controllers. New control strategies have been proposed such as direct power control (DPC) [41].

Direct Power Control (DPC) provides fast dynamic response, simple structure and proper operation in presence of parameter variations [42].

In this chapter, we study the control strategies of wind energy conversion system (WECS), we then present a direct power control (DPC) based PI controller and a DPC based fuzzy logic controller, additionally we present the results of simulation.

IV.2 Control strategies of WECS

The classification of control strategies for wind energy conversion systems (WECS) based on Doubly-Fed Induction Generators (DFIG) encompasses three primary categories:

- *Vector control*
- *Direct Torque Control (DTC)*
- *Direct Power Control (DPC)*

IV.2.1 Vector control

Most existing control methods use classical vector control based on voltage orientation control (VOC), or field-oriented control (FOC) [43].

Vector control occupies a significant place in today's industry. It was invented during the 1970s based on the control of separately excited DC machines, ensuring both dynamic and static performance via internal current control loops with a linear proportional-integral (PI) controller. However, it has poor dynamic performance, and its performance depends on machine parameters and the quality of the control loop, which is strongly influenced by grid voltage.

IV.2.1.1 Stator flux orientation

Aligning the control vector with the stator flux simplifies control and enhances performance under varying conditions. It ensures efficient utilization of the DFIG's capabilities.

IV.2.1.2 Rotor flux orientation

Similar to stator flux orientation, aligning the control with the rotor flux improves control over torque and power outputs. It optimizes the machine's performance in different operating scenarios.

IV.2.1.3 Voltage orientation

By aligning control with the system voltage, this method optimizes DFIG operation in response to voltage variations. It ensures stable operation and efficient power conversion.

IV.2.2 Direct torque control (DTC)

Direct Torque Control (DTC) emerged in the late 1980s as a control technique for squirrel-cage induction motors [44]. Later, in 2002, this method was expanded to Doubly Fed Induction Generators (DFIG) [45]. The DTC control relies on a vector representation of the output voltage space of the rotor-side converter, typically a two-level voltage source inverter. It excels in regulating both the flux and torque of the induction machine with greater precision, robustness, and speed compared to traditional vector control methods. The DTC control achieves this with a simplified control algorithm that is less sensitive to induction machine parameters.

IV.2.3 Direct power control (DPC)

Direct Power Control (DPC) emerged approximately twenty years ago to govern three-phase rectifiers. Unlike conventional techniques, the DPC control primarily concentrates on active and reactive powers as the primary variable signals [46] [47]. The DPC control eliminates the necessity for a pulse width modulation block and internal loops of controlled variables. Additionally, it removes the need for estimating control variables since active and reactive stator powers can be directly calculated from stator voltages and currents. Figure IV.1 illustrate the schematic structure of DFIG connected to the grid system.

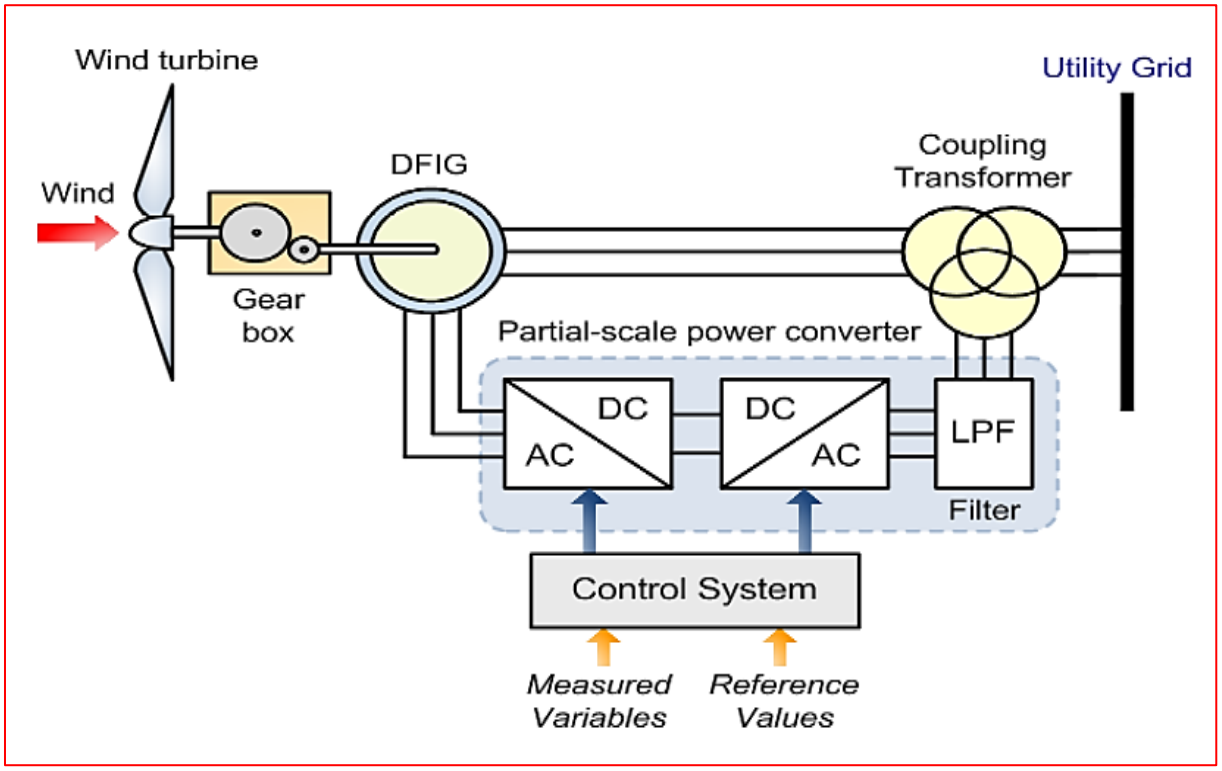

Figure IV.1 Schematic structure of DFIG connected to the grid

IV.2.3.1 Hysteresis band control based DPC

This method involves maintaining torque and flux within predefined bands. While it offers a straightforward control scheme, it may lead to higher ripples in torque and flux [48][49].

IV.2.3.2 Direct predictive power control based DPC

This method optimizes control actions to achieve desired power outputs. By forecasting system behavior, it can adapt control strategies in real-time.

IV.2.3.3 Sliding mode control based DPC

A robust approach, sliding mode control deals with uncertainties and disturbances by guiding system states towards equilibrium along a predefined surface. It ensures stability and robust performance.

IV.2.3.4 Pulse width modulation (PWM) / vector modulation

This method controls the switching of power electronics, such as inverters, to effectively regulate the speed and torque of the DFIG. By adjusting voltage and frequency, it maintains desired performance characteristics.

IV.2.3.5 Artificial intelligence (ai) based DPC

Techniques like neural networks, fuzzy logic, and genetic algorithms are employed to enhance control performance._ Fuzzy logic has been implemented in the direct power control of Doubly Fed Induction Generators (DFIG) by replacing the hysteresis-based controller and

conventional switching table with fuzzy logic-based controllers. While these enhancements aim to improve DPC performance, they concurrently introduce more intricate schemes. Figure IV.2 shows the classification of control strategies

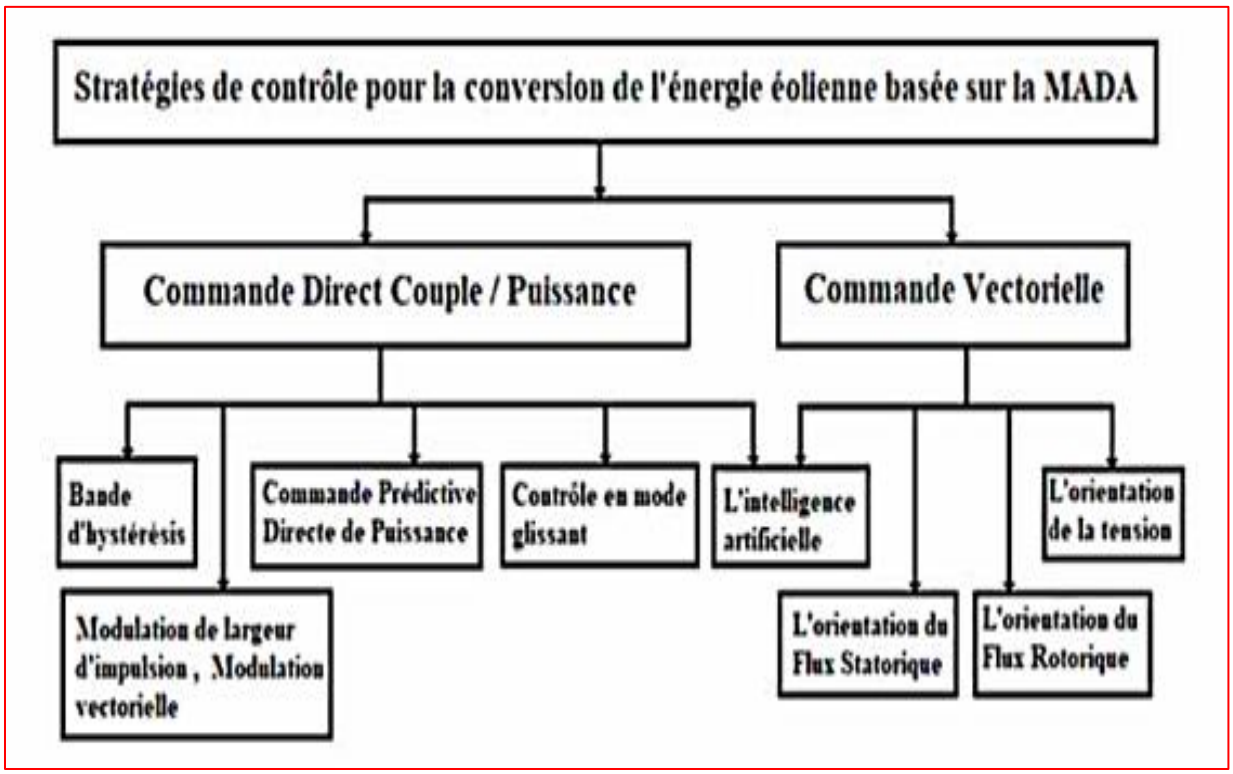

Figure IV.2 Classification of control strategies for wind energy conversion systems with doubly-fed induction generators [50]

In this work, the Direct Power Control (DPC) strategy is chosen for its simpler algorithm and good dynamic performance. This strategy estimates instantaneous variables with all harmonic components, leading to improved power factor and efficiency. Additionally, DPC offers decoupled control of active and reactive power.

IV.3 Direct power control based on pi controller

Direct Power Control (DPC) based on PI controller control strategy is used in power electronics and electrical drives to manage the power delivered by an inverter to a load, such as an electric motor or a power grid. The method relies on Proportional-Integral (PI) controllers to regulate the power flow by directly controlling the inverter's switching states.

IV.3.1 PI controller based direct power control

DPC is a technique used to control the active and reactive power in power converters without needing an intermediate voltage or current control loop. It involves measuring the power and using it directly to determine the switching states of the inverter, this technique is used the tow PI controllers

IV.3.2.1 Implementation steps of dpc using pi controller

- **Power calculation**

Measure the instantaneous active power (P) and reactive power (Q) from the inverter output.

These can be calculated using voltage and current measurements from the inverter output.

- **Error calculation**

Calculate the errors for active and reactive powers are given by:

$$(e_P = P_{ref} - P) \quad \textbf{(IV.1)}$$

$$(e_Q = Q_{ref} - Q) \quad \textbf{(IV.2)}$$

Where:

P_{ref} and Q_{ref} are the reference values for active and reactive power, respectively.

- **PI controller**

In DPC control, tow PI controllers are used for active and reactive power errors (figure IV.2). The output of these PI controllers will provide the control signals needed to adjust the inverter's switching states.

- **Switching state determination**

Based on the control signals from the PI controllers, determine the appropriate switching states for the inverter. The goal is to adjust the switching to minimize the power errors and achieve the desired power flow.

- **Inverter switching:**

Apply the calculated switching states to the inverter. This action adjusts the output voltage and current, thereby controlling the power delivered by DFIG.

IV.4 Fuzzy logic controller based direct power control

The principle of Fuzzy Logic-based Direct Power Control (DPC) involves integrating fuzzy logic techniques into the control strategy to enhance the robustness and adaptability of DPC in power electronic systems. Unlike conventional DPC, which relies on precise mathematical models and deterministic control rules, fuzzy logic-based DPC incorporates linguistic variables, fuzzy sets, and fuzzy rules to handle uncertainties and nonlinearities inherent in real-world systems. The core principle of fuzzy logic-based DPC revolves around the following key concepts:

IV.4.1 Fuzzy rule-based decision making

Fuzzy logic enables the formulation of fuzzy rules based on expert knowledge or empirical observations. These rules define relationships between input variables (such as error in active

and reactive power) and output control actions (such as switching states of the power converter). By leveraging linguistic variables (e.g., "low," "medium," "high") and fuzzy sets (e.g., "very low," "low," "medium," "high," "very high"), fuzzy logic-based DPC can handle imprecise and uncertain information effectively.

IV.4.2 Adaptive control strategy

Fuzzy logic-based DPC offers adaptability to varying operating conditions and system uncertainties. Instead of relying on fixed control rules, fuzzy logic allows for the adjustment of control actions based on real-time feedback and environmental changes. This adaptability enhances the robustness of DPC, making it suitable for dynamic and unpredictable systems such as renewable energy sources.

IV.4.3 Enhanced performance and flexibility

By incorporating fuzzy logic into DPC, the control system can exhibit improved performance and flexibility. Fuzzy logic-based DPC can accommodate a wider range of operating conditions and system dynamics compared to traditional DPC approaches. Additionally, it can handle non-linearities and uncertainties more effectively, leading to smoother and more reliable operation of power electronic systems.

The principle of fuzzy logic-based DPC involves leveraging fuzzy logic techniques to enhance the robustness, adaptability, and performance of DPC in power electronic systems. By incorporating linguistic variables, fuzzy sets, and fuzzy rules, fuzzy logic-based DPC can handle uncertainties and non-linearities inherent in real-world applications, making it a promising approach for various control challenges in power electronics.

IV.4.4 Equations and principles in fuzzy logic-based direct power control (DPC)

Fuzzy Logic-based Direct Power Control (DPC) involves a set of equations and principles to control active and reactive power. These equations form the basis of both the power control mechanism and the fuzzy logic system. Here is an outline of the key equations and steps involved in this control approach:

IV.4.4.1 Active and reactive power calculation

The first step in DPC is calculating the instantaneous active (P) and reactive (Q) power from the voltage and current measurements. These are typically calculated using the following equations:

$$P = v_{\propto} i_{\propto} + v_{\beta} i_{\beta} \quad \textbf{(IV.3)}$$

$$Q = v_{\propto} i_{\beta} - v_{\beta} i_{\propto} \quad \textbf{(IV.4)}$$

Here, v_α and v_β are the α-β components of the voltage, and $i_\alpha$and i_β are the α-β components of the current.

IV.4.4.2 Error calculation

The next step involves calculating the errors between the reference and actual values of active and reactive power:

$$e_P = P_{ref} - P_{actuel} \quad \textbf{(IV.5)}$$

$$e_Q = Q_{ref} - Q_{actuel} \quad \textbf{(IV.6)}$$

IV.4.4.3 Fuzzy logic controller

The fuzzy logic controller (FLC) processes the errors e_P and e_Q to determine the appropriate control actions. The FLC typically involves the following steps:

- **Fuzzification:**

Convert the numerical errors e_P and e_Q into fuzzy sets using membership functions.

- **Inference:**

Apply a set of fuzzy rules to the fuzzy inputs to determine the fuzzy output. The fuzzy rules can be expressed as:

- If (e_P is Low) and (e_Q is High) then (Control Action is Increase)
- If (e_P is High) and (e_Q is Low) then (Control Action is Decrease)

- **Defuzzification:**

Convert the fuzzy output back into a numerical value. This numerical value determines the adjustments to the switching states of the power converter.

IV.4.4.4 Switching state determination

Based on the output of the FLC, the appropriate switching states for the converter are determined. This involves mapping the fuzzy control action to specific switching signals for the converter switches._The switching state selection can be represented by a table or a set of conditional statements that translate the fuzzy controller's output into actions that adjust the switching states to minimize the power errors.

These steps collectively enable the fuzzy logic-based DPC to effectively regulate active and reactive power in power electronic systems, providing robust and adaptive control.

IV.5 Filter modeling

To minimize the ripple of the rectified voltage at the output of the rectifier, a capacitor C is placed in parallel at the output of the rectifier. This capacitor absorbs the difference between

the unidirectional current I and the current *Id*, thereby eliminating abrupt variations in U_{dc} during switching. However, to reduce the ripple in the current *Id* and protect the inverter against the critical rate of current increase, a smoothing inductance L with an internal resistance R is placed in series. Together, the L-R-C arrangement forms a low-pass filter [50], as illustrated in Figure IV.3.

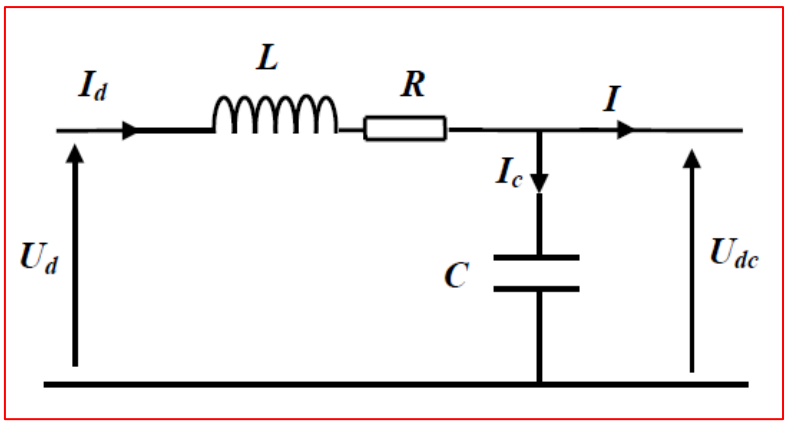

Figure IV.3 Representation of the low-pass filter

The equations of the filter are given by:

$$U_d(t) = L\frac{dI_d}{dt} + RI_d + U_{dc}(t) \quad \textbf{(IV.7)}$$

$$\frac{dU_{dc}(t)}{dt} = \frac{1}{c}(I_d(t) - I(t)) \quad \textbf{(IV.8)}$$

The transfer function of the filter is given by:

$$F(s) = \frac{U_{dc}(t)}{U_d(t)} = \frac{U_{filtered}}{U_{rectified}} = \frac{1}{L.C.s^2 + R.C.s + 1} \quad \textbf{(IV.9)}$$

It is a second-order filter with a cutoff frequency of [52]:

$$\omega_c = \frac{1}{\sqrt{L.C}} = 2.\pi.F_C \quad \textbf{(IV.10)}$$

Fc: is the cutoff frequency of the filter.

The simulation of the filter is shown in Figure IV.4.

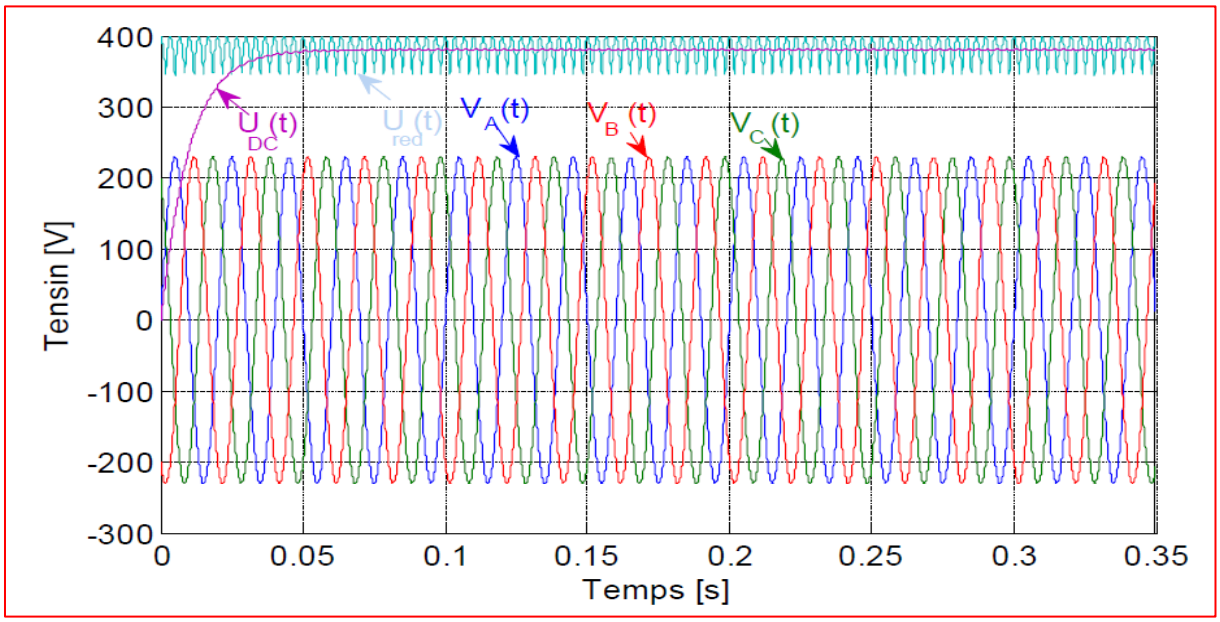

Figure IV.4 Filtered voltage [53]

IV.6 Voltage inverter modeling

After studying the rectifier and the filter, we now model the voltage inverter, which converts the DC voltage from a source into an AC voltage to power the rotor of the DFIG [52]. This inverter is composed of switching cells, typically IGBT thyristors for high power applications. The two-level three-phase inverter consists of six bidirectional switches, each made up of a transistor (T) and a diode (D) connected in an anti-parallel configuration in Figure IV.5.

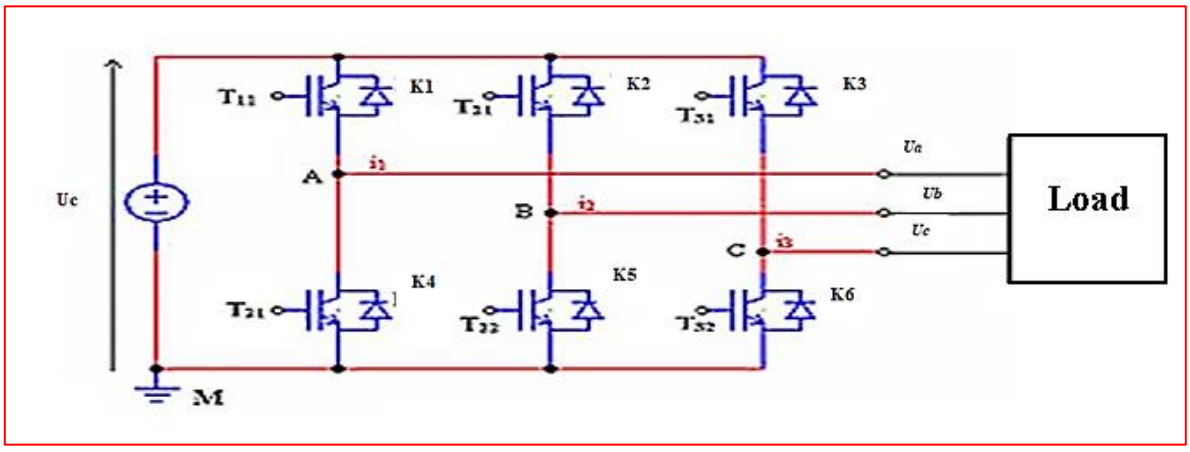

Figure IV.5 Two-level three-phase voltage inverter

The switches of each arm of the inverter are complementary; the same applies to the associated control signals. Therefore, we can write:

$$K_4 = 1 - K_1 \qquad K_5 = 1 - K_2 \qquad K_6 = 1 - K_3 \tag{IV.11}$$

The motor's phase voltages are denoted as: $V_A(t), V_B(t), V_C(t)$.

The motor's line-to-line voltages are denoted as: $U_{AB}(t), U_{BC}(t), U_{CA}(t)$

The voltage V_{AO} equals $\frac{V_{DC}}{2}$ when K_1=1 and K_4=0. It becomes $-\frac{V_{DC}}{2}$ when K_1=0 and K_4=1. The same reasoning applies to V_{BO} using the controls $K_2$and K_5 , and forV_{CO}using the controls K_3 and K_6.

The voltages V_{AO}, V_{BO}, V_{CO} are given by the following relations:

$$\begin{cases} V_{AO} = (K_1 - K_4)\frac{V_{DC}}{2} = (2K_1 - 1)\frac{V_{DC}}{2} \\ V_{BO} = (K_2 - K_5)\frac{V_{DC}}{2} = (2K_2 - 1)\frac{V_{DC}}{2} \\ V_{CO} = (K_3 - K_6)\frac{V_{DC}}{2} = (2K_3 - 1)\frac{V_{DC}}{2} \end{cases} \quad \textbf{(IV.12)}$$

The phase voltages are then expressed as follows:

$$\begin{cases} U_{AB} = V_{AO} - V_{BO} = (K_1 - K_2)V_{DC} \\ U_{BC} = V_{BO} - V_{CO} = (K_2 - K_3)V_{DC} \\ U_{CA} = V_{CO} - V_{AO} = (K_3 - K_1)V_{DC} \end{cases} \quad \textbf{(IV.13)}$$

The voltage system V_A , V_B,and V_C is balanced, which allows us to establish the expressions for the phase voltages:

$$\begin{cases} V_A = \frac{U_{AB} - U_{CA}}{3} \\ V_B = V_A - U_{AB} = \frac{-2U_{AB} - U_{CA}}{3} \\ V_A = V_A + U_{CA} = \frac{U_{AB} + 2U_{CA}}{3} \end{cases} \quad \textbf{(IV.14)}$$

By introducing the relations (IV.13), we finally obtain:

$$\begin{cases} V_A = (2K_1 - K_2 - K_3)\frac{V_{DC}}{3} \\ V_B = (2K_2 - K_1 - K_3)\frac{V_{DC}}{3} \\ V_C = (K_3 - K_1 - K_2)\frac{V_{DC}}{3} \end{cases} \quad \textbf{(IV.15)}$$

The state of the switches, assumed to be ideal, can be defined by three Boolean control variables $S_i(i = a, b, c)$:

- $S_i = 1$, when the upper switch is closed and the lower one is open.
- $S_i = 0$, when the upper switch is open and the lower one is closed.

Under these conditions, the phase voltages can be written in the following matrix form:

$$\begin{bmatrix} V_A \\ V_B \\ V_C \end{bmatrix} = \frac{V_{DC}}{3} \begin{bmatrix} 2 & -1 & -1 \\ -1 & 2 & -1 \\ -1 & -1 & 2 \end{bmatrix} \begin{bmatrix} S_a \\ S_b \\ S_c \end{bmatrix} \quad \textbf{(IV.16)}$$

IV.6.1 PWM control strategy

The principle of Pulse Width Modulation (PWM) involves switching between the inverter states such that the average value of the switched voltage matches the reference voltage. Since the voltage level of the inverter leg is constant, modulation is achieved by varying the pulse width (or its duty cycle). This technique is implemented in an analog circuit by comparing a fixed amplitude carrier signal $V_P(t)$with amplitude $V_P$to a sinusoidal reference signal $V_r(t)$with variable amplitude and frequency. The points of intersection between these signals determine the switching instances.

Two parameters characterize this strategy:

- The modulation index m, which is defined as the ration of the carrier frequency F_P the reference voltage frequency F:

$$m = \frac{F_P}{F} \quad \textbf{(IV.17)}$$

- The modulation rate M, which is the ratio of the reference voltage amplitude V_{ref} to that of the carrier (U_P)

$$M = \frac{V_{Pref}}{U_P} \quad \textbf{(IV.18)}$$

The maximum value of the phase voltage at the output of the inverter is exactly:

$$V_{max} = M.\frac{V_{DC}}{2} \quad \textbf{(IV.19)}$$

The control algorithm for a two-level inverter for a phase leg K can be summarized in two steps

- Step 1:

$$\begin{cases} V_{refk} \geq U_P \Rightarrow V_k = V_{DC} \\ V_{refk} < U_P \Rightarrow V_k = -V_{DC} \end{cases} \quad \textbf{(IV.20)}$$

Where V_{DC} is the DC bus voltage.

- Step 2:

$$\begin{cases} V_k = V_{DC} \Rightarrow S_k = 1 \\ V_k = -V_{DC} \Rightarrow S_k = 0 \end{cases} \quad \textbf{(IV.21)}$$

IV.7 Simulation results

IV.7.1 Simulation results of DPC based on pi controller for WECS

For this case, figure IV.6 presents the bloc diagram of proposed system in Matlab/Simulink, the system parameters of DFIG are presented in the table IV.1.

Table IV.1 The simulation parameters of the DFIG used for WECS

Parameters	Values
Nominal power	2000000 W
Voltage	690 V
Frequency	50 Hz
Stator resistance	0.0026 ohm
Stator inductance	0.002587 H
rotor resistance	0.0029 ohm
rotor inductance	0.002587 H
inertia	127 J(kg.m^2)
pole pairs	2

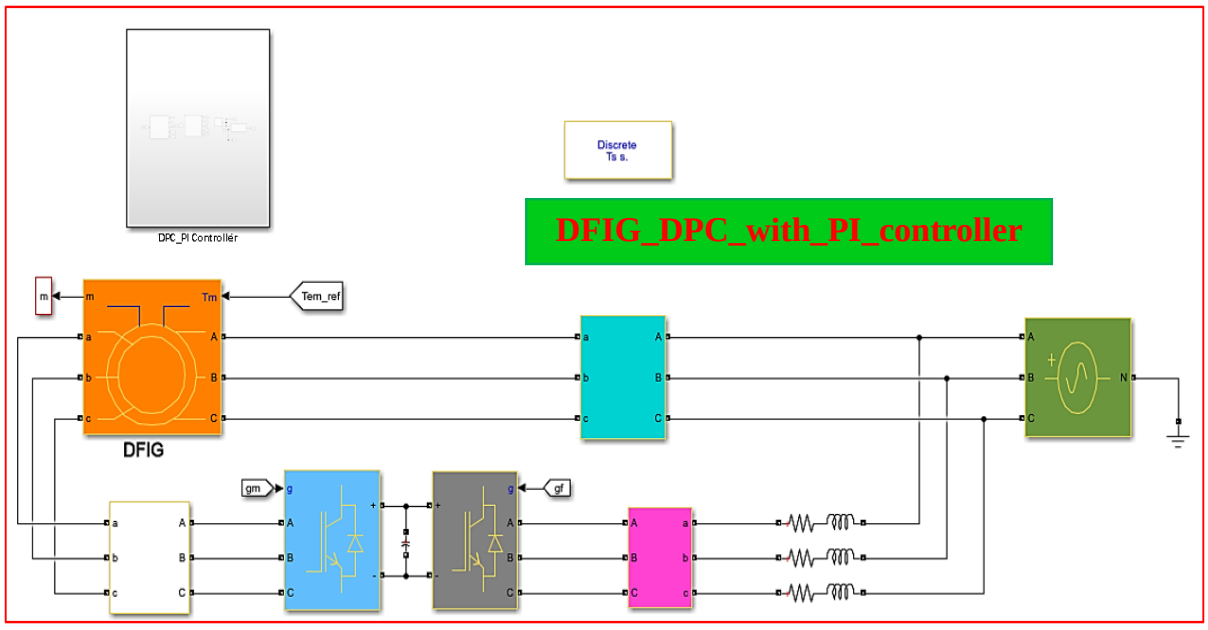

Figure IV.6 Block diagram of DFIG connected to wind turbine using DPC with PI controller

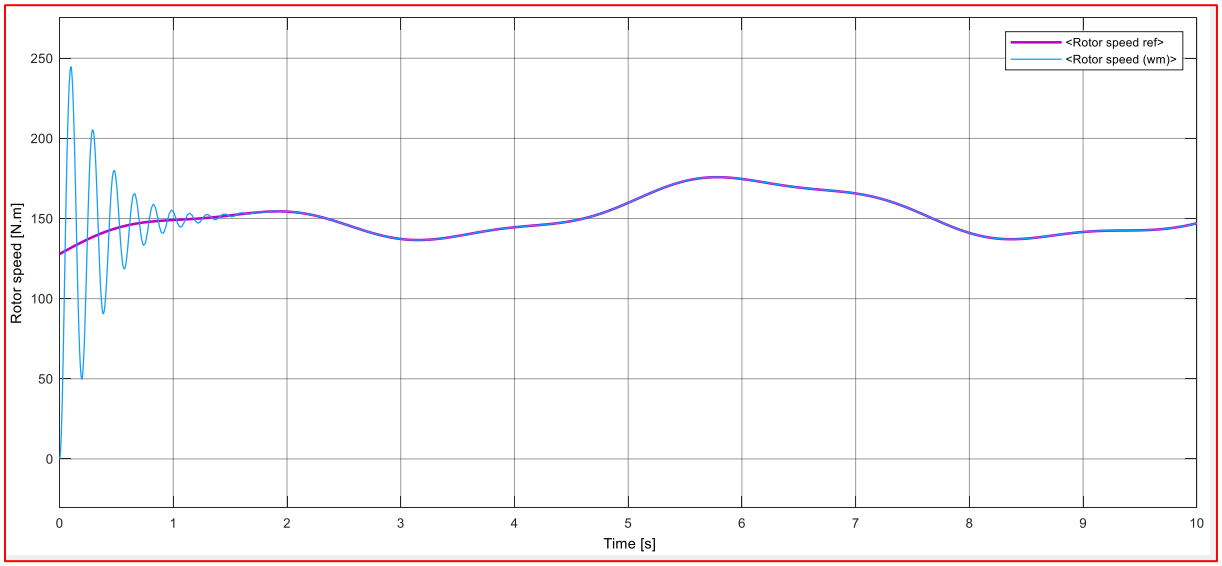

Figure IV.7 Mechanical speed using DPC with PI controller

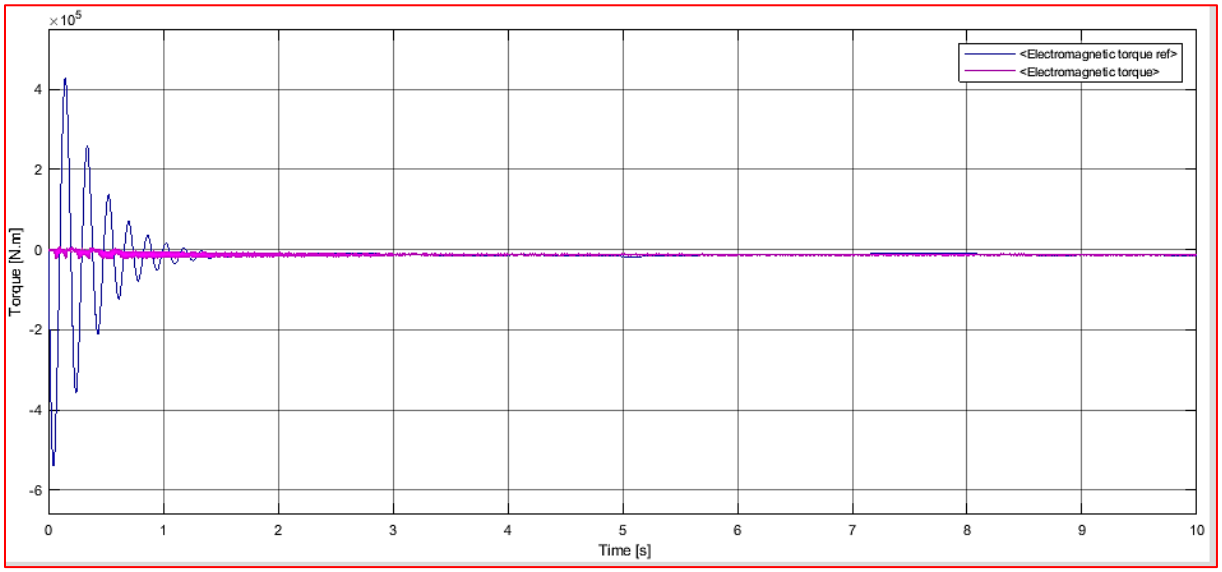

Figure IV.8 Electromagnetic torque using DPC with PI controller

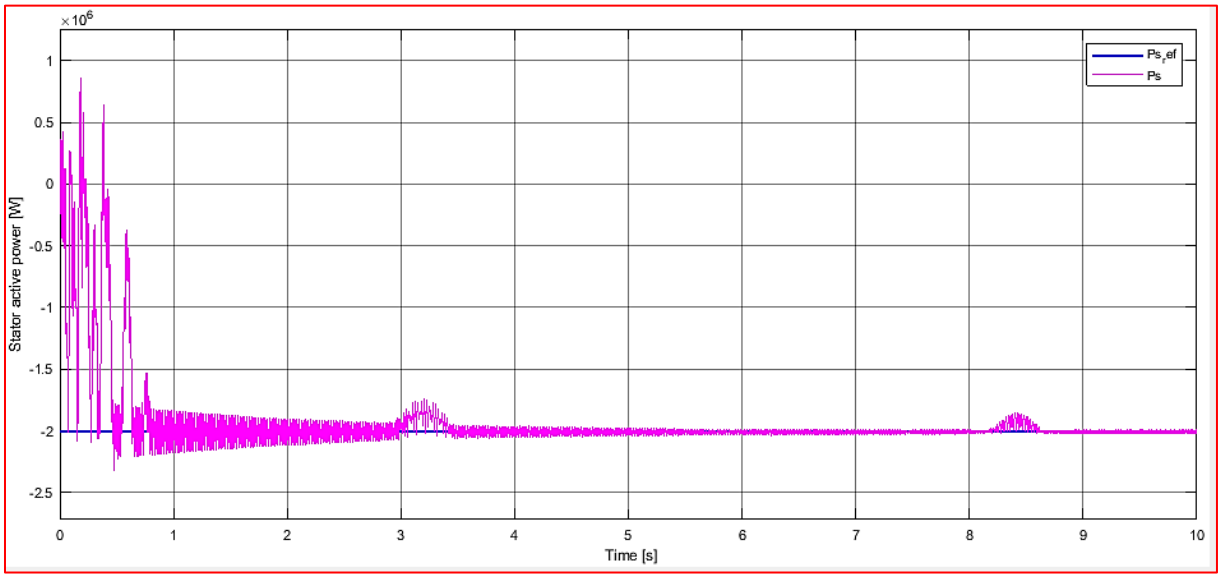

Figure IV.9 Stator active power using DPC with PI controller

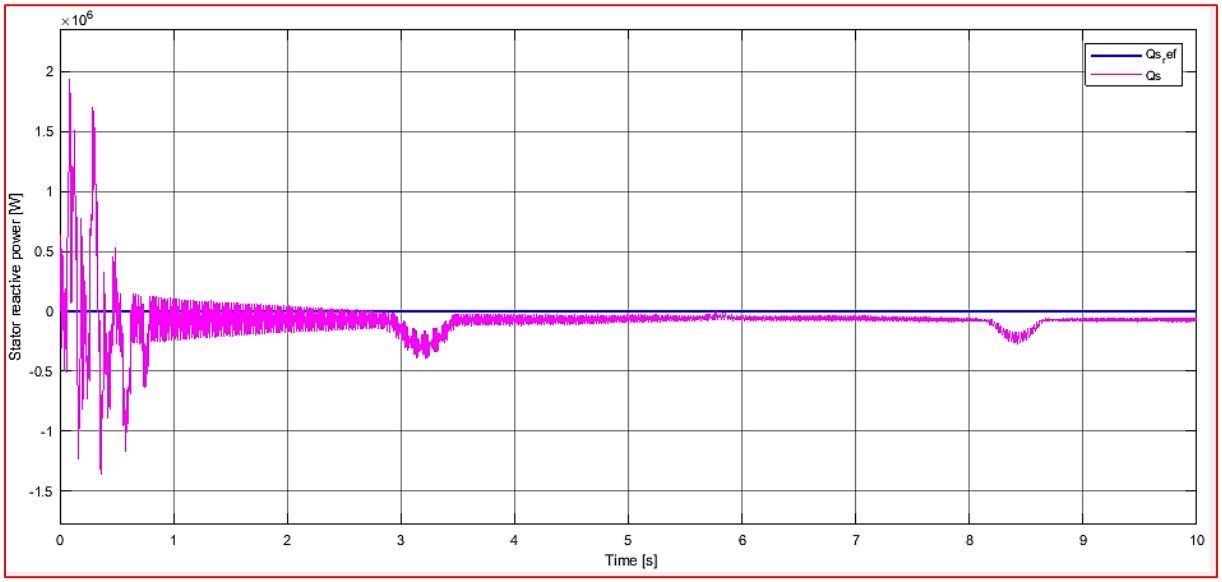

Figure IV.10 Stator reactive power using DPC with PI controller

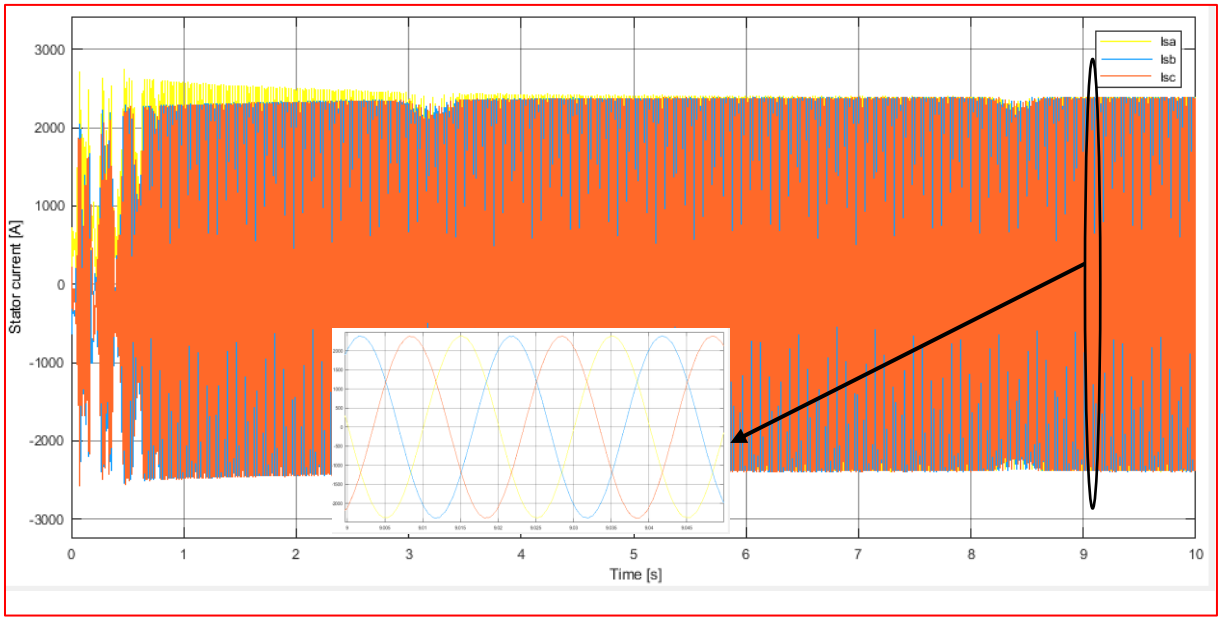

Figure IV.11 Stator currents using DPC with PI controller

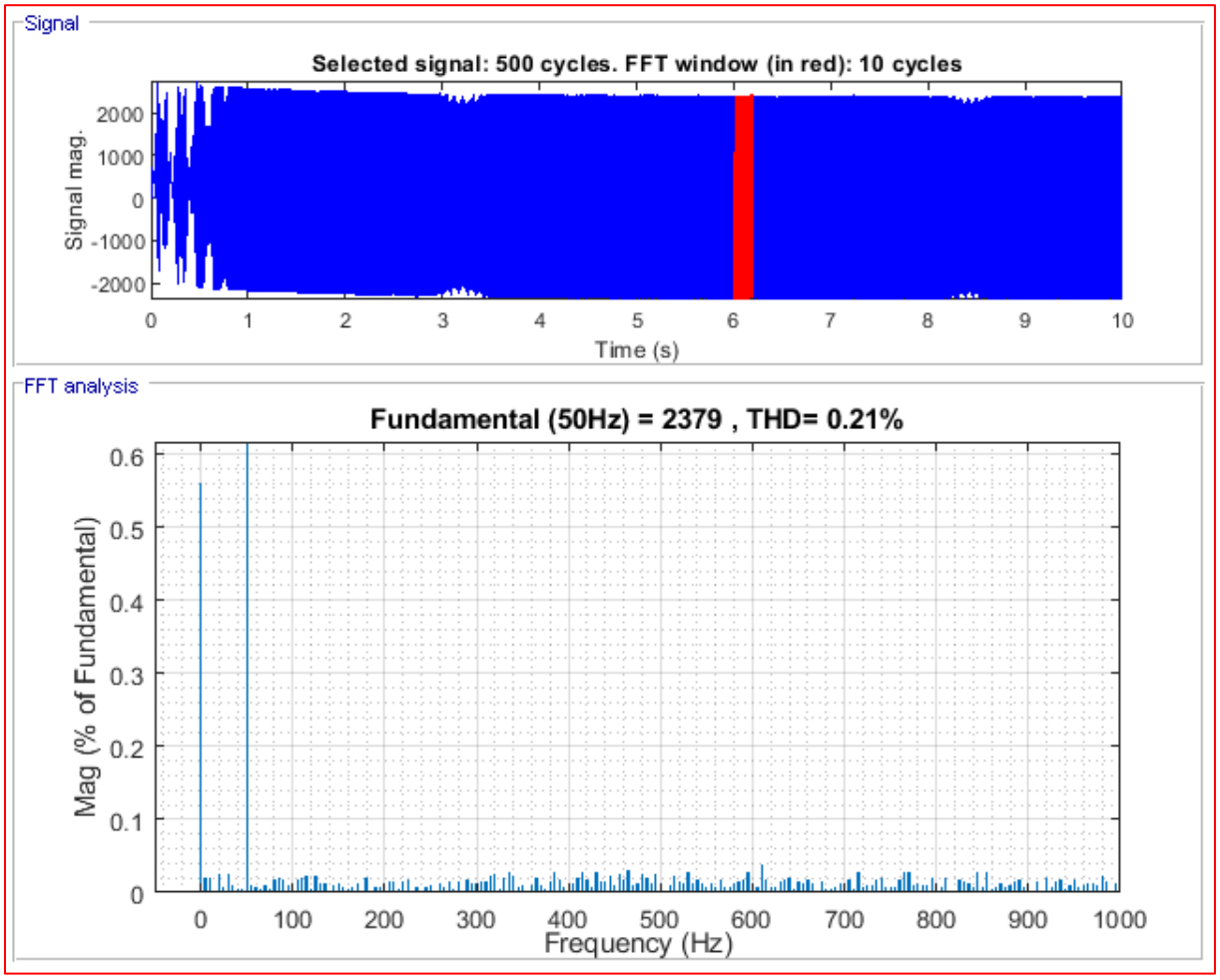

Figure IV.12 Spectrum harmonic analysis of stator currents using DPC with PI controller

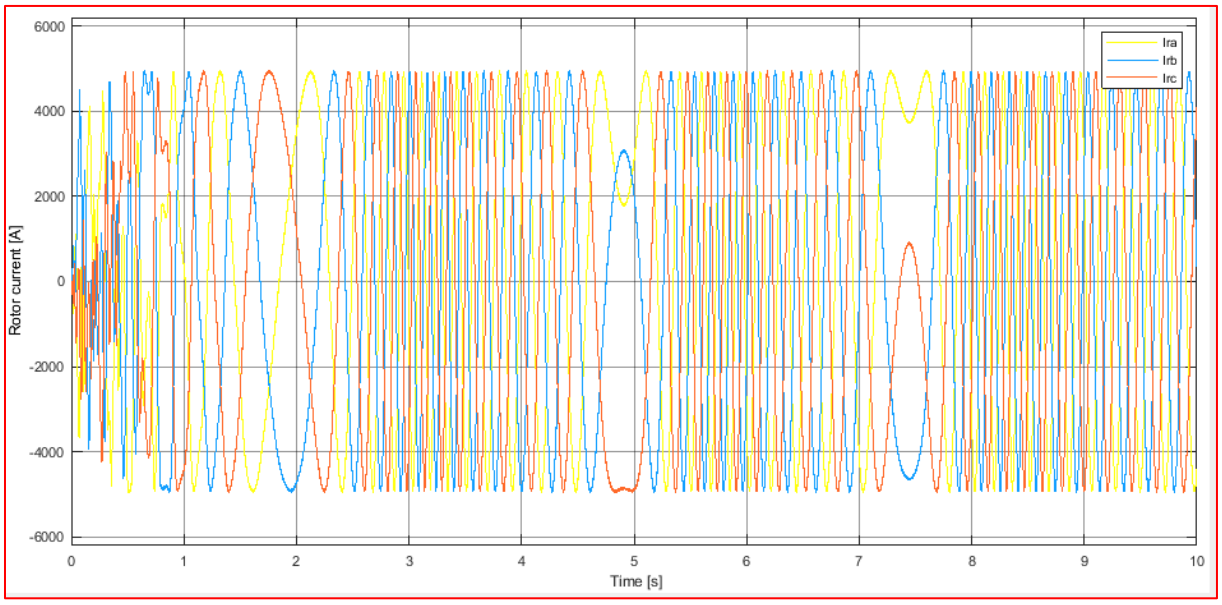

Figure IV.13 Rotor currents using DPC with PI controller

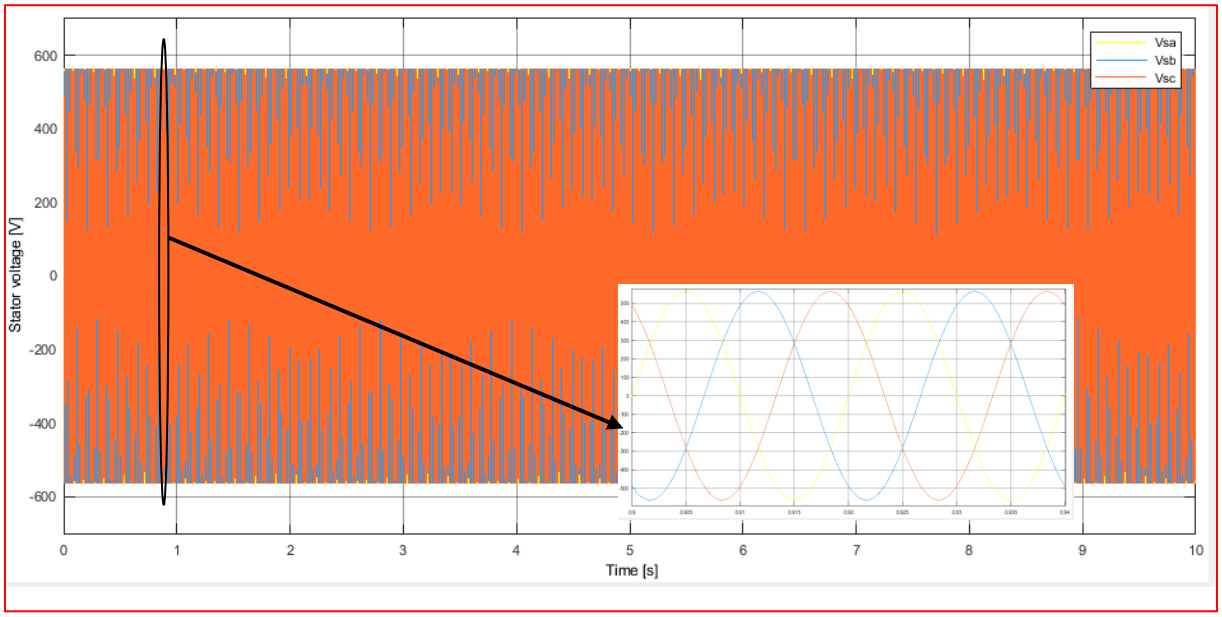

Figure IV.14 Stator voltage using DPC with PI controller

Figures VI.11 and VI.12 show the stator current and its harmonic spectrum analysis. These figures illustrate that the current waveform is almost sinusoidal, with a Total Harmonic Distortion (THD) of 0.21%.

Figure VI.13 presents the rotor current, which is also sinusoidal in nature; Figure VI.7 displays the mechanical speed and its reference, showing a perfect tracking of the reference speed.

Figures VI.9 and VI.10 illustrate the stator active power and stator reactive power, respectively. The active power tracks its reference at -2,000,000 W, and the reactive power tracks its reference at 0 var.

Finally, Figure VI.8 shows the electromagnetic torque, which accurately follows its reference.

In conclusion, these results demonstrate that direct power control with a PI controller provides excellent performance and maintains high accuracy in power control.

IV.7.2 Simulation results of DPC based on fuzzy logic controller for WECS

The simulation results have been validated through numerical simulation using MATLAB/Simulink software. The figures IV.15 presents the bloc diagram of proposed system.

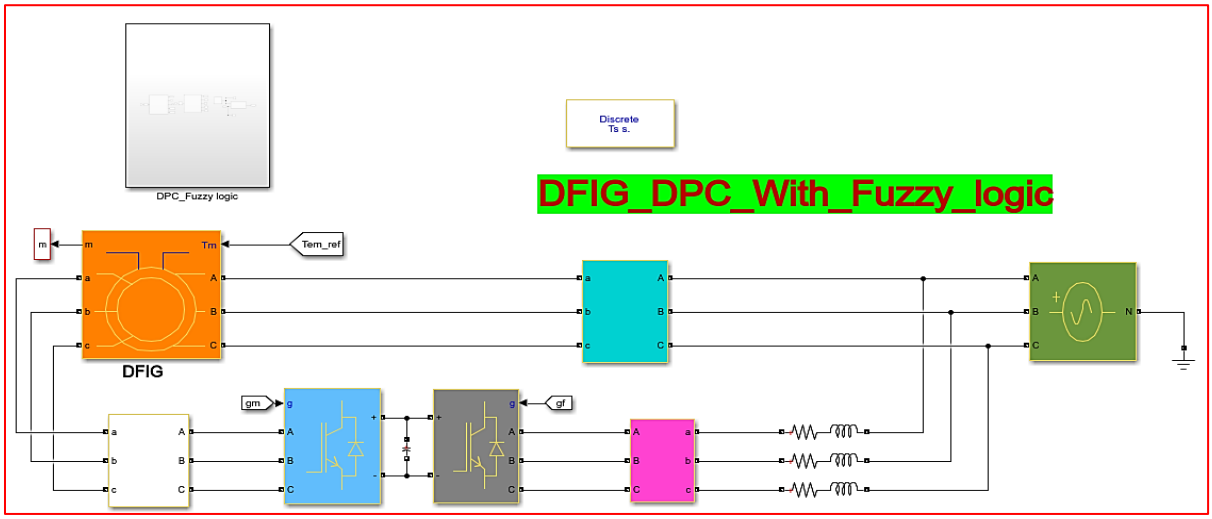

Figure IV.15 Block diagram of DFIG connected to wind turbine using DPC with fuzzy logic controller

The simulation results have been validated through numerical simulation. We observe in Figures below, the electromagnetic torque. This substantial torque signifies that the generator is generating a noteworthy amount of torque, essential for efficiently converting mechanical wind energy into electrical energy. Moreover, it demonstrates the DPC control capability to manage substantial torque fluctuations while upholding optimal performance.

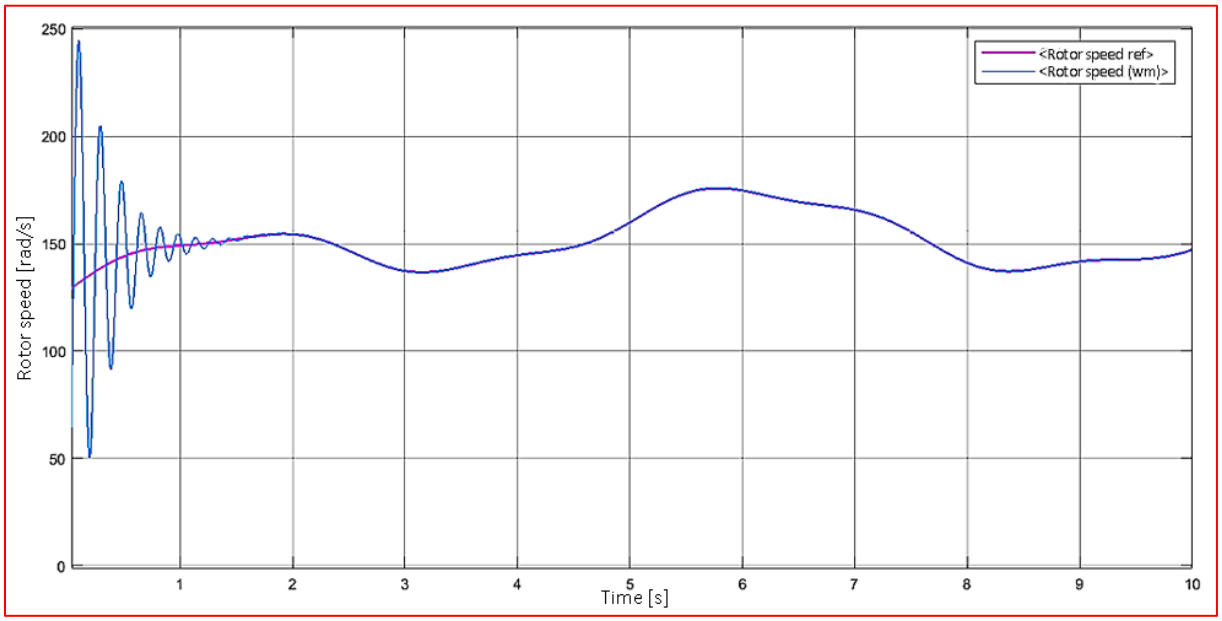

Figure IV.16 Mechanical speed using DPC with fuzzy logic controller

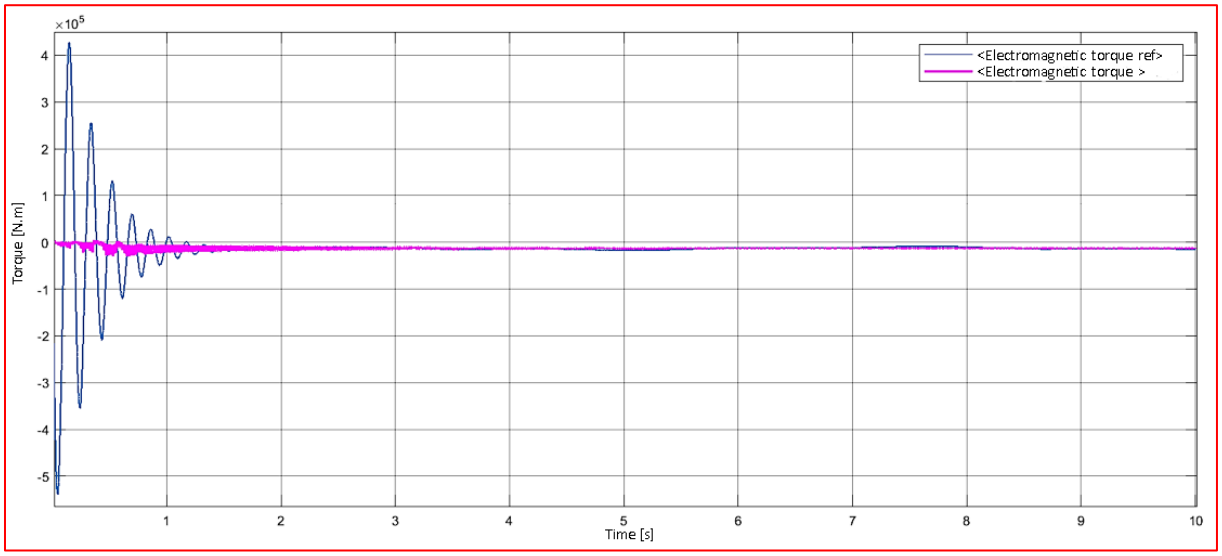

Figure IV.17 Electromagnetic torque using DPC with fuzzy logic controller

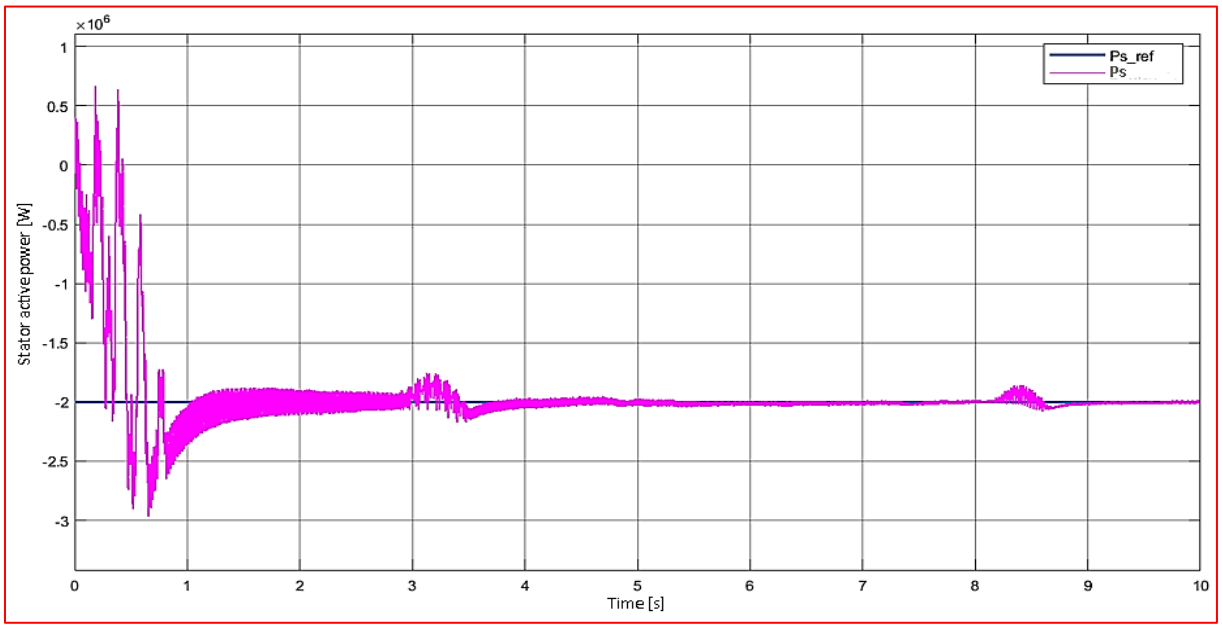

Figure IV.18 Stator active power using DPC with fuzzy logic controller

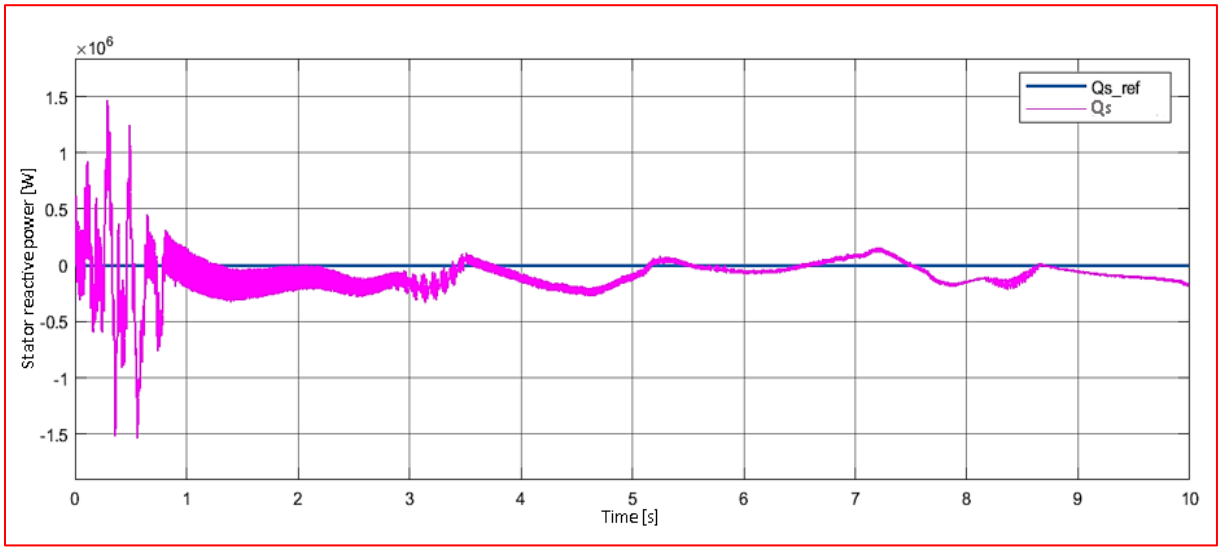

Figure IV.19 Stator reactive power using DPC with fuzzy logic controller

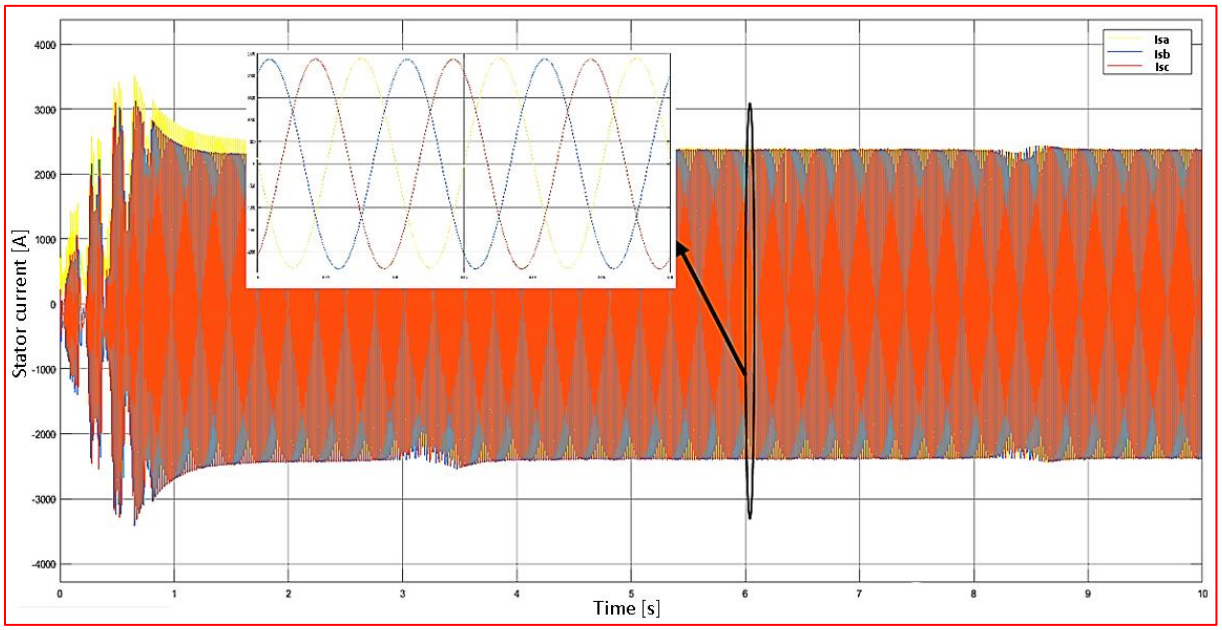

Figure IV.20 Stator currents using DPC with fuzzy logic controller

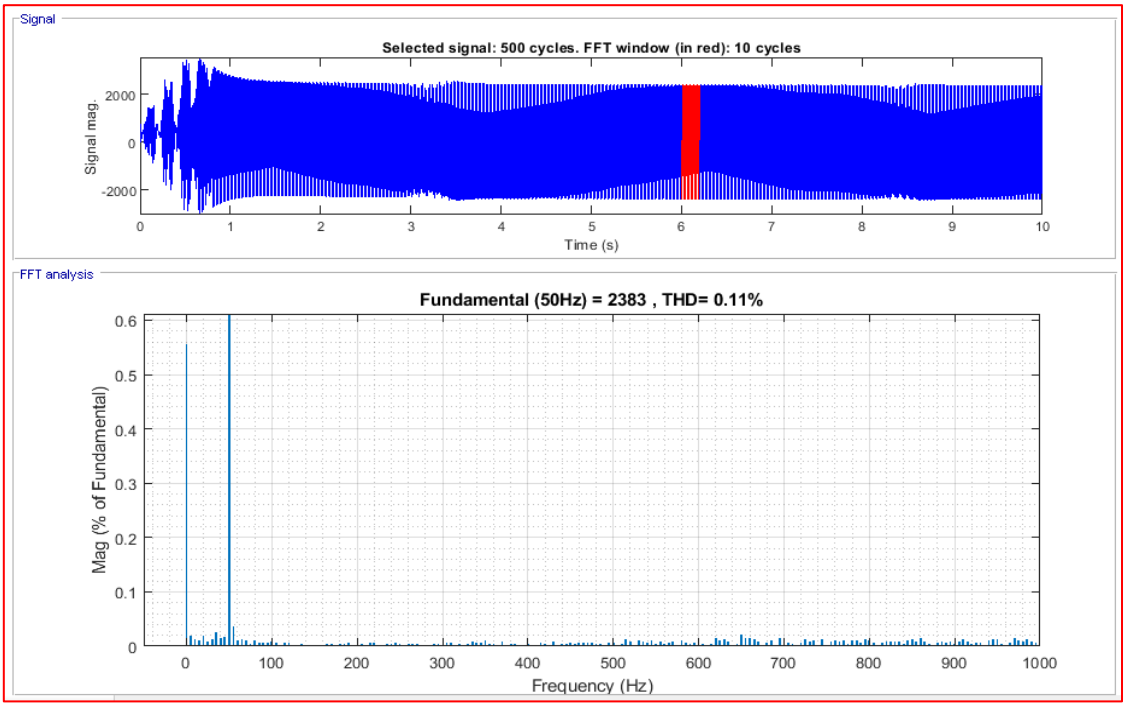

Figure IV.21 Spectrum harmonic analysis of stator currents

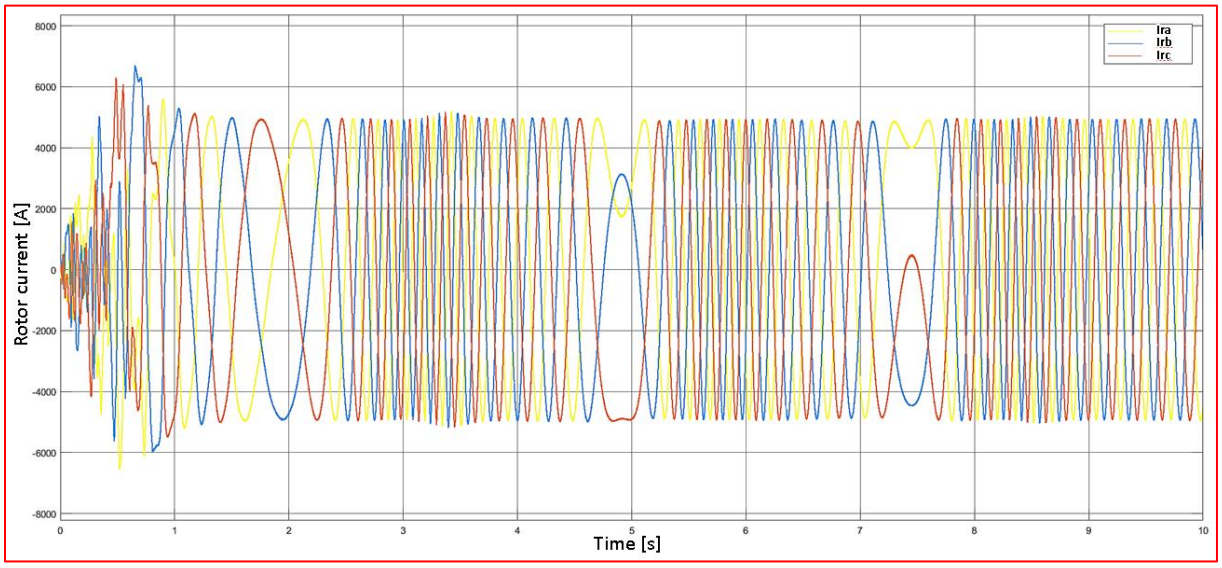

Figure IV.22 Rotor currents using DPC with fuzzy logic controller

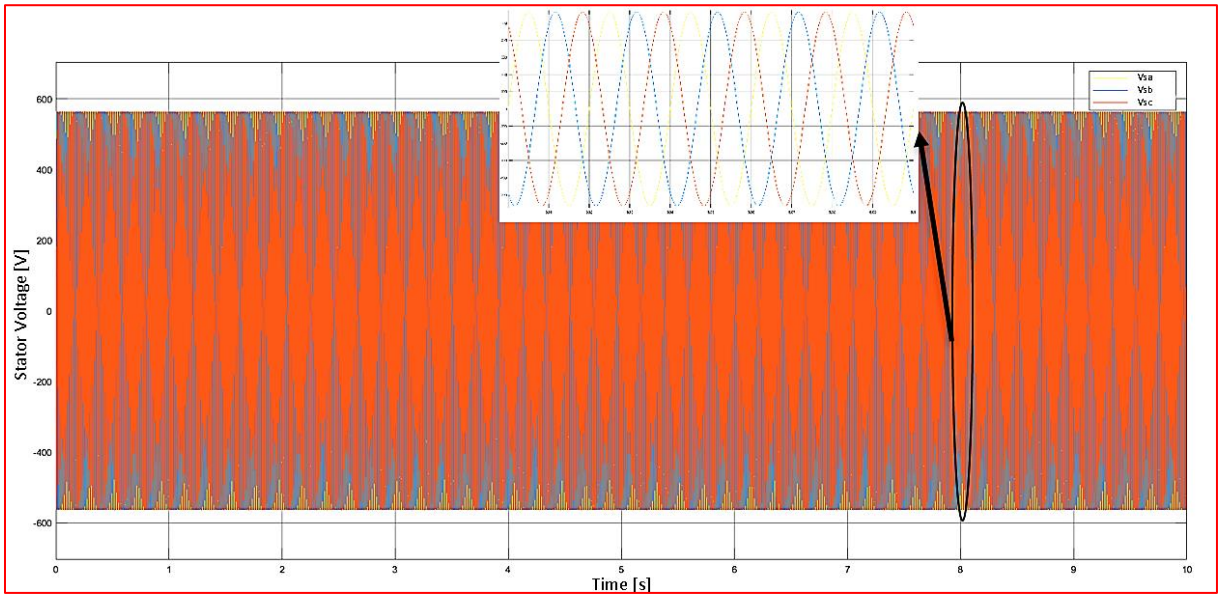

Figure IV.23 Stator voltage using DPC with fuzzy logic controller

With the integration of Fuzzy Logic Control (FLC) into the DPC system for a wind power system based on a Doubly-Fed Induction Generator (DFIG), we observe significant improvements across various parameters. The stator and rotor currents remain sinusoidal, indicating sustained stability and efficient operation. The active power closely follows the reference of -2000000 [W], demonstrating enhanced accuracy in power generation. The reactive power maintains zero VAR, reflecting superior compensation for inductive and capacitive components, thereby optimizing the power factor more effectively. Additionally, the rotor speed adheres precisely to the reference speed, indicating more refined control and higher efficiency in energy conversion. Overall, the incorporation of FLC with DPC results in a more robust and responsive system, enhancing stability, efficiency, and accuracy in power control.

The figure IV.24 demonstrates that the power of the DFIG follows the reference power, validating the effectiveness of the developed and utilized control strategy.

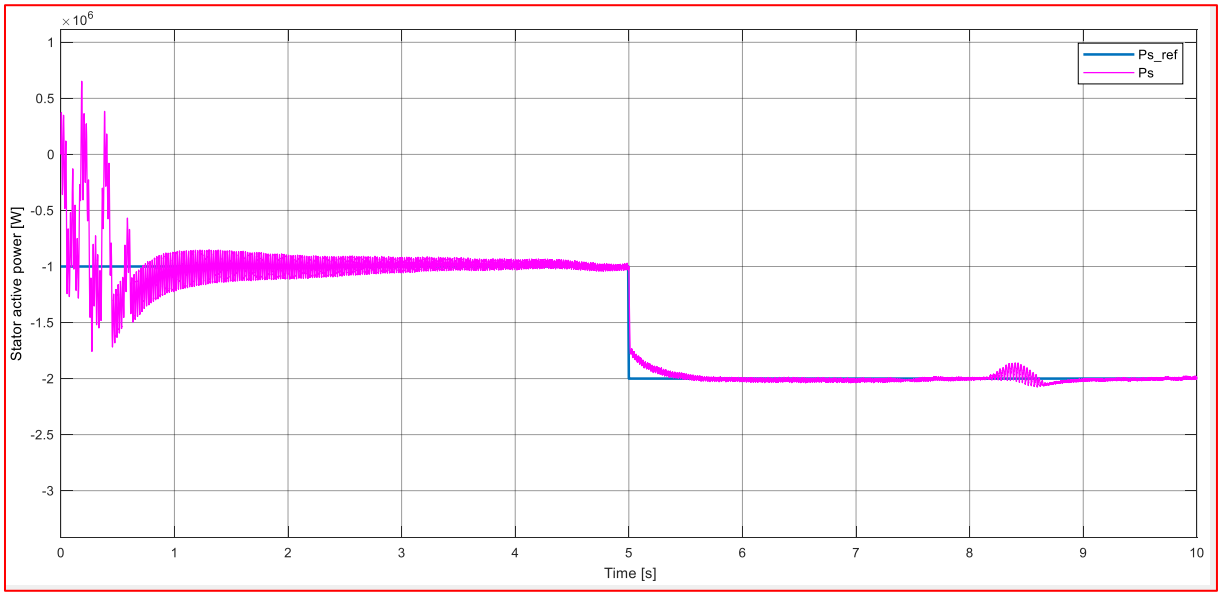

Figure IV.24 Stator active power with a variable values using DPC with fuzzy logic controller

From the comparison of the results with the PI controller and fuzzy logic, we observed that the quantities studied, such as the active power of DFIG, are almost the same. this is due to the precise calculation of the PI controller parameters as well as the parameters of the fuzzy logic controller.

IV.6 Conclusion

In this chapter, we explored control strategies for wind energy conversion systems using Doubly-Fed Induction Generators (DFIG), based on Direct Power Control (DPC) with the PI and fuzzy logic controller to improve the performance of the system. The results showed that the PI controller in DPC effectively reduced oscillations in torque and power, improving stability and performance. Incorporating fuzzy logic further improved the system's response to varying conditions, enhancing flexibility and long-term stability. This study advances our understanding of renewable energy systems and suggests pathways for developing more efficient and sustainable solutions.

GENERAL CONCLUSION

General conclusion

The work done in this project involves studying and simulating the control of a doubly-fed induction generator (DFIG) in a wind energy conversion system. To do this, we modeled and simulated the different parts of the conversion system. To capture the maximum power from a wind turbine, an MPPT (Maximum Power Point Tracking) control algorithm is used. The control of the active and reactive powers of the DFIG is done using direct power control.

To achieve our goal, we introduced general information about renewable energy, its different types, and their advantages and disadvantages in the first chapter. We also discussed renewable energy strategies in Algeria in this chapter.

In the second chapter, we established the mathematical model of the main components of the electromechanical conversion system in the wind turbine. We focused on the study of the mechanical part of the wind turbine and its control. We developed a technique to maximize the extracted power. The simulation results of these algorithms (MPPT) showed the effectiveness of the control in tracking the optimal operating point.

Then, in the third chapter, we studied the mathematical model of the DFIG and presented it in both three-phase and two-phase reference frames with the simulation of the DFIG directly connected to the electrical grid. We examined its electrical and electromagnetic characteristics.

Since the induction generator is used for energy production in the wind energy field, it is very useful to think in terms of power. Therefore, in the fourth chapter, we developed a direct power control method that allows the control of both active and reactive power. The results obtained show good tracking of the setpoints for both active and reactive power by the actual powers delivered by the stator of the machine, proving the effectiveness of the applied control.

This work is completed with a simulation of the overall conversion system with the DFIG directly connected to the grid in the MATLAB/SIMULINK environment

REFERENCES

References

[1] YOUMATTER world, "Energie renouvelable : définitions, exemple, avantage et limites ", https://youmatter.world/fr/definitions/energies-renouvelables-definition, 24sep2020.

[2] "Les energies renouvlables : les contraintes techniques, les contraintes economiques", from https://lms.fun-mooc.fr/c4x/ENSMP/76001S02/asset/M1-V3.docx.

[3] HERISSI Belgacem, "Commande d'une Eolienne basée sur les modèles flous de Takagi-Sugeno", Thèse master, 2016.

[4] L. Hamane, "Les ressources éoliennes de l'Algérie (2003) Revue des Energies Renouvelables", - N°3- CDER.

[5] N. Kasbadji Marzouk, "Quel avenir pour l'Energie Eolienne en Algérie? ", Bul. Ene. Ren, CDER, N°14, Dec 2008, p.6-7.

[6] A. Hadj arab, B. Ait driss, R. Amimeur, E. Lorenzo, "Photovoltaic systems sizing for Algeria. Solar Energy", 54 (1995) pp. 99-104.

[7] A. Rahmane, A. Bentafat, A. Sellami, "Eploitation of Solar Energie Between the German Leadership and The Reality of The Algerian Experience: Analytical Study During The Period (2000-2017) ", january 2019.

[8] AZIZI Amina, "Modélisation optimisation d'un système de production d'énergie photovoltaïque avec un système de stockage hybride", Thèse doctorat, 2019.

[9] "disadvantages of renewable energy", EnergySage, from https://www.energysage.com/about-clean-energy/advantages-and-disadvantages-of-renewable-energy/.

[10] Algerian Official Gazette, 2020, p. 53.

[11] Our World in Data. (n.d.). "Algeria : Energy Country Profile", Retrieved May 22, 2024, from Our World in Dat.

[12] Aggoun Ghania, "Etude qualitative de l'association convertisseur machine pour l'entrainement électrique d'une système de génération éolien-ou", mémoire de magister, Université tizi-ouzou, 2010.

[13] J. Martin, "Energies éoliennes", Techniques de l'Ingénieur, traité de Génie énergétique, pp. B 8 585 1- B 8 585 21,2002.

[14] L. HAMANE, "les ressources éoliennes de l'Algérie ", Bul. Ene. Ren, CDER, N°3, juin 2003. P 10-11.

[15] N. laverdure, I. Valero, S. Bacha, L.Gerbaud, " Optimisation de l'interfaçage de puissance dans les systèmes éoliens", GEVIQ'2002, merseille, 2002.

[16] Z. Stein, "Wind Energy Conversion System (WECS) ", february 5,2024.

[17] S. N. Bhadra, D. Kastha, S. Banerjee, "Wind Electrical Systems ", Oxford University Press 2005.

[18] B. BELTRAN, "contribution à la commande robuste des éoliennes à base de la GADA : du mode glissant classique au mode glissant d'ordre supérieur ", Thèse de Doctorat, Université de Bretagne occidentale, juillet 2010.

[19] F. POTIERS, " Etude et commande de génératrices asynchrones pour l'utilisation de l'énergie éolienne ", thèse de doctorat de l'université de Nantes, 2003.

[20] S. EL AIMANI, " Modélisation de différents technologies d'éoliennes intégrées dans un réseau de moyenne tension ", Thèse de doctorat, 2004, Ecole central de LIILE.

[21] LUO Cheng-xian."State Status and Prospect Forecast of World Wind Power" [J] .China& Foreign Energy, 2012, (03): 24-31.

[22] M. MALKI, S. BELARBI, " Etude et simulation d'un aérogénérateur connecter au réseau (Turbine + MADA + Réseau) en mode continu et discret ", Université Aboubeker Belkaid Tlemcen, Master en électrotechnique, 2014.

[23] H.BOUKHAMKHAM"Diagnostique des défaillances dans une machine asynchrone utilisé dans une chaine éolienne " Magister en électrotechnique, université de Biskra, 2011

[24] I. Darouaz, S. Chikh salah, "Etude et controle intelligent d'une chaine de conversion eolienne utilisant une GSAP ", Université ibn-khaldoun Tiaret, Master en automatization et controle des systémes industriels.

[25] M. Bahia, " Etude et commande d'une turbine éolienne utilisant une Machine Asynchrone à Double Alimentation", Mémoire de Magister API Université de TLEMCEN, 2011.

[26] L. Khelfat, L. Maataoui, "Etude et Simulation d'une éolienne à base d'une Machine Asynchrone Doublement Alimentée", Memoire De Master UNIVERSITE BADJI MOKHTAR-ANNABA, 2017.

[27] S. A. BELARBI, M. MALKI, "Etude et Simulation d'un aérogénérateur connecté au réseau (Turbine + MADA + Réseau) en mode continu et discret", Mémoire De Master En Electrotechnique Université Aboubekr Belkaid Tlemcen, 20/10/2014.

[28] P. Frédéric, "etude et commande de generatrices asynchrones pour l'utilisation de l'energie eolienne -Machine asynchrone à cage autonome -Machine asynchrone à double alimentation reliée au réseau", Thèse de Doctorat en Electronique et Génie Electrique à l'Ecole polytechnique de l'Université de Nantes, 2003.

[29] L. M. Tahar, "Commande Floue de la Machine Synchrone à Aimant Permanant (MSAP) utilisée dans un système éolien", Mémoire de Magister en Électrotechnique Université Ferhat Abbas de Setif, 24 /06 /2012.

[30] L. Khelfat, L. Maataoui, "Etude et Simulation d'une éolienne à base d'une Machine Asynchrone Doublement Alimentée", Memoire De Master UNIVERSITE BADJI MOKHTAR-ANNABA, 2017.

[31] M. Smaili, "Modélisation Et Commande D'un Aérogénérateur À Machine Asynchrone À Double Alimentation En Vue de Simulation des Problèmes de Cogénération", Mémoire de la Maîtrise en Ingénierie Universite du Quebec En Abitibi-Temiscamingue, Août 2013.

[32] H. M. Amine, "Influence de la commande d'une GADA des systèmes éoliens sur la stabilité des réseaux électriques", Mémoire Magister en Electrotechnique Sétif, 2012.

[33] B. A. ASMA, "Etude de la commande d'un systeme éolien base sur une GADA", Université Hadj Lakhdar - Batna, 2016.

[34] H. TAMRABET, " Robustesse d'un Contrôle Vectoriel de Structure Minimale d'une Machine Asynchrone", mémoire de magister, université de Batna, 20 /05 /2006.

[35] M. Z.BOUDJEMAA, M. BOUNADJA, " Commande Non Linéaire par retour d'État d'un Moteur Asynchrone à Double Alimentation par Régulateur PI-Flou, Revue des Sciences et de la Technologie" –RST- Volume 1 N°2, janvier 2010.

[36] B. Meriem, "Contribution à la Commande Robuste de la Machine Asynchrone à Double Alimentation MADA", Mémoire De Magister En Génie Electrique Ecole Nationale Polytechnique d'Oran, 2013 / 2014.

[37] D. YOUCEF, "Commande par réseaux de neurones d'une MADA intégrée à un système éolien", MÉMOIRE Magister en Électrotechnique, SIDI BEL-ABBÈS, 2009.

[38] M. M. Baggu, L. D. Watson, J. W. Kimball and B. H. Chowdhury, "Direct Power Control of Doubly-Fed Generator Based Wind Turbine Converters to Improve Low Voltage Ride-Through during System Imbalance", twenty-fifth annual IEEE applied power Electronics conference and exposition (APEC), 2010, pp, 2121-2125.

[39] A. Mehdi, A. Reama, H.E. Medouce, S.E. Rezgui and H. Benalla, "Direct Active and Reactive Power Control of DFIG Based Wind Energy Conversion System", International Symposium on Power Electronics, Electrical Drives, Automation and Motion, 2014, pp, 1128-1133.

[40] J. Hu, H. Nian, B. Hu, Y. He, and Z. Q. Zhu, "Direct Active and Reactive Power Regulation of DFIG Using Sliding-Mode Control Approach", IEEE transactions on energy conversion, vol. 25, no. 4, december 2010, pp, 1028-1039.

[41] A. Daoud and F.B. Salem, "Direct Power Control of a Doubly Fed Induction Generator Dedicated to Wind Energy Conversions", 11th International multi-conference on systems, Signals and Devices, IEEE 2014, pp, 1-8.

[42] A. Ejlali and D. A. Khaburi, "Power Quality Improvement Using Nonlinear-Load Compensation Capability of Variable Speed DFIG Based on DPC-SVM Method ", The 5th Power Electronics, Drive Systems and Technologies Conference (PEDSTC 2014), Tehran, Iran, Feb 5-6, 2014, pp, 280-254.

[43] S. Muller, M. Deicke, and R. W. De Doncker, "Doubly fed induction generator systems for wind turbines", IEEE Industrial Application Magazine, vol. 17, no. 1, pp. 26–33, May/June 2002.

[44] I. Takahashi, T. Noguchi, "A new quick-response and high-efficiency control strategy of an induction motor", IEEE Transactions on Power Electronics, vol. 22, no. 5, pp. 820–827, 1986.

[45] S. Arnalte, J. C. Burgos, J. L. Rodríguez-Amenedo, "Direct torque control of a doubly-fed induction generator for variable speed wind turbines", Electric Power Components and Systems, vol. 30, no. 2, pp. 199–216, 2002.

[46] L Xu, P Cartwright. "Direct Active and Reactive Power Control of DFIG for Wind Energy Generation". IEEE Transactions on Energy Conversion, 21(3):750–758, Sept 2006.

[47] R. Datta, and V.T. Ranganathan, "Direct power control of grid-connected wound rotor induction machine without rotor position sensors", IEEE Transactions on Power Electronics, vol. 16, no. 3, pp.390–399, May 2001.

[48] P. Mutschler, R. Hoffmann, "Comparison of wind turbines regarding their energy generation", In 33rd Annual IEEE Power Electronics Specialists Conference, vol. 1, pp. 6–11, Australia, 23–27 June, 2002.

[49] M.V. Kazemi, M. Moradi, R.V. Kazemi, "Minimization of powers ripple of direct power controlled DFIG by fuzzy controller and improved discrete space vector modulation", Electrical Power System, vo l. 89, pp. 23-30, 2012.

[50] F. Senani, "La Machine Asynchrone à Double Alimentation : Stratégies de Commande et Applications ", Thèse de doctorat, Université des freres mentouri de constantine 1,2018.

[51] A. K. Djamila, "Commande sans capteur mécanique de la machine asynchrone à l'aide de régulateurs fractionnair," Université Mouloud Maameri de Tizi Ouzou.

[52] M. Abid, "Adaptation de la commande optimisée au contrôle vectoriel de la machine asynchrone alimentée par onduleur à MLI", Thèse de doctorat d'état en Electrotechnique, Université Djillali Liabes De Sidi Bel-Abbès, Algérie, 2009.

[53] N. Cherfia, "Etude d'une Chaine de Conversion de l'Energie Eolienne", Thèse doctorat en sciences, Université des Frères Mentouri de Constantine, Algerie, 2018.

Abstract

In the search for renewable energy resources that are non-polluting and have no undesirable effects on people and the environment, we will conduct this work. It provides a general overview of studying a wind energy system based on a doubly-fed induction generator (DFIG) operating as a generator (DFIG-G) for producing electrical energy. First, we presented the current state of wind energy and the conversion systems used. Then, we described the mathematical models for each part of the wind turbine, including the wind turbine itself and its MPPT control. After that, we applied direct power control (DPC) using PI controllers and fuzzy logic. The direct power control applied to the DFIG-G for regulating active and reactive power, as well as the simulation, was done in the Matlab/Simulink environment. The simulation results obtained from the DPC of the DFIG driven by a wind turbine are significantly valid.

Keywords: renewable energy, doubly-fed induction generator, wind turbine, fuzzy logic, direct power control.

الملخص

في البحث عن موارد الطاقة المتجددة التي لا تلوث ولا تسبب آثاراً غير مرغوبة على الناس والبيئة، قمنا بهذا العمل الذي يقدم نظرة عامة على دراسة نظام طاقة الرياح المستند إلى مولد الحث ذو التغذية المزدوجة المستخدم كمولد لإنتاج الطاقة الكهربائية. أولاً، قدمنا الحالة الحالية لطاقة الرياح وأنظمة التحويل المستخدمة، ثم وصفنا النماذج الرياضية لكل جزء من توربين الرياح، بما في ذلك التوربين نفسه والتحكم فيه بواسطة تقنية تتبع نقطة القدرة القصوى. بعد ذلك، طبقنا التحكم المباشر في الطاقة باستخدام وحدات التحكم التناسبية التكاملية ثم باستخدام المنطق الضبابي.

تم تطبيق التحكم المباشر في الطاقة على المولد الحثي مزدوج التغذية لتنظيم الطاقة النشطة وغير النشطة، وكذلك تمت المحاكاة برنامج الماتلاب النتائج التي تم الحصول عليها من المحاكاة للتحكم المباشر في الطاقة للمولد الحثي مزدوج التغذية المدفوع بواسطة توربين الرياح كانت ذات فعالية كبيرة.

الكلمات الرئيسية: الطاقة المتجددة، مولد الحث ذو التغذية المزدوجة، توربين الرياح، المنطق الضبابي، التحكم المباشر في الطاقة.